Comparative Experimental Study of Subcritical R134a and Transcritical R744 Refrigeration Systems for Mobile Applications

D. E. Boewe, R. P. McEnaney, Y. C. Park,
J. M. Yin, C. W. Bullard, and P. S. Hrnjak

ACRC CR-17 July 1999

For additional information:

Air Conditioning and Refrigeration Center
University of Illinois
Mechanical & Industrial Engineering Dept.
1206 West Green Street
Urbana, IL 61801

(217) 333-3115

The Air Conditioning and Refrigeration Center was founded in 1988 with a grant from the estate of Richard W. Kritzer, the founder of Peerless of America Inc. A State of Illinois Technology Challenge Grant helped build the laboratory facilities. The ACRC receives continuing support from the Richard W. Kritzer Endowment and the National Science Foundation. The following organizations have also become sponsors of the Center.

Amana Refrigeration, Inc.
Brazeway, Inc.
Carrier Corporation
Caterpillar, Inc.
Chrysler Corporation
Copeland Corporation
Delphi Harrison Thermal Systems
Frigidaire Company
General Electric Company
Hill PHOENIX
Honeywell, Inc.
Hussmann Corporation
Hydro Aluminum Adrian, Inc.
Indiana Tube Corporation
Lennox International, Inc.
Modine Manufacturing Co.
Peerless of America, Inc.
The Trane Company
Thermo King Corporation
Visteon Automotive Systems
Whirlpool Corporation
York International, Inc.

For additional information:

Air Conditioning & Refrigeration Center
Mechanical & Industrial Engineering Dept.
University of Illinois
1206 West Green Street
Urbana IL 61801

217 333 3115

TABLE OF CONTENTS

Page

LIST OF TABLES vii
LIST OF FIGURES ix
NOMENCLATURE xiii

1 Introduction 1

2 Experimental Setup 3

2.1 Environmental Chambers and Wind Tunnels 3
2.2 A/C System and Components 6
2.3 Data Reduction 6
2.4 Energy Balance Agreement 7

3 Test Matrix 9

4 Experimental Results 11

4.1 R134a Data 12
4.2 R744 Data 12
4.3 Compressors 13
4.4 Evaporator 15
4.5 Condenser/Gas Cooler 15
4.6 System Charging 24
4.7 Oil Concentration 26
4.8 Test Repeatability 26

5 Internal Heat Exchanger 39

5.1 Introduction 39
5.2 Apparatus and test conditions 39
5.3 Pressure Drop in Suction Line 41
5.4 System performance improvements 43
5.5 Simulation Model 47
5.6 Design optimization 51
5.7 Conclusion 53

References 55

Appendix A - Mobile Air Conditioning System Components 57

A.1 Compressors 58
A.2 Evaporator 61
A.3 Condenser/Gas Cooler 64
A.4 Expansion Device 67

A.5 Suction Accumulator 67
A.6 Internal Heat Exchanger 70
A.7 Valves 72
A.8 Pipes 74
A.9 Sight Glasses 76

Appendix B - Environmental Chambers 77

B.1 Evaporator and Condenser/Gas Cooler Chambers 77
B.2 Compressor Chamber 80

Appendix C - Evaporator and Condenser/Gas Cooler Wind Tunnels 81

C.1 Ducts 81
C.2 Air Straightener 81
C.3 Thermocouple Grid 81
C.4 Nozzles 84
C.5 Heaters 84
C.6 Blowers 85
C.7 Humidifier 85
C.8 Condensate Collection Stand 87
C.9 Coiling Coil and Chiller System 87

Appendix D - Compressor Stand 91

Appendix E - Instruments 93

Appendix F - Data Reduction 98

F.1 Input to EES data calculation model 98
F.2 Output to EES data calculation model 100
F.3 R134a sample EES data calculation model 102
F.4 R744 sample EES data calculation model 110

Appendix G - Internal Heat Exchanger Model 117

LIST OF TABLES

Page

Table 3-1 Test conditions identified for a/c system. Conditions in boldface were run using R134a system. Conditions shaded were run using R744 system. 10

Table 4-1 Charge influence on R134a performance. 25

Table 4-2 Comparison of R744 performance with various charges. 25

Table 4-3 Measured oil concentrations for R134a system. 27

Table 4-4 Influence of oil flow rate through the bypass line from the oil separator in R744 system. 27

Table 4-5 Influence of oil flow rate from suction accumulator in R744 system. 27

Table 4-6 Repeatability of the R134a experimental results in time. 28

Table 4-7 Repeatability of the R744 experimental results in time. 28

Table 4-8 R134a system and compressor data. 29

Table 4-9 R134a evaporator data. 30

Table 4-10 R134a condenser data. 31

Table 4-11 R134a system and compressor cycling data. 32

Table 4-12 R134a evaporator cycling data. 33

Table 4-13 R134a condenser cycling data. 34

Table 4-14 Summary of all R744 data taken listed by test condition. 35

Table 4-15 Summary of all R744 data taken in chronological order. 37

Table 5-1 Test conditions for R744 system. 41

Table 5-2 Idle and driving speed operating conditions at near-optimal COP. 44

Table 5-3 Counterflow IHX performance at high ambient and driving conditions (B and C). 53

Table A-1 Dimensions and characteristics of R134a compressor and R744 compressor. 58

Table A-2 Dimensions and characteristics of R134a evaporator and all three R744 evaporators. 62

Table A-3 Dimensions and characteristics of R134a condenser and all three R744 gas coolers. 65

Table A-4 Connecting line dimensions for R134a and R744 systems..... 74

Table B-1 Heat transfer coefficients and surface areas for transmission losses in environmental chambers. 79

Table C-1 Evaporator wind tunnel duct sections. 82

Table C-2 Condenser/gas cooler wind tunnel duct sections. 83

Table E-1 List of all instruments used in calculating the chamber balance. 94

Table E-2 List of all instruments used in calculating the air side balance..... 95

Table E-3 List of all instruments used in calculating the refrigerant side balance. 96

Table E-4 Data acquisition measurement accuracy. 97

LIST OF FIGURES

Page

Figure 2-1 Schematic of R134a system (left) and prototype R744 system (right). 4

Figure 2-2 Chamber (a) and air side (b) energy balance using both condensate scale and second chilled mirror 5

Figure 2-3 Energy balance comparison for R134a and prototype R744 systems. 8

Figure 4-1 Volumetric efficiency for R134a compressor and R744 compressor 2 and 3 used in mobile air conditioning system. 16

Figure 4-2 Isentropic efficiency for R134a compressor and R744 compressor 2 and 3 used in mobile air conditioning system. 16

Figure 4-3 Volumetric efficiency for all R744 compressors (1, 2, and 3) used in mobile air conditioning system. 17

Figure 4-4 Isentropic efficiency for all R744 compressors (1, 2, and 3) used in mobile air conditioning system. 17

Figure 4-5 Compressor isentropic efficiency plotted in order of data taken. Circled points indicate same pressure ratio points near arrow. Number is pressure ratio. 18

Figure 4-6 Air side pressure drop as a function of air mass flow rate for R134a evaporator showing different air inlet relative humidity. All data are for continuous runs 19

Figure 4-7 Air side pressure drop as a function of face velocity for R134a evaporator showing different air inlet relative humidity. All data are for continuous runs. 19

Figure 4-8 Air side pressure drop as a function of air mass flow rate for R744 evaporator showing different air inlet relative humidity. All data are for continuous runs 20

Figure 4-9 Air side pressure drop as a function of face velocity for R744 evaporators showing different air inlet relative humidity. All data are for continuous runs. 20

Figure 4-10 Air side pressure drop as function of air mass flow rate for R134a and R744 evaporators. Both curves are dry coil measurement 21

Figure 4-11 Air side pressure drop as function of face velocity for R134a and R744 evaporators. Both curves are dry coil measurement 21

Figure 4-12 Air side pressure drop as a function of air mass flow rate for R134a condenser and R744 gas cooler 22

Figure 4-13 Air side pressure drop as a function of face velocity for R134a condenser and R744 gas cooler 22

Figure 4-14 Refrigerant side pressure drop as a function of refrigerant mass flow rate for R134a and R744 evaporators. 23

Figure 4-15 Refrigerant side pressure drop as a function of refrigerant mass flow rate for R134a condenser and R744 gas cooler. 23

Figure 5-1 Cross section of the prototype internal heat exchanger I, II, and III 41

Figure 5-2 Schematic diagram of the R744 suction line. 42

Figure 5-3 Graphical presentation of pressure drop elements in suction line. 44

Figure 5-4 Influences of IHX length at hot idling condition B. 46

Figure 5-5 Effect of ambient temperature. 47

Figure 5-6 Predicted and measured capacity in parallel (PF) and counterflow (CF) configurations. 50

Figure 5-7 Predicted and measured compressor suction inlet density with IHX in parallel (PF) and counterflow (CF) configurations 50

Figure 5-8 Proposed IHX designs IV (top) and V (bottom) with hot stream in smaller ports. Design V allows for limited bending about major axis 51

Figure 5-9 Efficiency improvement due to IHX optimization at idle condition B 52

Figure 5-10 Efficiency improvement due to IHX optimization at driving condition C. 52

Figure A-1 Picture of some of the prototype R744 system components and instruments in the test facility 57

Figure A-2 Schematic of R134a air conditioning system components showing all refrigerant side measurements (excluding compressor torque meter and tachometer) 59

Figure A-3 Schematic of R744 prototype air conditioning system components showing all refrigerant side measurements (excluding compressor torque meter and tachometer). 59

Figure A-4 Photo of R134a compressor (left) and R744 compressor (right) taken to show size comparison. At this time, R744 compressor is connected to refrigeration system being tested. 60

Figure A-5 Picture of R134a evaporator (right) and R744 evaporator (left) 61

Figure A-6 Profile of evaporator microchannel tube (top) and manifold (bottom). All dimensions in mm. 62

Figure A-7 Schematic showing the number of passes and number of tubes for each of the three evaporators available for use in the mobile air conditioning prototype system. The airflow is out of the paper through the first slab and then the second. 63

Figure A-8 Picture of R134a condenser (left) and R744 gas cooler (right). 64

Figure A-9 Profile of gas cooler microchannel tube (top) and manifold (bottom). All dimensions in mm. 65

Figure A-10 Schematic showing the number of passes and number of tubes for each of the three gas coolers available for use in the mobile air conditioning prototype system. 66

Figure A-11 Schematic of fixed orifice tube used in the R134a system. 68

Figure A-12 Schematics of HOKE® 2300 Series Bar Stock Metering Valve (left) and TESCOM® 26-1700 Series Pressure Reducing Regulator (right) used for R744 expansion devices. 68

Figure A-13 Picture of R134a suction accumulator (left) and R744 suction accumulator (right) 69

Figure A-14 Visualization of separation of vapor, liquid, and oil in R744 suction accumulator. 70

Figure A-15 A view of the suction line heat exchanger located on the wall of the environmental chamber. 71

Figure A-16 A cross section of the internal heat exchanger used in all tests. The high pressure gas cooler exit flows through the inner tube and the low pressure accumulator exit flows through the outer channels. 71

Figure A-17 Flow curves for the metering valve used as expansion device (left) and oil flow regulator (right). Graphs provided by HOKE® 73

Figure A-18 Pressure drop predictions used in selection of valves placed on high-pressure side of R744 system. 75

Figure A-19 Pressure drop predictions used in selection of valves placed on low-pressure side of R744 system. 75

Figure A-20 Picture of sight glass located after evaporator in the R744 system. (System was not running at time of picture.) 76

Figure B-1 Blow up of environmental chamber used in mobile air conditioning lab. 77

Figure B-2 Illustration of the panel locking system in the Tyler walk-in cooler. 78

Figure B-3 Plot of data taken to calibrate the condenser chamber (left). Plot of measured heat transmission loss verses calculated loss using calibrated U values. 79

Figure C-1 Evaporator wind tunnel duct sections with wind tunnel components included. 82

Figure C-2 Condenser/gas cooler wind tunnel duct sections with wind tunnel components included. 83

Figure C-3 Side view of internal components of humidifier. 86

Figure C-4 Schematic of condensate collection stand. 88

Figure C-5 A schematic of the mobile and residential chiller systems. 90

Figure D-1 Schematic of compressor stand. 91

NOMENCLATURE

A	area
AFR	air flow rate
C_v	valve flow coefficient
CF	counterflow
COP	Coefficient of Performance
D	hydraulic diameter
DG	condensate flow rate
DP	pressure drop
DP_v	pressure drop across the valve
DTsub	superheat of condenser
DTsup	subcooling of evaporator
f	friction factor
F	two-phase convection multiplier
Fc	transducer force
h	enthalpy
Δh_s	isentropic work of compression
IHX, ihx	internal heat exchanger
k	conductivity
L	length
m	mass flow rate
ml	mass flow rate of oil exiting the accumulator
$\dot{m}$, m_r	mass flow rate of refrigerant
Nu	Nusselt number based on hydraulic diameter
P	pressure
PF, CC	parallel flow, cocurrent flow
Pr	Prandtl number
Q	heat exchange
Re	Reynolds number
RH	relative humidity
SG	specific gravity of refrigerant

T	temperature
v	specific volume
Vc	speed of the compressor
V_d	compressor displacement
W_{comp}	compressor power
x	vapor quality
X_{tt}	Lockhart-Martinelli parameter

Greek

α	heat transfer coefficient
ε	effectiveness
η_{isen}	compressor isentropic efficiency
η_v	compressor volumetric efficiency
μ	viscosity
ρ	density
ω	compressor speed

Subscripts

a	air
c, cond	condenser or gas cooler
ci	suction side inlet to IHX
co	suction side exit to IHX
cp	compressor
D	hydraulic diameter
e, evap	evaporator
hi	high side inlet to IHX
ho	high side exit to IHX
i	inlet
IHX	internal heat exchanger
l	liquid phase

lat, latent	latent heat of evaporator
o	outlet
oil	oil flowing through compressor bypass
r	refrigerant
ratio	pressure ratio
sens, sensible	sensible heat of evaporator
v	vapor phase

1 Introduction

Automobile air conditioning systems are known to be the largest contributor of refrigerant released into the atmosphere. This release contributes to the global warming impact of automobile air conditioning systems. One of the options for reducing this global warming impact is the transcritical R744 (CO_2) system.

This cycle has been well known for a long time. The first successful R744 machine was designed and built by an American named Thaddeus Lowe in 1866. He used this R744 machine to make commercial ice in Dallas, Texas and in Jackson, Mississippi. By 1930, R744 systems became dominant in refrigerated marine cargo ships as a safe refrigerant. These large and bulky systems were later (by 1950's) replaced by then invented R12. (Thavenot, 1979)

The transcritical R744 cycle was revisited by Lorentzen and Pettersen (1993). The major drawback opponents articulate are high operating pressure and poor thermodynamic properties. Reasons to rethink the feasibility of R744 systems are the advancements in manufacturing of aluminum microchannel tubing and new compressor technology. Several Air Conditioning and Refrigeration Center (ACRC) member companies have expertise in these areas. One of them, Hydro Aluminum, has supported our efforts to design, build, and test a prototype of the transcritical R744 system.

This thesis/report shows some of the results obtained by the prototype transcritical R744 system and also document the setup of the test facility.

Before this project began there was a huge debate in the professional arena about the energy efficiency of the transcritical R744 systems. We wanted to experimentally check the performance of a prototype R744 system. To be able to provide credible results, the comparison to some conventional system was necessary. A R134a Ford Escort mobile air conditioning system was chosen to be a good representative air conditioner. This R134a system is of a size that can be found in the US, European, and Japanese markets. The heat exchangers are of a type commonly used in conventional systems. The evaporator has brazed aluminum plates and fins (sometimes called drawn-cup or laminated evaporator) while the condenser is an aluminum tube and plate louvered fin type.

Due to higher pressure, heat exchangers for R744 need either smaller diameter tubes or thicker walls of the same material. We selected micro-channel heat exchangers with specially designed headers to sustain higher operating pressures. The entire experimental setup is given in more detail in Chapter 2 and Appendix A, B, C, D, and E.

Component (evaporator, condenser, accumulator and compressor) volumes of the R744 system were constrained to be less or equal to those of the R134a baseline system. Additionally the face areas were kept equal. This gives smaller core volume of the gas cooler in the R744 system due to smaller depth. Volumetric flow rates of air are designed to be the same, as are air-side pressure drops. As it will be shown in Chapter 4, air side pressure drops of the R744 system are actually lower.

The system test conditions are defined in a test matrix given in Chapter 3. This test matrix was to be large enough to use the data taken for the purpose of developing component and system simulation models, as well as supporting data-to-data comparisons at normal, seasonal and extreme operating conditions.

Recently, detailed system performance comparisons were published by McEnaney et al. (1999). Results showed the R744 system to have slightly lower capacity and COP (a few percent) at very high ambient temperatures (above 45°C) but much higher capacity and COP at lower ambient temperatures. All data taken for both the R134a and R744 systems are given in Chapter 4 in table format and on disk in file format.

The R744 system components are now being looked at more closely. An analysis of the prototype internal heat exchangers (IHX) is given in Chapter 5. The system effects of the IHX are discussed in this analysis. An IHX model has been created and compared to data taken. Then using this model, a redesign of the IHX is given.

2 Experimental Setup

The test facilities have been designed to give three procedures to determine system performance: refrigerant side, air side, and calorimetric chambers. Each side yields its own energy balance calculation to find the capacity of the system. With the three methods used, instead of two as required by all applicable standards, the determination of system capacities is more reliable. In some cases, when the evaporator refrigerant exit is two phase, only the air side and chamber balances are available. The test facility for each system is shown in Figure 2-1.

2.1 Environmental Chambers and Wind Tunnels

The environmental chamber walls have 30 cm of insulation. The inside dimensions of the chambers are 3.55 x 1.83 x 2.45m for the evaporator chamber and 3.55 x 2.13 x 2.45m for the condenser chamber. The chambers were carefully calibrated. The chambers have five thermocouples located on the inside and outside of the walls, floor, and ceiling. The temperatures yield a temperature drop across each wall, which is used to find transmission losses. Appendix B shows the calibration result of the condenser chamber. At a temperature difference close to 32°C, the transmission losses are only approximately 300 W. These calibration data were used in the chamber energy balance and are about 5% of the overall chamber energy balance.

A ±0.1°C accurate chilled mirror dew point sensor measures the humidity of the evaporator inlet air. Outlet humidity is determined by finding the condensate removal rate and calculating the outlet air conditions. The weight of the condensate extracted at the evaporator is measured by a 0-2.5 kg load cell (Sc) with ±0.1% FS accuracy and the clock in the computer measures time in the data acquisition system. The change in weight of condensate over time is the condensate removal rate. This procedure was verified by an additional chilled mirror placed at the exit of the evaporator air flow. The condensate removal rate was then backed out and compared to the weighed condensate. These results are shown in Figure 2-2.

The thermocouple grids (TG) are used for inlet temperatures of the heat exchangers. The evaporator thermocouple grid has 9 evenly spaced thermocouples and the condenser has 27. each

finds the representative inlet air temperature for the heat exchanger. The air temperatures are used in conjunction with relative humidity to find the air enthalpies and specific heats.

The flow straightener (FS) at the inlet of the wind tunnels in the calorimetric chambers serves to reduce turbulence. Uniformity of the velocity profile was checked and the difference in the nine grid points of the duct inlet is ±2.37% at a mean air velocity of 1.4 m/sec. Air flow rate is measured using ANSI standard nozzles (N). The nozzles are used with ±0.17% FS differential pressure transducers and a thermocouple to obtain the air flow rates.

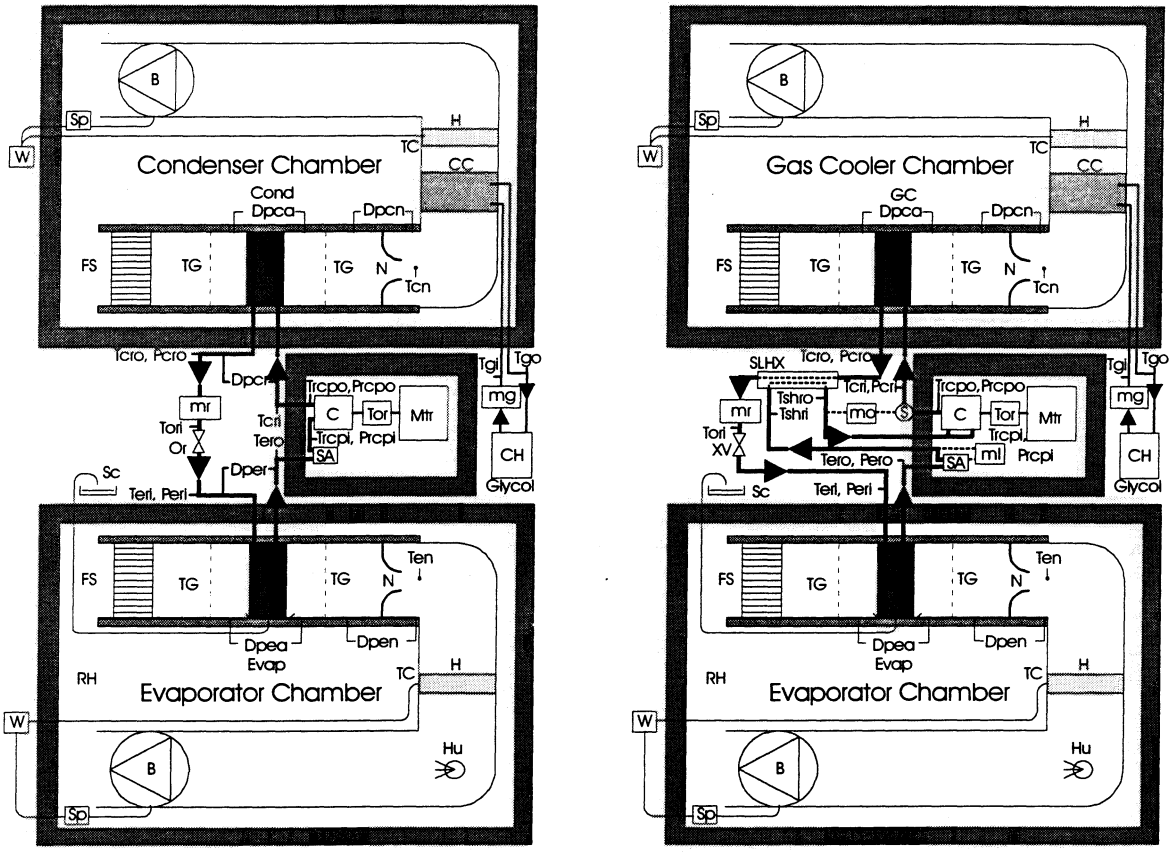

B – Blower, **C** – Compressor , **CC** – Cooling Coil, **CH** – Glycol Chiller, **Cond** – Mobile Condenser, **Dp** – Differential Pressure Transducer, **Evap** – Mobile Evaporator, **FS** – Flow Straightener, **GC** – Gas Cooler, **H** – Heater, **Hu** – Humidifier, **mg** – Glycol Mass Flow Meter, **ml** – Suction Accumulator Liquid Mass Flow Meter, **mo** – Oil Mass Flow Meter, **mr** – Refrigerant Mass Flow Meter, **Mtr** – Motor, **N** – Nozzle, **Or** – Orifice Tube, **P** – Pressure Transducer, **RH** – Relative Humidity Probe, **S** – Separator, **SA** – Suction Accumulator, **Sc** – Condensate Scale, **SLHX** – Suction Line Heat Exchanger, **Sp** – Speed Controller and Tachometer, **T** – Thermocouple, **TC** – Temperature Controller, **TG** – Thermocouple Grid, **Tor** – Torque Transducer, **W** – Watt Transducer, **XV** – Metering Expansion Valve
Indices: **a** – air, **c** – condenser, **cp** – compressor, **e** – evaporator, **g** – glycol, **i** – inlet, **n** – nozzle, **o** – outlet, **r** – refrigerant, **sh** – suction line heat exchanger

Figure 2-1 Schematic of R134a system (left) and prototype R744 system (right).

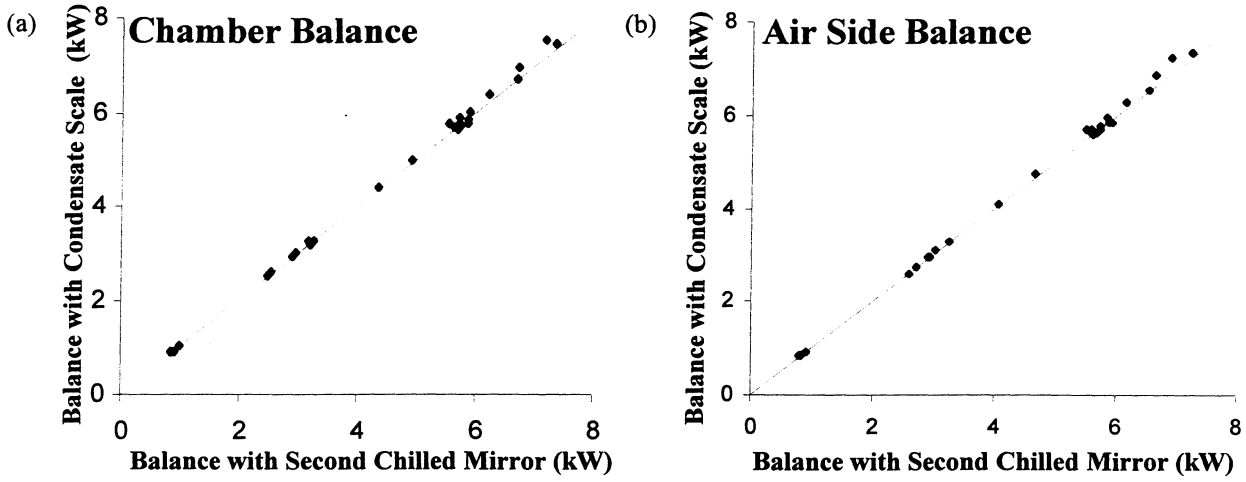

Figure 2-2 Chamber (a) and air side (b) energy balance using both condensate scale and second chilled mirror.

To determine cooling capacity by the chamber balance, all energy inputs and outputs are measured. Electrical heaters and blower motors provide sensible load. SCRs and PIDs control the heaters (H). The blowers (B) are controlled using variable speed controllers (Sp). The SCRs and speed controllers are located inside the chambers. In this way, all losses from the SCR and the controller are sensible load to the chambers. These and any other electrical sources going into the chambers are measured by ±0.2% watt transducers (W) located outside at regular power supply lines.

A PID controller controls the steam humidifier that provides latent load, whose capacity is varied by a heater. The humidity in the evaporator chamber is maintained in the range of ±0.2°C dew point temperature. Inlet enthalpy is determined by inlet temperature for a measured (almost atmospheric) pressure. Exit enthalpy is determined for a measured water temperature. The steam flow rate is measured by the weight of the condensate.

The condenser chamber uses an external glycol chiller with an aqueous solution of ethylene glycol to remove the heat. The mass flow rate of the glycol is measured using a ±0.1% FS accuracy Coriolis type mass flow meter (Mg). The inlet and exit temperatures (Tgi and Tgo) are found using T-type immersion thermocouples placed directly into the glycol streams.

The test facility described provides data for refrigerating capacities measured by independent procedures in a narrow error band. Figures 3 and 4 indicate those values for the evaporator and condenser chambers. The chambers, wind tunnel, and instruments are discussed in more detail in Appendices B, C, D, and E.

2.2 A/C System and Components

The air conditioning systems used are an off the shelf R-134a unit for a Ford Escort and a prototype R744 system. For the R134a system, the components were not modified in any way in order to replicate the original system as closely as possible. The only exception is the piping. The tube lengths were modified due to component locations in the test facilities. The tube diameters were not changed. All system components along with measurement locations for both systems are described in Appendix A and a system schematic is shown in Figures A-2 and A-3.

The refrigerant mass flow rate is measured using a ±0.1% Coriolis type mass flow meter (mr). For the R134a, the pressure transducers (P) for the high side are 0~3.5 MPa (±0.2% FS), and for the low side 0-0.7 MPa (±0.2% FS). Differential pressure transducers (DP) are used to measure the refrigerant pressure drop across the evaporator and condenser. Their range is 0-170 kPa (±0.17% FS). For the R744, the pressure transducers (P) for the high side are 0~20.7 MPa (±0.25% FS), and for the low side 0-6.9 MPa (±0.25% FS). All thermocouples (T) in the refrigerant loop are T-type shielded immersion thermocouple probes placed directly into the refrigerant flow.

The R744 system uses two additional ±0.1% Coriolis mass flow meters. One mass flow meter (mo) is used to measure the oil flow rate from an oil separator (S) at the exit of the compressor back to the inlet of the compressor (C). The other mass flow meter (ml) is used to measure the flow rate of oil exiting the bottom of the suction accumulator (SA).

2.3 Data Reduction

All data is taken with a Hewlett-Packard data acquisition system HP75000 and data acquisition software. All data are monitored via graphic windows and transferred to an Excel data sheet. Data stored in Excel are transferred to Engineering Equation Solver (EES) using a developed

Visual Basic program. The performance of the system is calculated in this EES program given in Appendix F, linked to REFPROP, and converted again to an Excel data sheet for drawing graphs of the results as a form of COP, capacity, flow rate, torque, etc. The data acquisition program was written using HPVEE.

2.4 Energy Balance Agreement

A comparison of the energy balances was made to ensure the correctness of the data. For the R134a evaporator, the air side energy balance is compared to the chamber energy balance in Figure 2-3a. They show to have a standard deviation of 0.07 kW, which is about 2% of the average evaporator capacity. For the R134a condenser, the air side energy balance is compared to the chamber energy balance in Figure 2-3b. They show to have a standard deviation of 0.15 kW, which is about 3% of the average condenser capacity. The refrigerant side energy balance for R134a condenser and evaporator shows not to be reliable since the refrigerant is in a two-phase condition at the exit for some conditions.

For the R744 evaporator, the air side energy balance and the chamber energy balance are compared in Figure 2-3c. They show to have a standard deviation of 0.04 kW, which is about 1.3% of the average evaporator capacity. The refrigerant side energy balance for the R744 evaporator shows not to be reliable since the refrigerant is in a two-phase condition at the exit for some conditions. For the R744 gas cooler, the refrigerant side energy balance and the chamber energy balance are compared in Figure 2-3d. They show to have a standard deviation of 0.18 kW, which is about 4% of the average gas cooler capacity. In this case, the refrigerant side energy balance proves to be good since the R744 does not go through a phase change. The air side energy balance showed to have large error since the supercritical R744 goes through a large temperature change. This large temperature change causes the exit air temperature to be difficult to accurately measure. The chamber energy balance is assumed the most accurate balance. As a check of the R744 gas cooler capacity, a comparison of the chamber energy balance with the calculated gas cooler capacity is shown in Figure 2-3e. The calculated gas cooler capacity comes from the addition of the evaporator capacity and the compressor work. This comparison shows to have a standard deviation of 0.15 kW, which is about 3.2% of the gas cooler capacity. This calculated comparison neglects all heat losses through the lines and compressor housing.

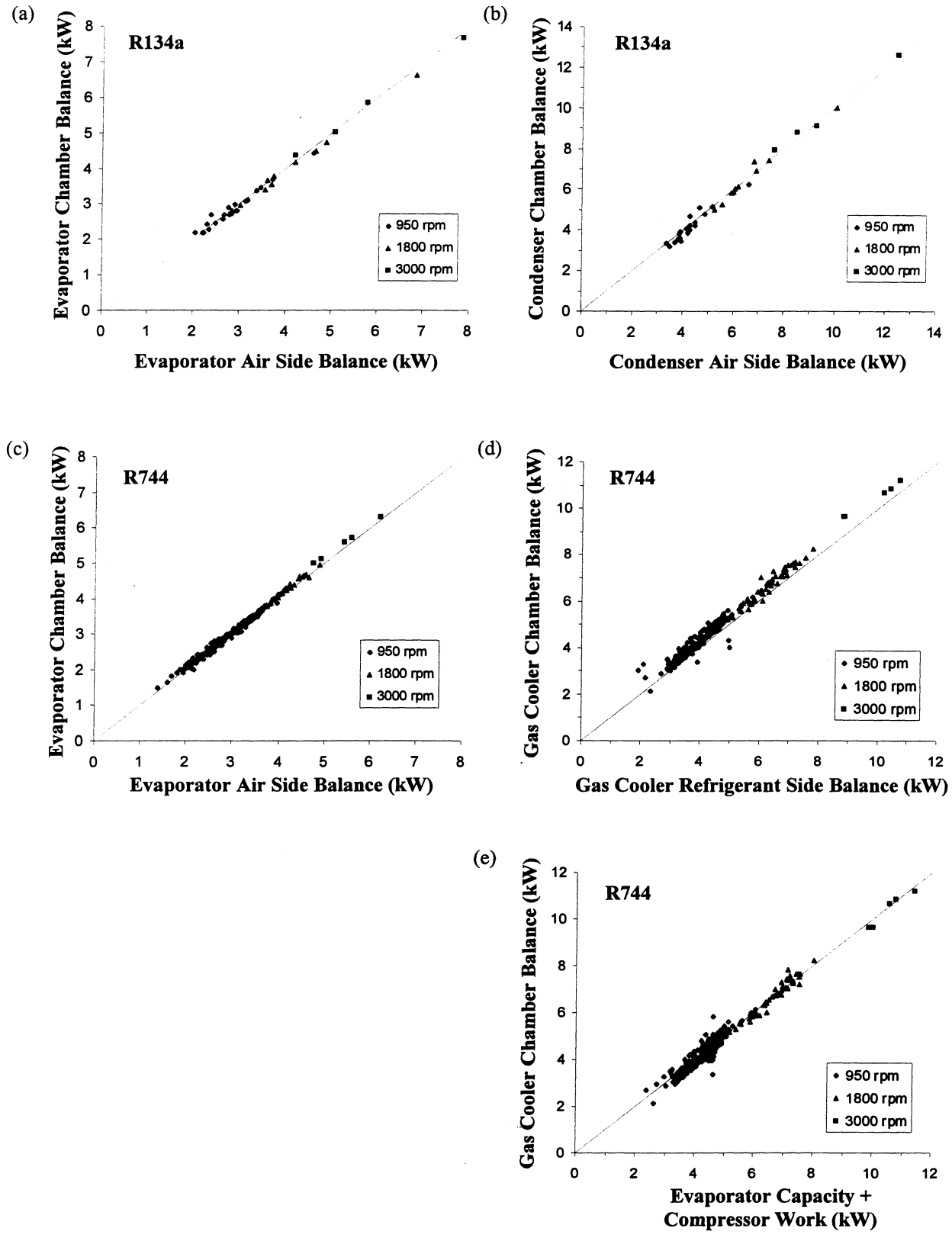

Figure 2-3 Energy balance comparison for R134a and prototype R744 systems.

3 Test Matrix

The test matrix was designed to provide system and component performance data to serve two main objectives: improving the system and its components, and verifying models. This matrix is shown in Table 3-1. The same test matrix was used for both the R134a system and R744 system. It is comprised of three compressor speeds: 950 rpm (shown as "I #"), which represents idling conditions, 1800 rpm (shown as "M #"), which represents medium speed driving operation, and 3000 rpm (shown as "H #"), which represents high speed operation. Also, one mid-speed condition of 1400 rpm (shown as "N #") was added to better see the effect of compressor speed. For all but two conditions (I40 and I41), the condenser/gas cooler air flow rates are related to the compressor speed.

The conditions that are in bold in the test matrix are those for which the R134a system has had testing performed. The conditions shaded in are those for which the R744 system operated. Conditions with an asterisk denote conditions that cycled. These cycling data are discussed in Ryan McEnaney's thesis. Test conditions denoted by a T at the end of the test condition are part of a reduced test matrix. This reduced test matrix was found to be important for TEWI calculations (Yin et. al. 1999).

Table 3-1 Test conditions identified for a/c system. Conditions in boldface were run using R134a system. Conditions shaded were run using R744 system.

Compressor Speed, RPM (Condenser/Gas Cooler Flow Rate)	Condenser/ Gas Cooler Inlet Air Temp., °C	Evaporator		Relative Humidity, %				
		Flow Rate, m^3/min	Inlet Air Temp., °C	70	50	40	25	Dry
3000 (35.40 m^3/min)	43.3	7.080	43.3		**H1**			
			32.2		**H2**	**H3T**	**H4**	
			21.1	**H5***	**H6***	**H7***	**H8***	
	32.2	4.956	26.7	**H9***	**H10***	**H11T***	**H12***	
	21.1	2.832	21.1	**H13***	**H14***	**H15T***	**H16***	
1800 (26.90 m^3/min)	43.3	7.080	43.3		**M1**	**M0**		
			32.2		**M2**	**M3T**	**M4**	
			26.7			**M5**		
			21.1	**M6**	**M7**	**M8**	M9*	
	32.2	7.080	26.7			**M10**		
		4.956	26.7		**M11***	**M12T***	**M13***	
			21.1			**M14***		
	26.7	4.956	26.7			**M15***		
			21.1			**M16***		
		2.832	21.1			**M27***		
	21.1	4.956	32.2		**M17**	**M18***	**M19***	
		2.832	26.7			**M20***		
			21.1	**M21***	**M22***	**M23T***	**M24***	
	15.5	2.832	26.7			**M25***		
			21.1			**M26T***		
1400 (25.06 m^3/min)	43.3	7.080	26.7			N1		
950 (22.65 m^3/min)	60	7.080	43.3		**I1**			
			32.2		**I2**	**I3**	**I4**	
	54.4	7.080	26.7			I38		
			32.2		**I5**	**I6T**	**I7**	
	43.3	7.080	43.3			I39		
			32.2		**I8**	**I9**	**I10**	
			26.7			**I11**		I35
			21.1	**I15**	**I16**	**I17**	**I18**	
		4.956	26.7	I34	**I12**	**I13T**	**I14**	I36
		2.832	26.7			I42		I37
	32.2	7.080	26.7			**I19**		
		4.956	26.7			**I20**		
		2.832	26.7			**I31***		
			21.1	**I21***	**I22***	**I23T***	**I24***	
	26.7	7.080	26.7			I44		
		2.832	26.7			**I32***		
			21.1			**I33***		
	21.1	7.080	26.7			**I25**		
		2.832	26.7			**I26***		
			21.1	**I27***		**I28***		
	15.5	2.832	26.7			**I29***		
			21.1			**I30T***		
950 (26.90 m^3/min)	43.3	7.080	26.7			I41		
950 (35.40 m^3/min)						I40		

4 Experimental Results

This chapter contains tables with experimental results broken by refrigerant (R134a and R744) and type of operation (continuous and cycling). Due to the extreme number of results of R744, the data are not printed but are available in electronic form.

Also given in this chapter are a few basic component comparisons (compressor efficiencies, refrigerant side pressure drops in heat exchangers, and air side pressure drops in heat exchangers). These comparisons are first step efforts to aid in the development and validation of the component models.

At the end of the chapter several system checks (system charging, oil concentration, and test repeatability) are given. These checks are to validate some basic assumptions used throughout the testing period, i.e. R744 charge is not important.

System performance is being analyzed and various publications have been made by our group. These publications are listed as follows:

Boewe, D., Park, Y.C., Yin, J., Bullard, C.W., Hrnjak, P.S., "The Role of a Suction Line Heat Exchanger in Transcritical R744 Mobile A/C Systems." SAE International Congress and Exposition, Paper 1999-01-0583, 1999.

McEnaney, R.P., Boewe, D.E., Yin, J.M., Park, Y.C., Bullard, C.W., Hrnjak, P.S., "Experimental Comparison of Mobile A/C Systems when Operated With Transcritical CO_2 Versus Conventional R134a." International Refrigeration Conference at Purdue, pp. 145-150, 1998.

McEnaney, R.P., Park, Y.C., Yin, J.M., Hrnjak, P.S., "Performance of the Prototype of Transcritical R744 Mobile A/C System." SAE International Congress and Exposition, Paper 1999-01-0872, 1999.

Park, Y.C., McEnaney, R., Boewe, D., Yin, J.M., Hrnjak, P.S., "Steady State And Cycling Performance Of A Typical R134a Mobile A/C System." SAE International Congress and Exposition, Paper 1999-01-1190, 1999.

Yin, J., Park, Y.C., Boewe, D., McEnaney, R., Beaver, A., Bullard, C.W., Hrnjak, P.S., "Experimental and model comparison of transcritical CO2 versus R134a and R410 system performance." Natural Working Fluids '98, IIR - Gustav Lorentzen conference, Oslo, pp. 331-340, 1998.

Yin, J.M., Pettersen, J., McEnaney, R., Beaver, A., "Performance Of TEWI Comparison of R744 and R134a Systems for Mobile Air Condition." SAE International Congress and Exposition, Paper 1999-01-0582, 1999.

4.1 R134a Data

The R134a system was operated in both continuous and cycling mode. All continuous data was measured and averaged for 10 minute time periods for each data point. These continuous data are given in the following tables at the end of this chapter:

a) Table 4-8 System and compressor data,
b) Table 4-9 Evaporator data,
c) Table 4-10 Condenser data.

The process of cycling and method of taking data is explained in detail in Ryan McEnaney's thesis. The following tables are given to present the R134a cycling data at the end of this chapter:

a) Table 4-11 System and compressor cycling data,
b) Table 4-12 Evaporator cycling data,
c) Table 4-13 Condenser cycling data.

4.2 R744 Data

Two tables, Table 4-14 and Table 4-15, located at the end of this chapter summarize the R744 steady state data. Table 4-14 presents data by test condition. It has twelve columns:

1) Point – The test condition run
2) Date – Date of run
3) Comp – Compressor (1, 2, or 3) described in Section
4) # runs – Number of times data was taken for that point, usually to find the COP maximizing pressure
5) IHX – Internal heat exchanger (0, 1.0, 1.5, 2.0 m) described in Chapter 5 and Appendix A
6) Flow – The type of flow being used in the internal heat exchanger (CC – cocurrent or parallel flow, CF – counterflow)
7) and 8) Pressure Range – The range of high side pressures over the number of runs made
9) and 10) COP Range – The high and low value of COP found over the number of runs and pressure range
11) and 12) Rows – Location of data in the detailed data file (R744 data.xls) used to look up and plot various data

The second table, Table 4-15, has the same data as Table 4-14 only sorted by date. Its purpose is to give an indication of the objective of some tests performed and also list the data in chronological order. Cycling data is given in Ryan McEnaney's thesis.

An Excel program called 'R744 data.xls' has been made with a complete listing of all R744 steady state data. In Table 4-14 and Table 4-15, a list of rows for each data set is given. These rows correspond to the rows in the program. Within this program, up to ten sets of data can be viewed and plotted by specifying the rows from the table. In addition, up to ten specific points can be chosen to make a P-h or T-h diagram. On the T-h diagram, the air side temperatures can be plotted for the first two points chosen.

4.3 Compressors

The same R134a compressor was used during all of the testing data being reported. Three R744 compressors were used over the testing period. The first compressor developed a leak at the shaft seal after approximately 400 hours of use and was then replaced with the second compressor. After approximately 100 hours of use, the second compressor developed leaks around the bolt heads used to hold the compressor together and was also replaced with a third compressor. The third compressor was actually the first compressor after being rebuilt and was used for the completion of testing. Both systems were operated in idling (950 rpm), driving (1800 rpm), and highway (3000 rpm) conditions. The volumetric and isentropic efficiencies of compressors 2 and 3 along with the R134a compressor are shown in Figure 4-1 and Figure 4-2. In both cases, the efficiencies of all the compressors appear to fall along the same line. More details on the compressors are given in Appendix A.

The R744 compressor has greater scatter in the efficiency data. A further analysis indicates this is consequence of the compressor used. Figure 4-3 and Figure 4-4 show the variation of efficiencies for the three different compressors. In these figures, the third compressor's efficiencies were always below the second compressor and the first compressor appears to be inconsistent with its performance. This led us to look at the compressors' isentropic efficiency for the data in test order.

Figure 4-5 shows the compressor efficiency plotted in the order of tests taken. There are three sets of two arrows, one set for each compressor. These arrows are connecting isentropic efficiencies for the same pressure ratio in time. The decreasing direction of the two arrows for the first compressor indicate that compressor was degrading over the testing period. This degradation was found to reduce the repeatability of the test conditions and the compressor was replaced after developing a leak around the shaft seal.

For the second and third compressors, the arrows appear to remain horizontal in Figure 4-5, which would suggest no significant compressor degradation. The removal of the second compressor was necessary when leakage of oil was detected. This leakage occurred around the head of the bolts holding the compressor together. The third compressor still appears to be good and will be used in the future.

The volumetric efficiency is calculated using Equation (4.1).

$$\eta_v = \frac{m_r \cdot v_v}{\omega \cdot V_d} \tag{4.1}$$

Where m_r is the refrigerant mass flow rate (kg/s), v_v is the specific volume of the suction vapor entering the compressor (m^3/kg), ω is the compressor speed (rev/sec), and V_d is the compressor displacement (m^3).

The isentropic efficiency is calculated using Equation (4.2),

$$\eta_{isen} = \frac{m_r \cdot \Delta h_s}{W_{comp}} \tag{4.2}$$

where m_r is again the refrigerant mass flow rate (kg/s), Δh_s is isentropic work of compression (kJ/kg), and W_{comp} is the power supplied to the compressor (kW). The inlet and exit conditions are determined in the suction and discharge lines as shown in Figure A-2 for the R134a compressor and Figure A-3 for the R744 compressor. Isentropic work of compression is determined assuming isentropic compression from suction condition to discharge pressure, Prcpo.

As expected, larger pressure ratio compressors have both lower volumetric and isentropic efficiencies. Therefore, it is advantageous to the performance of a system to have a lower pressure ratio.

4.4 Evaporator

The measured R134a and R744 evaporator air side pressure drops are given as a function of mass flow rate in Figure 4-6 and Figure 4-8 and as a function of face velocity in Figure 4-7 and Figure 4-9. These figures show the measured data for different relative humidity along with a pressure drop curve for the dry coil. The pressure drop curve for the dry coil was made using an inclined manometer connected to the inlet and exit air pressures of the dry evaporator. The other points are from the data taken during system testing. Figure 4-10 and Figure 4-11 compare these two pressure drop curves for the R134a and R744. The R744 evaporator has a lower air side pressure drop than that of the R134a evaporator at the dry condition. These data can now be used to help create and validate air side pressure drop models for the evaporators. The characteristics of the R134a and R744 evaporators are discussed in more detail in Appendix A.

The refrigerant side pressure drops for the evaporators are given as a function of mass flow rate in Figure 4-14.

4.5 Condenser/Gas Cooler

The measured R134a condenser and R744 gas cooler air side pressure drop curves are given as a function of air mass flow rate in Figure 4-12 and as a function of face velocity in Figure 4-13. These pressure drop curves were made using an inclined manometer connected to the inlet and exit air pressures. The R744 gas cooler has a lower air side pressure drop than that of the R134a condenser. This data can now be used to help create and validate air side pressure drop models for the condenser and gas cooler. The characteristics of the R134a condenser and R744 gas cooler are discussed in more detail in Appendix A.

The refrigerant side pressure drops in the R134a condenser and R744 gas cooler are given as a function of mass flow rate in Figure 4-15. The R744 microchannel gas cooler has more than twice the pressure drop as the R134a tube and louvered fin condenser on the refrigerant side.

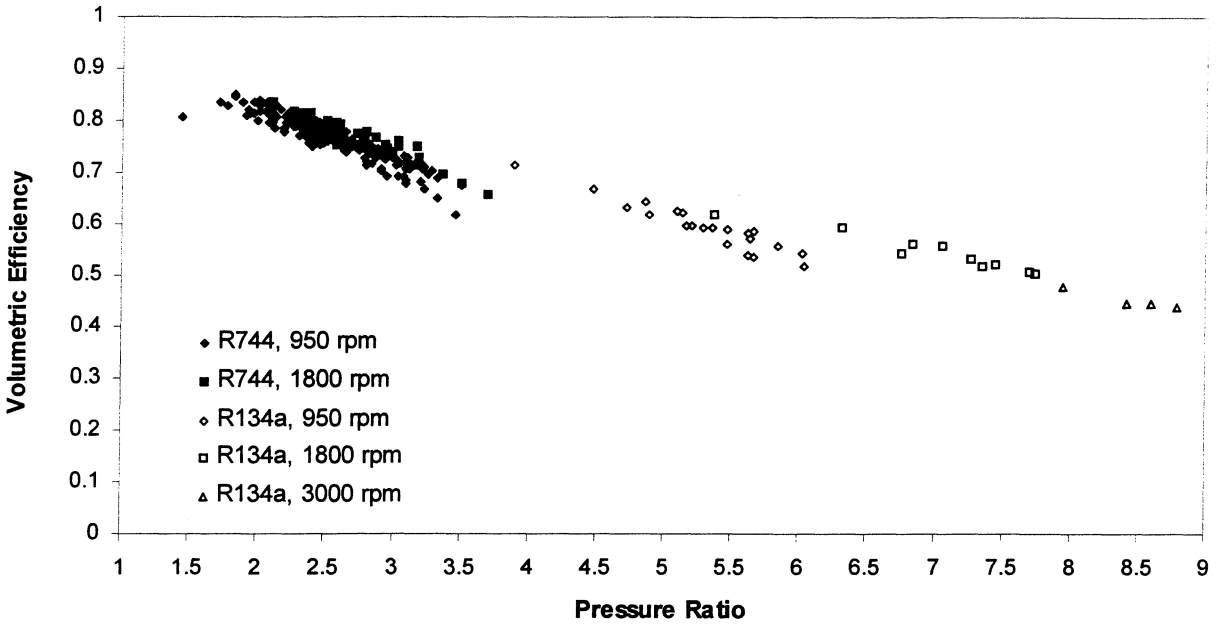

Figure 4-1 Volumetric efficiency for R134a compressor and R744 compressor 2 and 3 used in mobile air conditioning system.

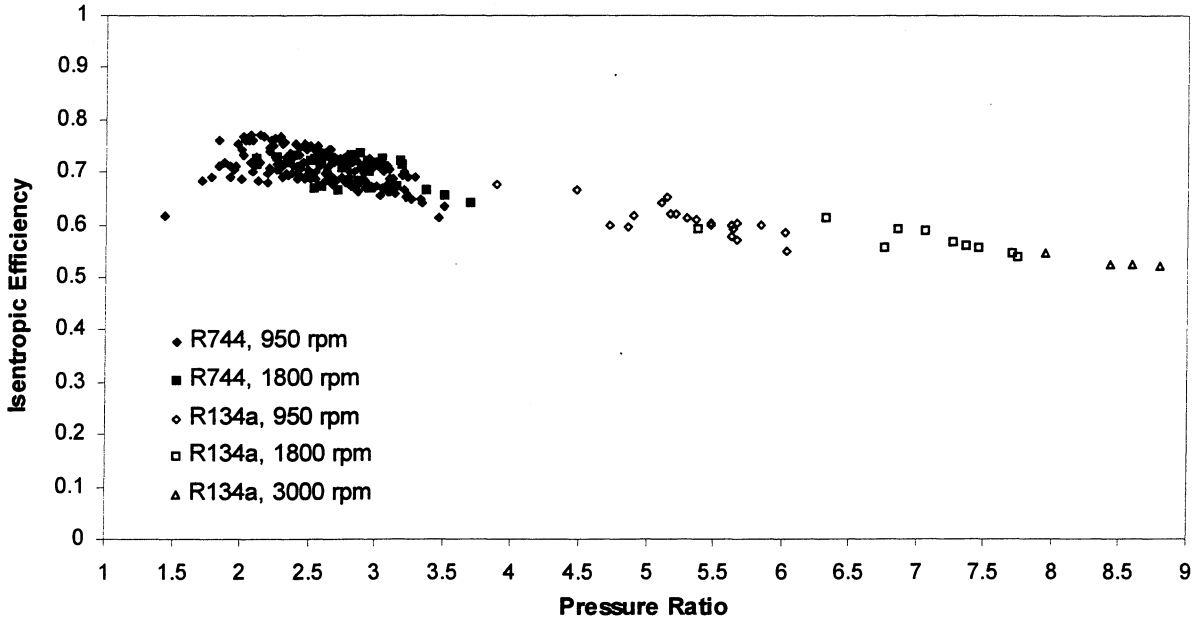

Figure 4-2 Isentropic efficiency for R134a compressor and R744 compressor 2 and 3 used in mobile air conditioning system.

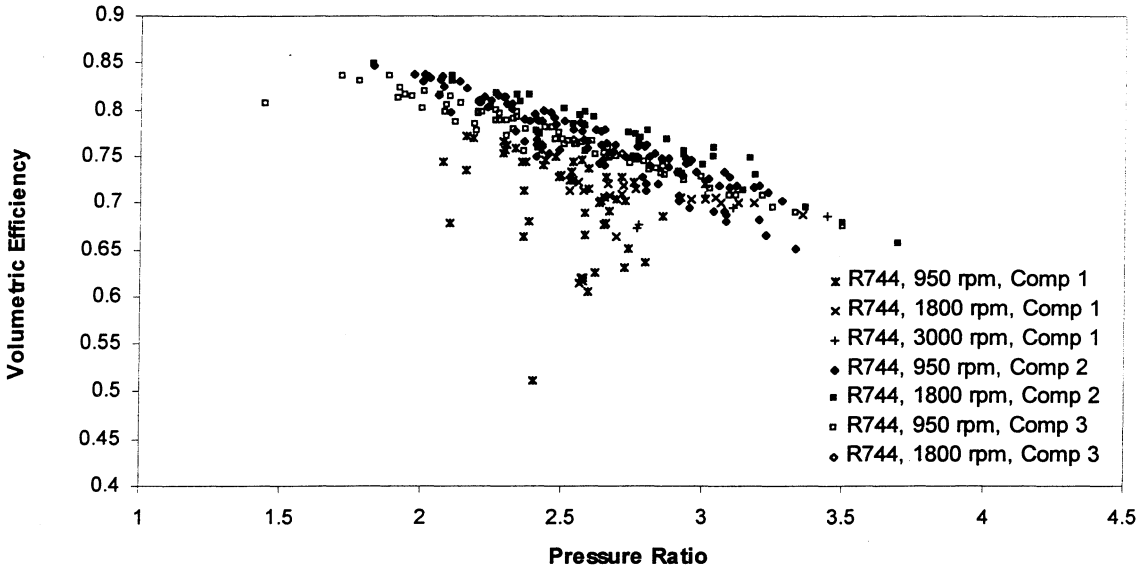

Figure 4-3 Volumetric efficiency for all R744 compressors (1, 2, and 3) used in mobile air conditioning system.

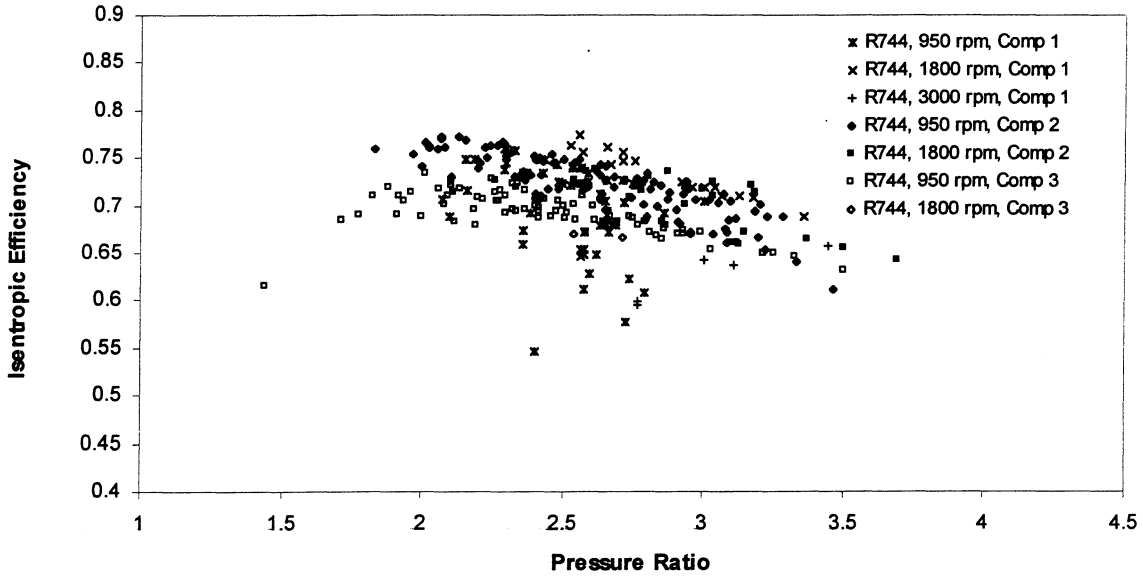

Figure 4-4 Isentropic efficiency for all R744 compressors (1, 2, and 3) used in mobile air conditioning system.

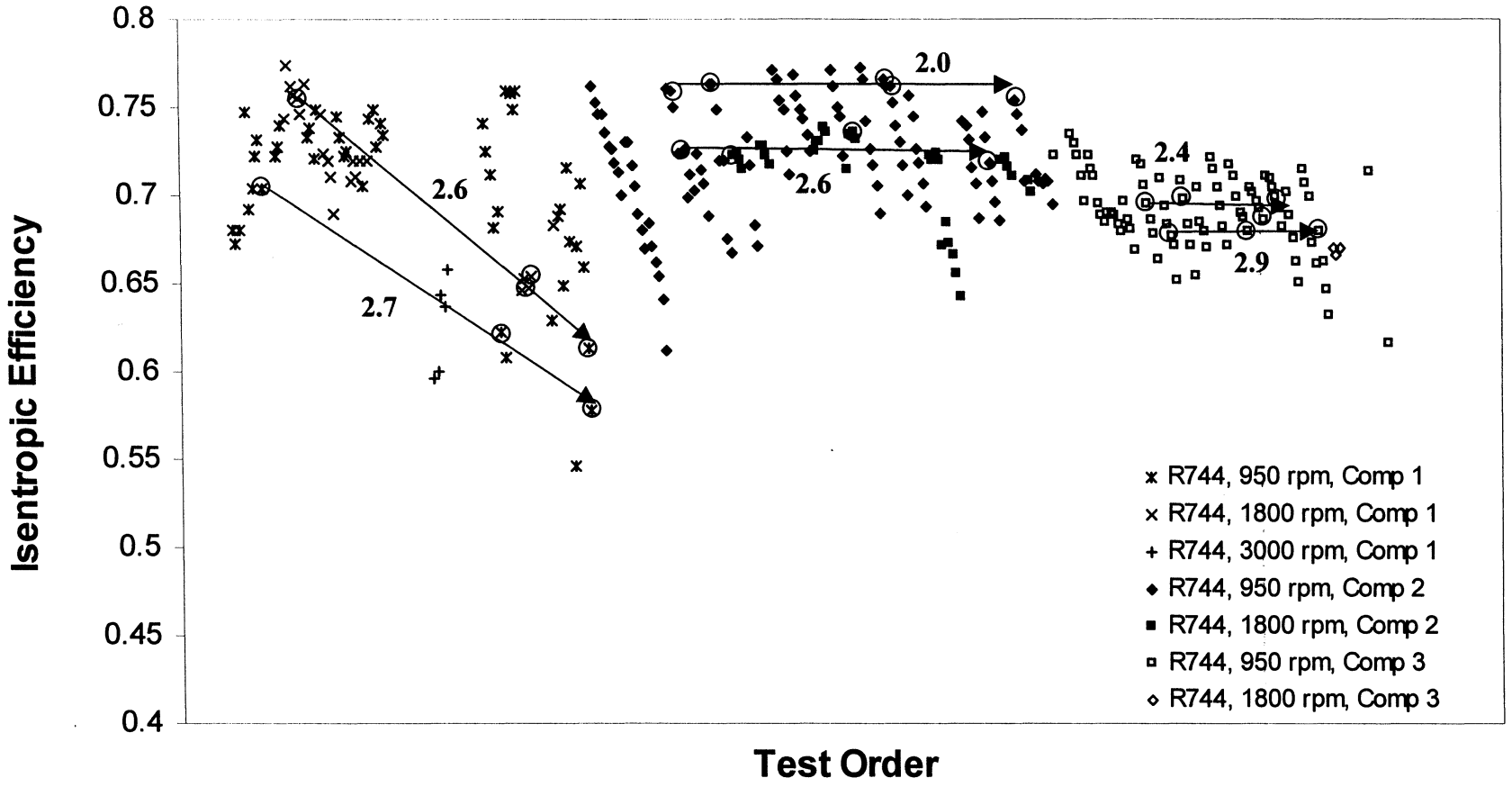

Figure 4-5 Compressor isentropic efficiency plotted in order of data taken. Circled points indicate same pressure ratio points near arrow. Number is pressure ratio.

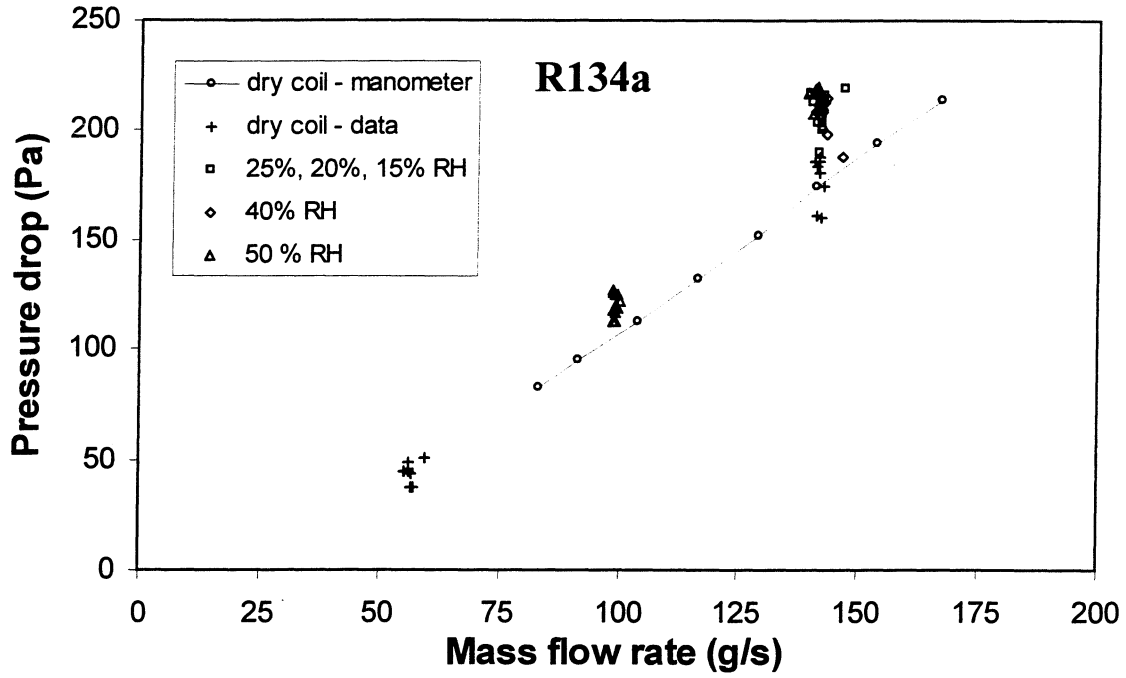

Figure 4-6 Air side pressure drop as a function of air mass flow rate for R134a evaporator showing different air inlet relative humidity. All data are for continuous runs.

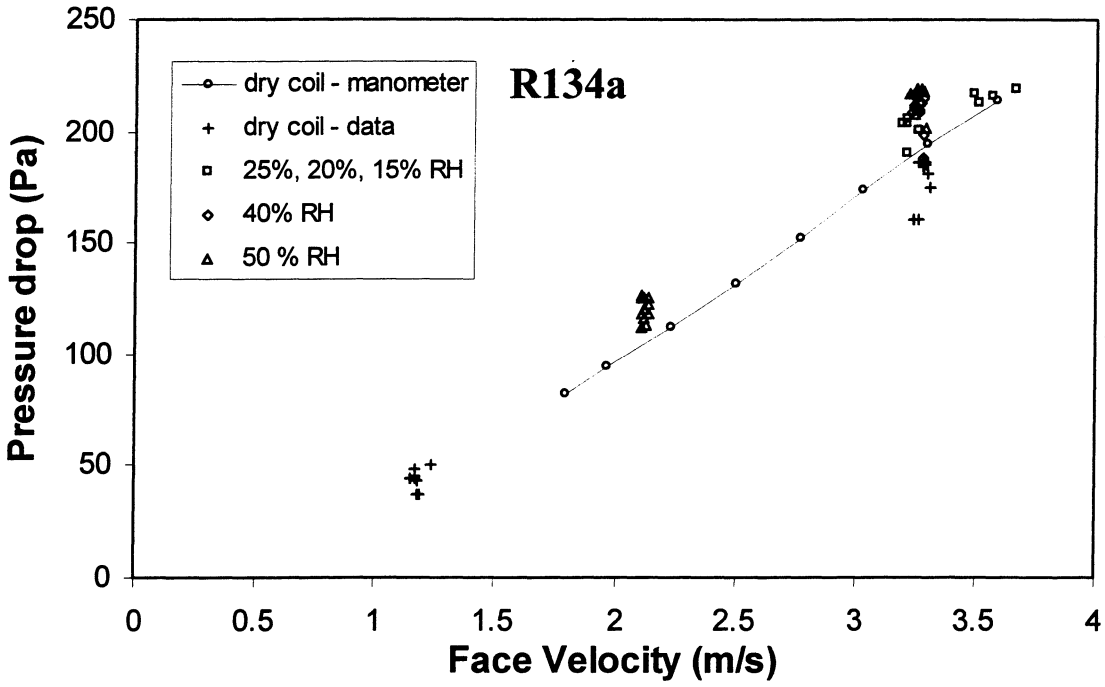

Figure 4-7 Air side pressure drop as a function of face velocity for R134a evaporator showing different air inlet relative humidity. All data are for continuous runs.

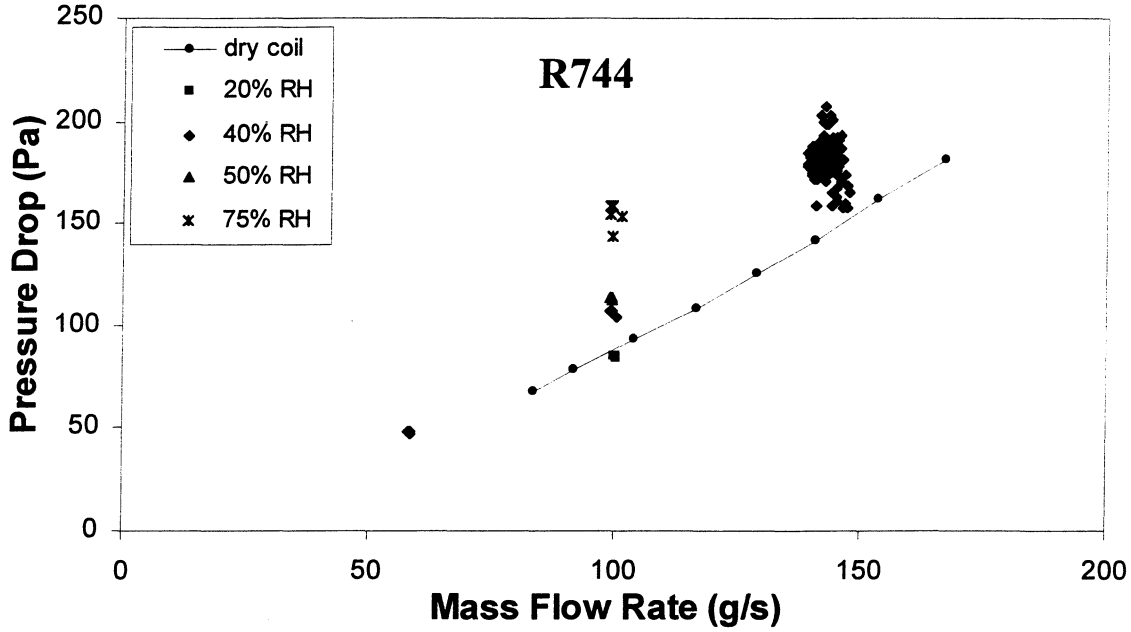

Figure 4-8 Air side pressure drop as a function of air mass flow rate for R744 evaporator showing different air inlet relative humidity. All data are for continuous runs.

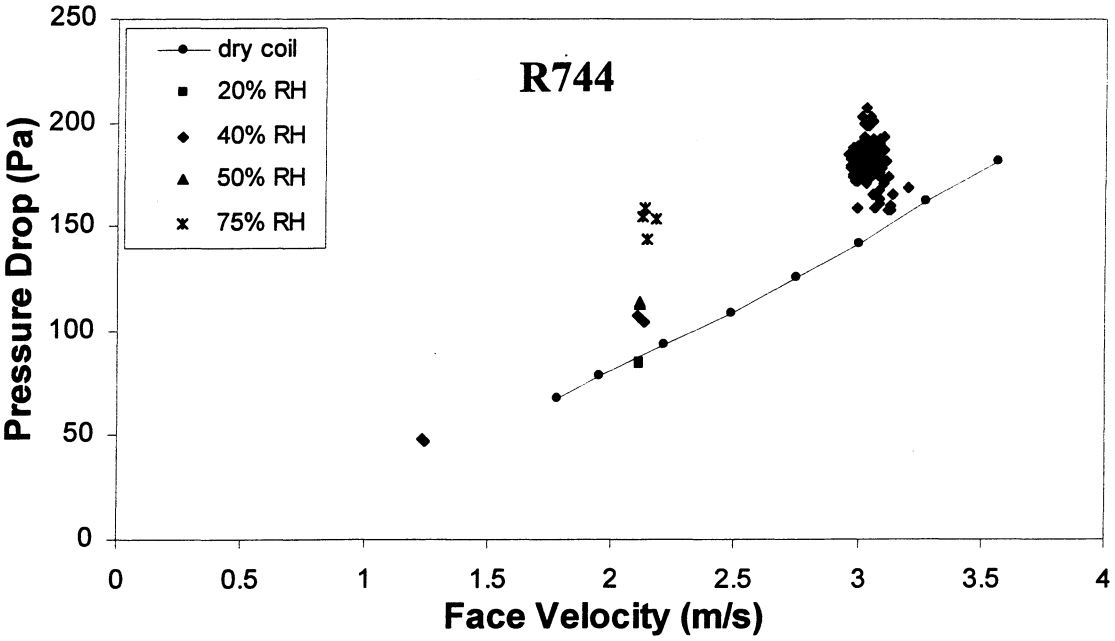

Figure 4-9 Air side pressure drop as a function of face velocity for R744 evaporators showing different air inlet relative humidity. All data are for continuous runs.

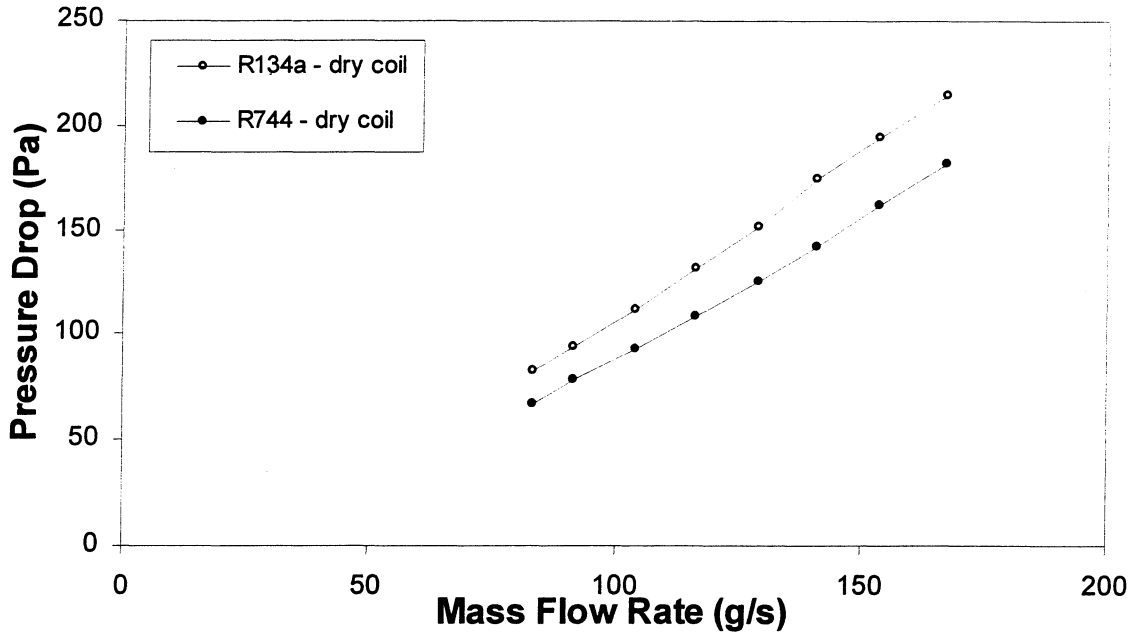

Figure 4-10 Air side pressure drop as function of air mass flow rate for R134a and R744 evaporators. Both curves are dry coil measurement.

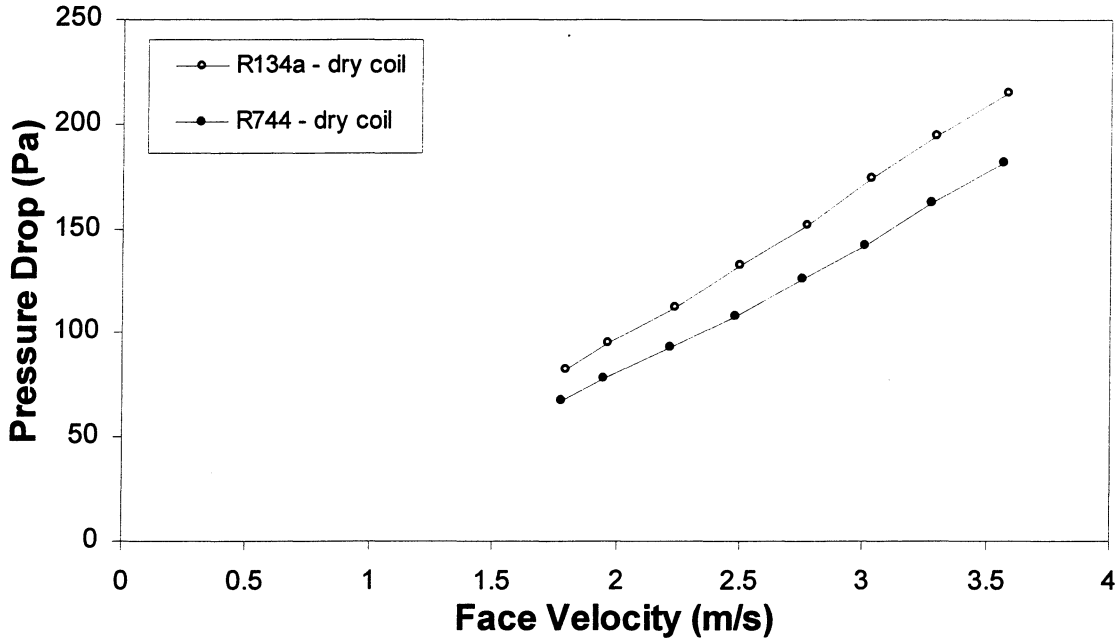

Figure 4-11 Air side pressure drop as function of face velocity for R134a and R744 evaporators. Both curves are dry coil measurement.

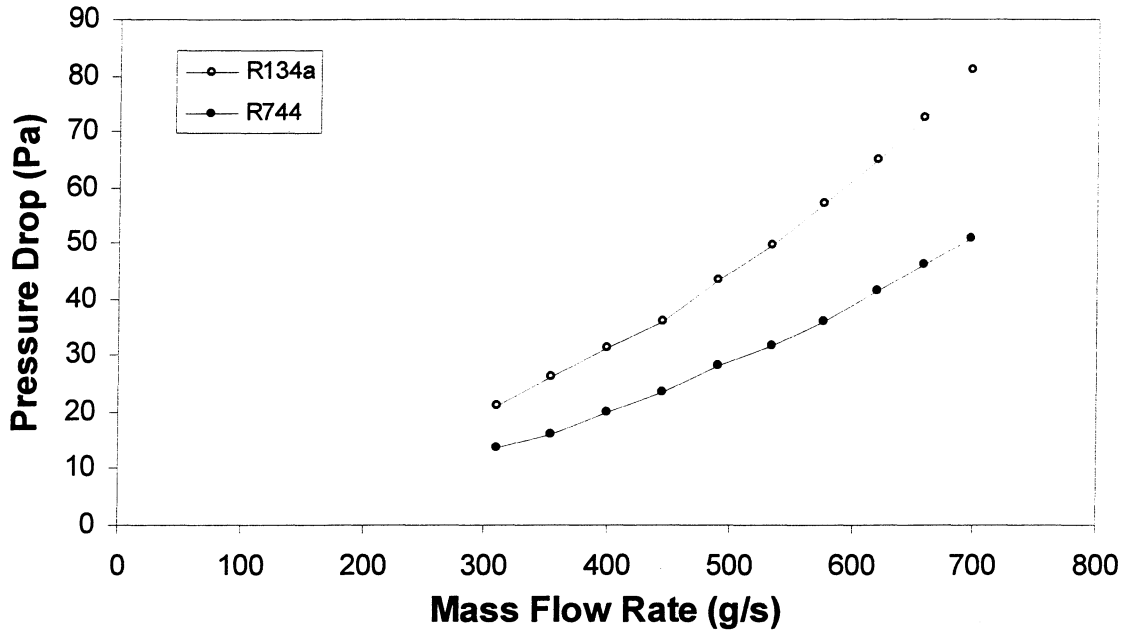

Figure 4-12 Air side pressure drop as a function of air mass flow rate for R134a condenser and R744 gas cooler.

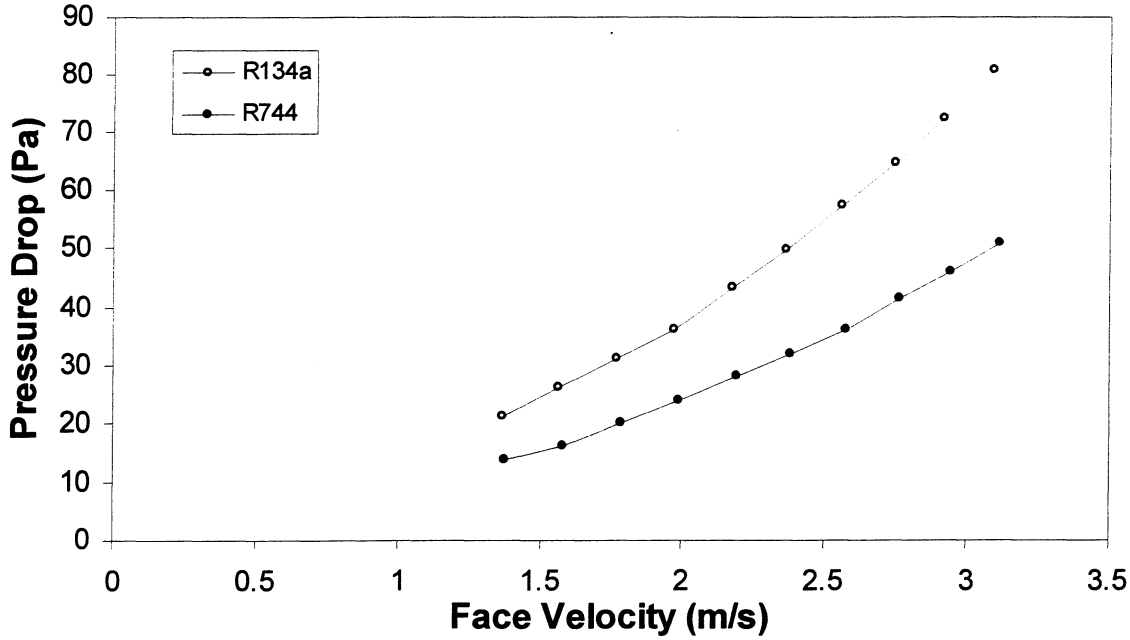

Figure 4-13 Air side pressure drop as a function of face velocity for R134a condenser and R744 gas cooler.

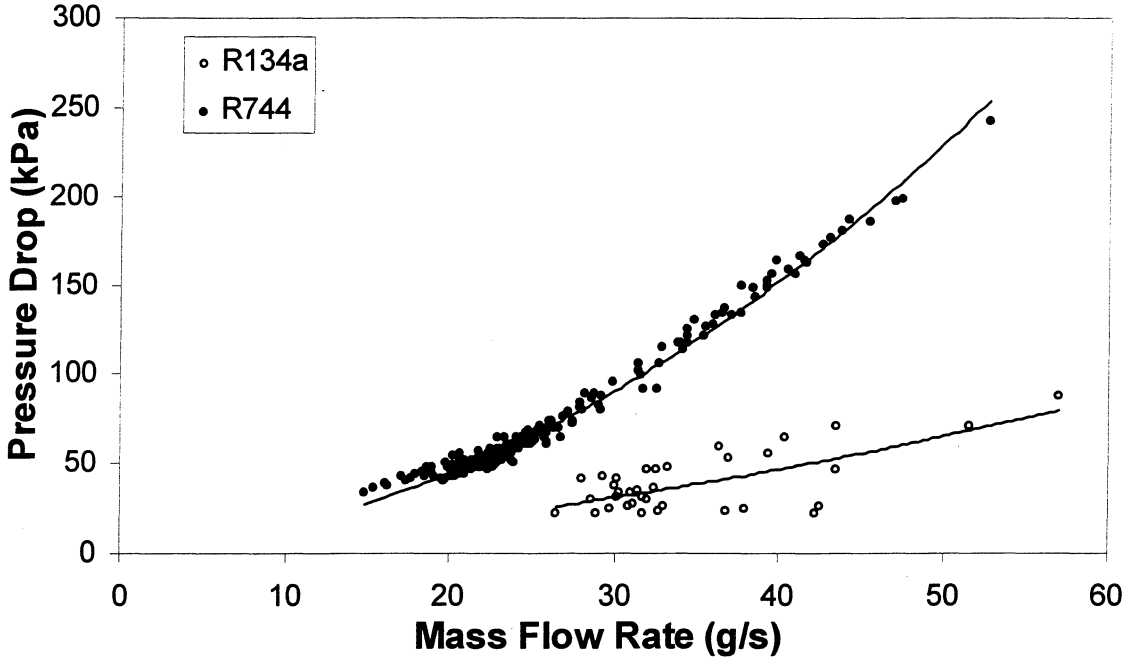

Figure 4-14 Refrigerant side pressure drop as a function of refrigerant mass flow rate for R134a and R744 evaporators.

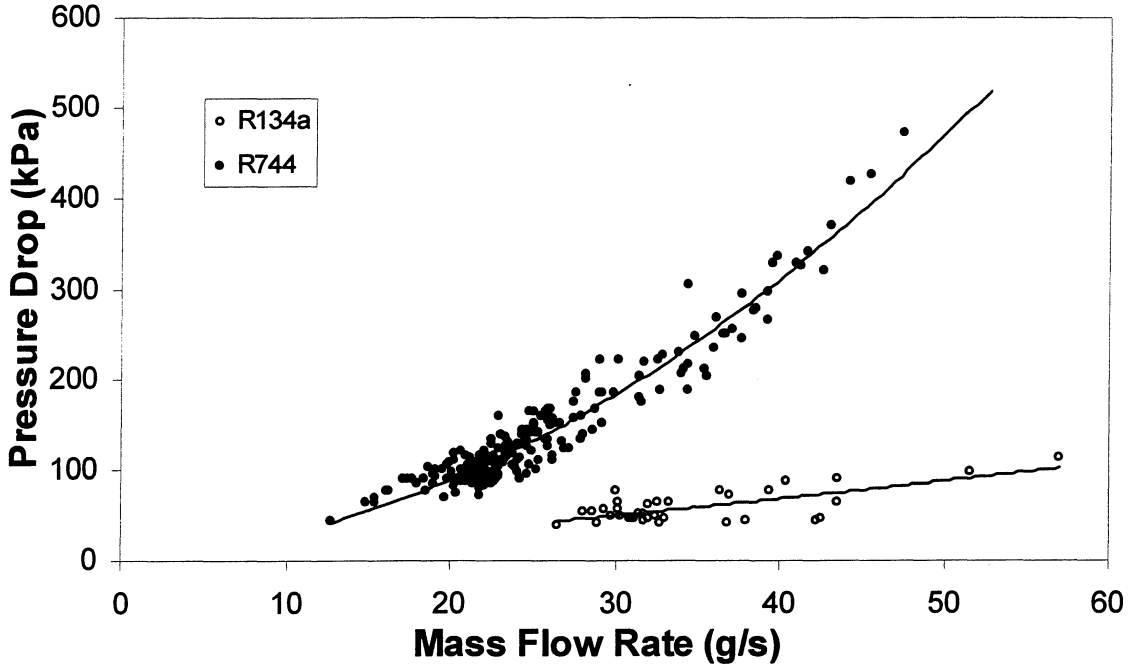

Figure 4-15 Refrigerant side pressure drop as a function of refrigerant mass flow rate for R134a condenser and R744 gas cooler.

4.6 System Charging

For R134a, the system charge is an important factor in the performance of the system. The charging procedures were to add refrigerant until the evaporator outlet refrigerant temperature is less than (as a result of pressure drop) or equal to the evaporator inlet temperature. The charge procedure was conducted at the M0 test condition and that charge was used for all tests. This method is not a direct method to find out the optimum COP or capacity, but is widely used in practice.

The influence of the refrigerant charge was determined before conducting the tests. Table 4-1 shows four different charging conditions (A, B, C and D) and three test conditions (Wh, M1 and M0). The only difference between the three test conditions is relative humidity. All tests are at intermediate compressor speed (1800 rpm), condenser and evaporator inlet temperatures are 43.3°C, and the air flow rates over the condenser and the evaporator are 26.9 m^3/min and 7.08 m^3/min respectively.

The dry coil test was performed first (charges A and B). At charge A, the temperatures at the evaporator inlet (6.3°C) and outlet (8.7°C) were apart. Refrigerant was added and the result shows very close temperatures across the evaporator. At this charge (charge B), the test condition was changed from dry coil test (Wh) to 50% relative humidity condition (M1). As the humidity increased, the temperature difference increased over 10°C (charge C1). To reduce the temperature difference, the system was charged a little more (charge C2) and it showed only 1°C difference.

The typical suggested charging conditions by manufacturers are at 40% relative humidity. Due to this, the relative humidity was changed from 50% to 40% and the results show that the evaporator outlet temperature is a little lower than the inlet temperature. The performance of the system, which is properly charged at the condition suggested by the manufacturer (charge D1), shows that capacity is approximately 6.0 kW and COP is 1.84. When the system is overcharged (charge D2), the capacity and COP are reduced.

For the R744 system, the charging conditions were not as strict. The system only needed to have enough charge to maintain some liquid R744 in the accumulator. All data was taken in this manner. A check of the system performance was made with three levels (low, middle, and high)

of R744 in the accumulator and is shown in Table 4-2. The three levels were checked using test condition i19. The system performance was unchanged for the three tests. This check shows that so long as the accumulator has some liquid R744 in it, the correct charge is being used.

Table 4-1 Charge influence on R134a performance.

Test		Wh*	Wh*	M1	M1	M0	M0
Test Cond.	T_{cai} (°C)	43.4	42.9	43.1	43.2	43.1	43.1
	T_{eai} (°C)	43.7	43.7	43.1	43.2	43.1	43.2
	RH_e (%)	10.45	10.57	50.22	50.16	40.14	40.11
RESULTS	W_{comp} (kW)	2.51	2.53	3.38	3.50	3.25	3.34
	DG_{gs} (g/s)	0	0	1.59	1.61	1.22	1.14
	T_{evap} (°C)	2.9	3.1	13.3	14.9	12.4	13.3
	T_{eri} (°C)	6.3	6.6	16.8	18.5	16.3	17.2
	T_{ero} (°C)	8.7	6.5	26.1	19.5	15.6	15.0
	P_{ero} (kPa)	227	229	363	388	350	363
	P_{cro} (kPa)	2001	2005	2481	2558	2419	2535
	Q_{evap} (kW)	4.10	4.11	6.60	6.72	5.99	5.68
	COP	1.63	1.62	1.96	1.92	1.84	1.70
Charge		A	B	C1	C2	D1	D2

* Dry coil test – test condition not shown in Test Matrix

Table 4-2 Comparison of R744 performance with various charges.

Test		I19	I19	I19
Test Cond.	T_{cai} (°C)	32.1	32.2	32.3
	T_{eai} (°C)	26.6	26.6	26.7
	RH_e (%)	40.75	40.61	40.47
RESULTS	W_{comp} (kW)	1.36	1.36	1.36
	DG_{gs} (g/s)	0.37	0.36	0.37
	T_{evap} (°C)	6.2	6.1	6.1
	T_{eri} (°C)	7.7	7.9	8.0
	T_{ero} (°C)	7.3	7.4	7.6
	P_{ero} (kPa)	4033	4025	4028
	P_{cro} (kPa)	9516	9513	9536
	Q_{evap} (kW)	3.28	3.27	3.30
	COP	2.41	2.41	2.43
Charge		Low	Middle	High

4.7 Oil Concentration

Both the R134a and R744 systems have oil circulating in the system with the refrigerant. For the R134a, the oil was circulated throughout the entire loop along with the refrigerant. The amount of oil in the system was approximately 200 ml of a Pyrol PAG RL244 Low viscosity oil inserted directly into the compressor. The oil concentration was then measured for the R134a system using an impactor. For the impactor, a sample of the refrigerant/oil mixture was taken from the liquid line exiting the condenser. The sampling apparatus was a short tube with valves at the inlet and exit. The sampling apparatus was weighed with and without the sample to find the sample refrigerant/oil mass. The refrigerant/oil sample was then passed through the impactor, which separated out the oil from the refrigerant. The initial and final weights of each stage of the impactor gives the total weight of the oil for the sample. Great care was taken during the weighing to ensure not to contaminate the different stages of the impactor. Oil concentration measurements are given in Table 4-3 and range from 1.0% to 2.1%.

For the R744 system, the amount of oil in the system was approximately 100 ml. A majority of the oil was bypassed from the exit of the compressor back to the inlet of the compressor using an oil separator. The bypassed oil's flow rate (m_{oil}) was measured using a ±0.1% Coriolis type mass flow meter. This oil flow rate was varied at two different conditions to see the effect of oil bypass shown in Table 4-4. The data shows no significant change in COP or capacity (Q_{evap}).

Some oil does get past the separator and circulates through the primary refrigerant loop. This oil is collected in the bottom of the suction accumulator before being returned back into the refrigerant flow through the bottom of the accumulator. Another ±0.1% Coriolis type mass flow meter is used to measure this oil flow rate (ml). The effect of this oil flow rate is shown in Table 4-5. This flow rate is used to find the oil concentration in the circulating refrigerant/oil mixture.

4.8 Test Repeatability

Table 4-6 shows the repeatability of the R134a experiments. All R134a test results were taken between January 25, 1998 and March 6, 1998. A repeatability check was made four times in that test period. The data are taken at the same condition to check the possible leakage of the refrigerant and to verify the test results through repeatability of the tests.

Table 4-7 shows the repeatability of the R744 experiments. All R744 test results were taken between April 20, 1998 and February 4, 1999. A repeatability check was made 4 times over a 4-month period. The data are taken at the same condition to verify the test results through repeatability of the tests..

Table 4-3 Measured oil concentrations for R134a system.

Test point		M1	-	H3	I9	-
Set Condition	T_{cai} (°C)	43.3	21.1	43.3	43.3	43.3
	T_{eai} (°C)	43.3	43.3	32.2	32.2	43.3
	RH_e (%)	50	Dry	40	40	Dry
	AFR_c (m^3/min)	26.90	22.65	35.40	26.90	26.90
	AFR_e (m^3/min)	7.08	7.08	7.08	7.08	7.08
Oil Concentration (%)		1.4	2.1	1.3	1.0	1.4

Table 4-4 Influence of oil flow rate through the bypass line from the oil separator in R744 system.

Test Condition	I13	I13	I13	M3	M3
m_{oil} (g/s)	0.40	1.49	2.57	0.96	3.61
COP	1.678	1.675	1.663	1.593	1.569
Q_{evap} (kW)	2.32	2.30	2.28	4.67	4.64
η_m (%)	0.674	0.704	0.703	0.707	0.720
η_v (%)	0.714	0.741	0.757	0.743	0.762
T_{rcpi} (°C)	29.0	34.0	38.1	31.9	38.6
T_{rcpo} (°C)	113.5	112.0	111.0	124.1	123.9

Table 4-5 Influence of oil flow rate from suction accumulator in R744 system.

Test Condition	I19	I19
ml (g/s)	0.54	3.05
System Oil Concentration (%)	2.4	12.8
COP	2.444	2.350
Q_{evap} (kW)	3.33	3.20
η_m (%)	0.71	0.71
η_v (%)	0.76	0.76
T_{rcpi} (°C)	27.6	21.5
T_{rcpo} (°C)	97.9	91.2

Table 4-6 Repeatability of the R134a experimental results in time.

Repeat Date		Jan.23,98	Feb.05,98	Feb.13,98	Mar.06,98
Test point		M0	M0	M0	M0
Measured conditions	T_{cai} (°C)	43.1	43.9	43.5	43.5
	T_{eai} (°C)	43.1	43.6	43.3	43.3
	RH_e (%)	40.0	39.6	40.8	40.2
	AFR_c (m^3/min)	26.95	26.94	26.92	27.02
	AFR_e (m^3/min)	7.11	7.088	7.11	7.255
Results	W_{comp} (kW)	3.249	3.325	3.298	3.287
	DG_{gs} (kg/s)	1.222	1.182	1.223	1.210
	DT_{sub} (°C)	19.4	19.5	19.9	19.5
	DT_{sup} (°C)	3.2	3.8	3.6	4.9
	P_{cro} (kPa)	2419	2473	2453	2434
	P_{ero} (kPa)	350.1	359.6	360.8	358.0
	Q_{evap} (kW)	5.988	6.022	6.147	6.169
	COP	1.843	1.811	1.864	1.877

Table 4-7 Repeatability of the R744 experimental results in time.

Repeat Date		Aug.05,98	Sep.09,98	Oct.29,98	Nov.16,98
Test point		I19	I19	I19	I19
Measured conditions	T_{cai} (°C)	32.3	32.2	32.9	32.5
	T_{eai} (°C)	26.5	26.7	27.0	26.5
	RH_e (%)	40.4	40.3	39.2	40.6
	AFR_c (m^3/min)	27.10	27.10	27.22	26.92
	AFR_e (m^3/min)	8.50	8.54	8.69	8.53
Results	W_{comp} (kW)	1.346	1.325	1.352	1.384
	DG_{gs} (kg/s)	0.353	0.351	0.327	0.370
	DT_{sup} (°C)	1.6	1.6	1.6	1.5
	P_{cro} (kPa)	9436	9438	9398	9429
	P_{ero} (kPa)	3978	4003	4078	4004
	Q_{evap} (kW)	3.242	3.285	3.243	3.329
	COP	2.408	2.479	2.399	2.405

Table 4-8 R134a system and compressor data.

Test Point	Date	COP	Q_{evap} (kW)	Q_{lat} (kW)	Q_{sens} (kW)	W_{comp} (kW)	Q_{cond} (kW)	M_r (g/s)	η_m (-)	η_v (-)	P_{ratio} (-)	P_{rcpi} (kPa)	T_{rcpi} (°C)	T_{rcpo} (°C)	Fc (in-lb)	Vc (rpm)
i1	2/12/98	2	4.517	2.562	1.96	2.255	6.702	43.6	0.653	0.62	5.14	598	28.1	104	201	950.5
i2	2/12/98	1.58	2.871	1.128	1.74	1.817	4.564	32.5	0.6	0.56	5.85	453	14	91.6	161	952.1
i3	2/12/98	1.5	2.614	0.618	2	1.743	4.253	31	0.585	0.54	6.02	427	11.5	89.7	155	952.4
i4	2/12/98	1.4	2.351	-0.03	2.38	1.677	3.886	31.8	0.548	0.52	6.04	415	9.11	87.6	149	951.8
i5	2/5/98	1.8	3.108	1.269	1.84	1.724	4.447	31.5	0.599	0.56	5.47	443	13.3	88.1	153	950.8
i6	2/4/98	1.76	2.939	0.76	2.18	1.675	4.89	30.4	0.577	0.54	5.62	421	11.2	85.4	149	952.4
i7	2/5/98	1.6	2.54	-0.13	2.67	1.583	3.639	32	0.57	0.53	5.67	402	7.52	82.9	141	950.8
i8	1/26/98	2.4	3.708	1.681	2.03	1.545	5.421	30.2	0.594	0.64	4.86	403	12.6	80.2	137	952.1
i9	1/26/98	2.27	3.365	1.092	2.27	1.484	5.076	28.6	0.616	0.62	4.89	389	9.48	77.2	132	951.9
i10	1/27/98	2.05	2.824	0.135	2.69	1.379	4.533	30.9	0.64	0.63	5.1	351	4.17	71.9	123	951.2
i11	1/28/98	2.03	2.773	0.767	2.01	1.364	4.096	33	0.619	0.6	5.21	344	4.18	72.7	121	951.9
i12	2/11/98	2.04	2.749	1.192	1.56	1.346	4.034	42.5	0.613	0.59	5.29	336	3.38	71.9	120	952.1
i13	2/4/98	1.9	2.475	0.742	1.73	1.301	3.606	38.1	0.603	0.59	5.47	317	1.13	69.4	116	952.2
i14	2/11/98	1.75	2.187	0.194	1.99	1.25	3.491	29	0.603	0.59	5.66	298	-0.5	68.5	111	951.9
i15	2/25/98	2.11	2.873	1.543	1.33	1.361	4.304	31.2	0.619	0.6	5.17	344	4.43	72.2	121	952
i16	1/26/98	1.79	2.32	0.709	1.61	1.295	3.932	36.9	0.61	0.59	5.36	322	1.09	70	115	951.7
i17	1/26/98	1.75	2.208	0.408	1.8	1.264	3.696	32.8	0.599	0.58	5.63	302	0	69	112	951.9
i18	1/26/98	1.72	2.113	-0.03	2.14	1.228	3.412	26.5	0.591	0.57	5.63	297	-1.1	68.2	109	951.9
i19	1/28/98	2.58	3.142	0.953	2.19	1.216	4.491	29.8	0.664	0.67	4.48	322	2.51	63.7	108	951.3
i20	1/29/98	2.33	2.678	0.905	1.77	1.147	4.064	42.2	0.597	0.63	4.72	291	-1.6	60.3	102	952.3
i25	1/28/98	3.22	3.464	1.096	2.37	1.076	5.014	31.8	0.676	0.71	3.89	297	1.63	58	95.7	950.6
m1	1/25/98	1.92	6.721	4.242	2.48	3.502	10.24	51.7	0.613	0.59	6.32	420	20.5	109	164	1800
m2	1/25/98	1.64	4.567	2.351	2.22	2.789	7.586	39.4	0.591	0.56	6.85	323	6.57	96.1	131	1800
m3	1/25/98	1.58	4.194	1.66	2.53	2.659	7.118	37	0.588	0.56	7.06	302	3.76	93.5	125	1800
m4	1/26/98	1.47	3.627	0.634	2.99	2.475	6.407	33.3	0.567	0.53	7.27	277	-0.1	89.9	116	1801
m5	1/28/98	1.44	3.48	1.133	2.35	2.419	5.675	32	0.555	0.52	7.45	268	-0.7	90.4	114	1801
m6	2/25/98	1.5	3.622	1.976	1.65	2.411	6.144	32.6	0.558	0.52	7.36	271	0.65	91.4	113	1802
m7	1/26/98	1.31	2.981	1.08	1.9	2.282	5.761	29.4	0.544	0.51	7.7	249	-4.2	86.9	107	1801
m8	1/26/98	1.27	2.817	0.704	2.11	2.214	5.278	28.1	0.54	0.5	7.75	243	-5.4	85.7	104	1801
m10	1/28/98	1.68	3.754	1.226	2.53	2.232	6.481	30.2	0.555	0.54	6.76	247	-0.2	87	105	1801
m17	2/10/98	2.31	4.8	2.539	2.26	2.082	7.172	30	0.592	0.62	5.38	244	6.98	84.9	97.7	1801
h1	3/6/98	1.53	7.756	4.946	2.81	5.067	12.57	57	0.546	0.48	7.95	351	20.5	129	142	3006
h2	3/5/98	1.27	5.036	2.509	2.53	3.982	9.354	43.6	0.524	0.45	8.59	270	6.28	115	112	3006
h3	3/5/98	1.55	5.805	2.919	2.89	3.738	8.827	40.5	0.525	0.45	8.42	256	4.44	112	105	3008
h4	3/5/98	1.24	4.295	0.891	3.41	3.455	7.837	36.4	0.522	0.44	8.8	233	0.63	109	97.1	3008

Table 4-9 R134a evaporator data.

Test Point	Q_{evap} (kW)	Rh_e (-)	T_{eai} (°C)	AFR_{Evap} (scfm)	m_{ea} (kg/s)	DG_{kgs} (kg/s)	DP_{er} (kPa)	DT_{sup} (°C)	P_{eri} (kPa)	P_{ero} (kPa)	T_{eao} (°C)	T_{eri} (°C)	T_{ero} (°C)	T_{ori} (°C)	T_{evap} (°C)
i1	4.517	0.511	43.71	250.5	0.1419	9.73E-04	46.3	3.85	679	633	30.2	25.5	27.14	73.41	23.29
i2	2.871	0.482	32.55	250.8	0.142	4.11E-04	35.9	1.24	514	478	19.8	16.3	15.51	71.15	14.28
i3	2.614	0.384	32.51	249.5	0.1413	2.25E-04	33.5	1.23	481	448	18.2	14.4	13.53	71.2	12.3
i4	2.351	0.279	32.55	251.8	0.1426	9.41E-06	31.1	0.81	458	427	16.9	12.6	11.65	70.76	10.84
i5	3.108	0.486	32.4	248.6	0.1408	4.77E-04	34.5	1.75	491	457	19.2	15.1	14.66	65.62	12.91
i6	2.939	0.4	32.43	254.2	0.144	3.07E-04	33.3	1.65	469	436	18.1	13.8	13.11	65.36	11.46
i7	2.54	0.259	32.38	255.5	0.1447	2.51E-06	30	1.07	437	407	16	11.4	10.5	64.72	9.433
i8	3.708	0.492	32.55	252.9	0.1433	6.41E-04	31.5	1.79	458	426	18.6	12.6	12.61	53.43	10.82
i9	3.365	0.399	32.49	254.7	0.1442	4.21E-04	29.7	1.49	432	403	17.1	10.9	10.58	52.91	9.096
i10	2.824	0.244	31.8	255.4	0.1446	7.49E-05	26.3	1.42	385	359	14.3	7.82	7.166	51.35	5.748
i11	2.773	0.395	26.98	251.7	0.1426	2.73E-04	26.2	0.9	381	354	12.3	6.84	6.261	52.16	5.359
i12	2.749	0.486	27.04	175.8	0.0996	4.37E-04	25.6	1.11	373	348	18.2	6.57	5.91	51.91	4.797
i13	2.475	0.396	26.81	175.8	0.0995	2.80E-04	23.9	1.32	352	328	18.8	5.15	4.461	51.06	3.139
i14	2.187	0.253	26.95	178.7	0.1012	6.88E-05	22.2	1.02	332	310	17.2	3.22	2.586	50.84	1.563
i15	2.873	0.681	21.49	255.4	0.1447	5.58E-04	27.1	1.1	387	360	11.2	7.48	6.934	51.27	5.832
i16	2.32	0.495	21.31	252.7	0.1431	2.56E-04	23.8	1.28	350	326	9.62	4.93	4.261	51.26	2.986
i17	2.208	0.4	21.33	254	0.1439	1.49E-04	22.8	1.42	334	312	8.67	3.77	3.122	50.96	1.704
i18	2.113	0.277	21.39	256.7	0.1454	1.24E-05	21.9	1.01	324	302	7.61	2.47	1.832	50.9	0.8199
i19	3.142	0.396	27	251.3	0.1423	3.46E-04	24.1	0.98	355	331	11.1	4.64	4.391	39.71	3.411
i20	2.678	0.401	26.85	175.5	0.0994	3.43E-04	21.3	1.2	319	298	9.04	2.08	1.668	38.51	0.4667
i25	3.464	0.399	26.9	252.4	0.143	4.16E-04	21.4	1.3	330	308	10.4	2.45	2.713	27.3	1.41
m1	6.721	0.502	43.22	251.7	0.1426	1.61E-03	70.3	4.61	558	487	26	18.5	19.51	57.86	14.91
m2	4.567	0.498	32.52	251.9	0.1427	8.75E-04	55.7	1.94	426	370	16.3	10.4	8.564	54.16	6.629
m3	4.194	0.397	32.54	252.1	0.1428	6.31E-04	52.5	1.82	400	347	14.9	8.52	6.59	53.33	4.766
m4	3.627	0.253	32.52	252	0.1427	2.54E-04	47.3	1.82	359	312	12.2	5.55	3.537	52.35	1.717
m5	3.48	0.397	26.9	251.3	0.1423	4.01E-04	45.8	1.42	347	301	9.41	4.1	2.191	52.88	0.7667
m6	3.622	0.683	21.47	254.8	0.1443	7.19E-04	46.7	1.99	354	307	8.82	5.1	3.268	52.09	1.28
m7	2.981	0.496	21.28	252.5	0.143	3.96E-04	42.6	2.07	320	277	7.46	2.64	0.561	52.16	-1.505
m8	2.817	0.396	21.35	253.3	0.1435	2.61E-04	40.7	1.81	309	268	6.46	1.41	-0.65	52.06	-2.457
m10	3.754	0.399	26.82	251	0.1422	4.73E-04	41	2.07	324	283	9.36	2.69	1.08	42.77	-0.9929
m17	4.8	0.507	32.01	175	0.0991	9.33E-04	36.7	2.85	313	276	7.51	1.12	1.206	28.84	-1.64
h1	7.756	0.499	43.24	253.3	0.1435	1.88E-03	88.1	7.65	530	441	24.1	16.7	19.51	56.63	11.86
h2	5.036	0.488	32.44	248.9	0.141	9.51E-04	70.3	2.5	410	340	14.5	9.31	6.651	53.79	4.149
h3	5.805	0.402	32.39	248.9	0.141	1.13E-03	64.7	2.51	379	314	12.7	7.06	4.455	50.84	1.943
h4	4.295	0.249	32.46	251.6	0.1425	3.72E-04	59	2.14	345	286	10	4.2	1.502	50.53	-0.6361

Table 4-10 R134a condenser data.

Test Point	Q_{cond} (kW)	T_{cai} (°C)	AFR_{Cond} (scfm)	m_{ca} (kg/s)	DP_{cr} (kPa)	DT_{sub} (°C)	P_{cro} kPa	T_{cao} (°C)	T_{cri} (°C)	T_{cro} (°C)	T_{cond} (°C)
i1	6.702	59.78	813	0.4605	64.52	12.6	3010	74.76	103	73.79	86.39
i2	4.564	60.12	814.7	0.4614	49.06	7.981	2598	70.29	90.38	71.44	79.42
i3	4.253	59.99	814.3	0.4612	46.45	6.674	2524	69.5	88.4	71.39	78.06
i4	3.886	59.98	815.3	0.4617	44.01	6.241	2461	68.77	86.19	70.66	76.9
i5	4.447	55.17	811.4	0.4595	50.58	8.952	2370	66.02	87.22	66.21	75.17
i6	4.89	55.16	814.2	0.4611	48.77	8.252	2317	65.28	84.56	65.87	74.12
i7	3.639	55.05	811.8	0.4598	45.37	7.319	2234	64.41	82.17	65.15	72.47
i8	5.421	43.57	803.2	0.4549	56.67	11.85	1901	56.04	79.31	53.44	65.3
i9	5.076	43.48	803.7	0.4552	53.31	11.1	1850	55.26	76.46	53.01	64.11
i10	4.533	42.9	802.4	0.4544	47.41	9.894	1743	53.57	71.63	51.66	61.55
i11	4.096	43.63	799.1	0.4526	46.42	9.951	1745	53.28	71.57	51.63	61.58
i12	4.034	43.96	794.8	0.4501	45.14	9.598	1732	53.3	71	51.68	61.28
i13	3.606	43.39	801.9	0.4542	43.28	8.858	1689	52.82	69	51.34	60.2
i14	3.491	43.91	798	0.452	40.35	8.342	1647	51.94	67.9	50.8	59.14
i15	4.304	43.15	802.8	0.4546	47.14	10.11	1733	53.17	71.42	51.18	61.3
i16	3.932	43.35	803.1	0.4548	42.28	8.755	1684	52.66	69.47	51.32	60.07
i17	3.696	43.38	803.4	0.455	40.39	8.451	1657	52.14	68.43	50.94	59.39
i18	3.412	43.66	803.6	0.4551	38.66	8.08	1633	51.66	67.5	50.7	58.78
i19	4.491	32.76	793.9	0.4496	49.57	13.23	1392	42.98	62.89	38.97	52.2
i20	4.064	32.47	799.4	0.4527	42.98	11.99	1333	42.13	60.16	38.46	50.45
i25	5.014	21.12	792.5	0.4488	51.66	16.62	1104	32.95	57.39	26.48	43.1
m1	10.24	43.23	961.9	0.5447	97.36	21.22	2558	62.45	107.5	57.47	78.68
m2	7.586	43.25	951.9	0.5391	77.13	16.63	2135	57.63	94.55	53.8	70.43
m3	7.118	43.16	950.6	0.5383	72.71	15.71	2059	56.73	92.09	53.09	68.8
m4	6.407	43.15	951.7	0.539	65.36	14.15	1949	55.4	88.72	52.23	66.38
m5	5.675	43.89	948.6	0.5372	62.81	13.76	1932	54.69	89.08	52.24	66
m6	6.144	43.25	955.4	0.5411	63.73	13.87	1928	55.16	90.07	52.04	65.91
m7	5.761	43.45	951.1	0.5387	57.7	11.93	1859	54.59	86.27	52.38	64.32
m8	5.278	43.66	951.5	0.5389	55.07	11.39	1824	53.99	84.95	52.11	63.5
m10	6.481	34.6	946.3	0.5359	65.61	15.12	1606	47.24	86.28	42.95	58.07
m17	7.172	20.93	938.7	0.5316	76.85	19.57	1238	34.64	83.82	27.96	47.53
h1	12.57	43.5	1249	0.7076	112.9	24.48	2677	61.47	127.7	56.34	80.82
h2	9.354	43.79	1252	0.7088	90.33	18.57	2233	57.37	113	53.89	72.45
h3	8.827	42.1	1253	0.7098	86.52	17.91	2067	54.65	110.7	51.06	68.97
h4	7.837	42.67	1253	0.7096	78	16.17	1968	53.69	107.8	50.64	66.81

Table 4-11 R134a system and compressor cycling data.

Test Point	COP	Q_{evap} (kW)	Q_{lat} (kW)	Q_{sens} (kW)	W_{comp} (kW)	Q_{cond} (kW)	P_{ratio} (-)	P_{rcpi} (kPa)	T_{rcpi} (°C)	T_{rcpo} (°C)	Fc (in-lb)	Vc (rpm)	Cycle Time	% ON
l21	2.784	1.677	0.898	0.778	0.602	2.390	4.02	295	-1.11	52.32	54	950	41.9	0.61
l22	2.007	1.427	0.508	0.919	0.711	2.201	3.74	301	-1.63	48.94	64	950	34.8	0.72
l23	1.897	1.219	0.275	0.945	0.643	1.979	3.73	304	-0.97	47.32	58	950	27.6	0.65
i24	1.798	0.969	-0.050	1.019	0.539	1.579	3.52	308	-0.72	44.70	49	950	24.8	0.57
i26	2.998	1.781	0.603	1.178	0.594	2.132	3.08	297	-0.24	42.87	53	950	29.9	0.63
i27	2.443	1.131	0.582	0.549	0.463	1.436	2.69	308	0.57	38.82	41	950	36.4	0.52
i28	2.671	1.141	0.207	0.934	0.427	1.703	2.60	318	0.02	36.52	39	950	27.7	0.48
i29	3.517	1.696	0.520	1.176	0.482	2.136	2.58	304	0.08	36.44	43	950	27.6	0.55
i30	3.109	1.132	0.186	0.947	0.364	1.772	2.31	313	0.18	32.56	33	950	30.5	0.43
i31	1.905	1.290	0.358	0.932	0.677	2.190	3.80	299	-1.40	50.59	60	950	55.7	0.43
i32	2.257	1.260	0.331	0.929	0.558	1.959	3.20	306	-0.41	44.72	50	950	46.2	0.67
i33	1.876	0.812	0.147	0.665	0.433	1.344	2.92	311	0.19	39.79	39	950	35.5	0.58
m9	1.335	2.049	-0.037	2.085	1.535	3.707	5.90	283	-1.85	76.50	73	1800	14.3	0.76
m11	1.777	3.444	1.544	1.900	1.938	5.661	5.94	255	-1.61	79.51	91	1800	57.4	0.92
m12	1.820	2.548	0.834	1.714	1.400	4.179	4.68	288	-1.14	68.79	67	1800	20.7	0.67
m13	1.801	2.213	0.204	2.008	1.229	3.615	4.39	288	-1.29	65.68	58	1800	19.7	0.64
m14	1.394	1.523	0.025	1.498	1.093	3.194	4.21	292	-0.16	62.17	53	1800	14.3	0.56
m15	2.154	2.779	0.891	1.887	1.290	4.325	4.14	284	-0.71	64.67	61	1800	20.9	0.63
m16	2.045	1.869	0.388	1.481	0.914	2.939	3.37	309	0.60	55.48	44	1800	14.6	0.49
m18	2.444	3.756	1.576	2.180	1.537	5.537	4.33	272	3.47	71.55	73	1800	24.9	0.78
m19	2.386	2.995	0.551	2.443	1.255	4.419	3.64	289	0.68	62.78	60	1800	18.7	0.61
m20	2.223	1.697	0.582	1.115	0.763	2.209	2.96	306	1.78	51.13	37	1800	14.8	0.44
m21	2.308	1.735	0.991	0.744	0.752	1.846	2.78	311	2.53	50.10	36	1800	14.8	0.46
m22	2.129	1.338	0.467	0.871	0.629	2.040	2.75	311	2.35	46.82	31	1800	14.3	0.41
m23	2.035	1.107	0.172	0.935	0.544	1.664	2.64	312	2.39	42.42	27	1800	14.0	0.33
m24	1.896	0.943	-0.042	0.985	0.498	1.495	2.63	312	2.02	40.91	24	1800	13.0	0.33
m25	2.557	1.659	0.522	1.137	0.649	2.302	2.47	315	2.66	46.14	32	1800	15.1	0.39
m26	2.375	1.051	0.210	0.841	0.443	1.467	2.25	317	2.84	38.90	22	1800	14.1	0.29
h5	1.154	3.636	1.885	1.751	3.151	6.915	8.23	237	-0.07	104.4	89	3000	52.1	0.94
h6	1.240	2.936	1.085	1.851	2.367	5.117	6.41	270	-0.65	91.67	67	3000	14.4	0.73
h7	1.123	2.351	0.389	1.962	2.094	4.400	6.02	278	-0.06	88.72	59	3000	12.7	0.65
h8	1.111	2.068	-0.065	2.133	1.862	3.657	5.75	282	0.71	84.68	52	3000	11.3	0.58
h9	1.461	3.750	2.150	1.600	2.567	6.720	6.10	253	0.24	91.03	72	3000	19.0	0.79
h10	1.472	3.019	1.310	1.709	2.051	5.136	5.05	276	0.39	83.25	58	3000	14.0	0.64
h11	0.954	1.687	-0.110	1.797	1.768	4.362	4.69	285	0.59	80.02	50	3000	13.1	0.57
h12	1.425	1.930	-0.061	1.991	1.354	3.196	3.98	303	1.89	72.44	38	3000	11.6	0.44
h14	1.609	1.275	0.494	0.782	0.792	3.508	2.65	316	3.06	55.53	22	3000	12.0	0.29
h15	1.518	1.085	0.264	0.821	0.715	3.252	2.52	324	2.85	51.91	20	3000	11.4	0.27
h16	1.352	0.878	-0.007	0.885	0.649	2.646	2.47	327	3.08	50.02	18	3000	11.2	0.25

Table 4-12 R134a evaporator cycling data.

Test Point	Q_{evap} (kW)	Rh_e (-)	T_{eai} (°C)	AFR_{Evap} (scfm)	m_{ea} (kg/s)	DG_{kgs} (kg/s)	DP_{er} (kPa)	P_{eri} (kPa)	P_{ero} (kPa)	T_{eao} (°C)	T_{eri} (°C)	T_{ero} (°C)	T_{ori} (°C)	T_{evap} (°C)
i21	1.677	0.682	20.91	103	0.0582	3.26E-04	14.7	314	300	6.06	1.12	1.65	36.23	0.60
i22	1.427	0.489	20.87	104	0.0586	1.92E-04	13.2	314	301	5.13	0.79	0.76	35.28	0.75
i23	1.219	0.395	21.26	106	0.0599	1.14E-04	11.7	316	305	6.33	1.27	1.34	35.98	1.07
i24	0.969	0.250	21.45	106	0.0598	0.00E+0	9.5	317	308	6.24	1.38	1.50	35.40	1.36
i26	1.781	0.400	27.14	103	0.0582	2.34E-04	11.9	313	301	7.42	0.00	1.26	25.05	0.77
i27	1.131	0.691	20.94	107	0.0606	2.04E-04	10.3	315	305	10.36	-0.02	0.91	23.39	1.11
i28	1.141	0.395	21.34	104	0.0591	9.42E-05	8.6	325	316	6.99	1.04	1.86	23.59	2.11
i29	1.696	0.386	27.10	102	0.0579	2.14E-04	10.4	319	309	8.32	0.00	1.57	18.70	1.47
i30	1.132	0.396	21.27	104	0.0591	8.17E-05	8.1	322	314	6.34	0.44	1.75	17.59	1.94
i31	1.290	0.401	26.91	106	0.0600	1.43E-04	12.8	311	298	12.06	0.87	2.38	36.15	0.44
i32	1.260	0.400	26.89	104	0.0590	1.40E-04	11.0	317	306	12.47	1.16	1.53	29.80	1.19
i33	0.812	0.409	20.82	104	0.0589	5.41E-05	9.2	319	310	9.45	1.41	1.35	28.83	1.58
m9	2.049	0.288	21.27	252	0.1425	0.00E+0	26.1	329	303	7.30	3.24	2.37	50.08	0.95
m11	3.444	0.482	26.94	175	0.0990	5.67E-04	35.5	319	283	6.69	2.05	0.89	39.78	-0.91
m12	2.548	0.401	26.86	176	0.0994	3.18E-04	24.4	333	309	9.74	3.20	2.63	37.82	1.47
m13	2.213	0.249	26.94	177	0.1004	7.51E-05	20.3	330	310	6.98	2.66	2.14	37.16	1.54
m14	1.523	0.389	21.12	179	0.1014	0.00E+0	18.5	327	309	6.04	2.44	2.55	35.39	1.43
m15	2.779	0.393	26.82	178	0.1005	3.38E-04	23.0	335	312	8.08	2.99	2.72	30.63	1.73
m16	1.869	0.385	21.23	179	0.1015	1.38E-04	14.5	335	320	6.21	2.28	2.81	29.14	2.48
m18	3.756	0.399	32.05	176	0.0995	5.80E-04	27.4	337	310	9.24	2.79	3.51	26.91	1.54
m19	2.995	0.255	32.02	177	0.1004	2.21E-04	22.2	332	310	8.47	2.15	2.41	24.49	1.54
m20	1.697	0.400	27.15	103	0.0581	2.22E-04	12.6	328	315	8.12	1.11	2.14	23.70	2.03
m21	1.735	0.680	21.06	105	0.0596	3.54E-04	11.6	334	322	6.44	0.90	2.21	23.05	2.65
m22	1.338	0.484	21.52	107	0.0608	1.74E-04	11.1	331	319	6.91	1.53	2.64	22.68	2.40
m23	1.107	0.391	21.36	104	0.0590	7.92E-05	9.6	332	322	6.84	1.71	2.83	22.81	2.67
m24	0.943	0.274	21.41	105	0.0597	6.23E-06	9.3	332	322	6.99	1.48	2.58	22.21	2.65
m25	1.659	0.393	27.09	102	0.0579	2.13E-04	10.8	333	322	8.83	1.03	2.70	17.58	2.65
m26	1.051	0.377	21.57	105	0.0593	7.73E-05	9.0	332	323	7.23	1.08	2.83	17.26	2.73
h5	3.636	0.669	21.41	249	0.1408	6.88E-04	53.6	342	288	7.85	3.85	1.68	49.83	-0.46
h6	2.936	0.485	21.42	251	0.1420	3.98E-04	36.7	343	306	7.87	4.10	2.65	47.82	1.23
h7	2.351	0.393	21.39	254	0.1437	1.48E-04	31.1	344	313	7.83	4.00	2.86	48.35	1.79
h8	2.068	0.302	21.38	255	0.1442	0.00E+0	26.6	341	315	7.64	3.94	3.06	48.19	1.99
h9	3.750	0.647	26.90	173	0.0982	7.81E-04	42.2	347	305	8.60	4.25	2.91	38.25	1.07
h10	3.019	0.484	26.93	174	0.0984	4.86E-04	30.2	344	314	8.94	4.03	3.27	36.76	1.90
h11	1.687	0.389	26.95	175	0.0988	0.0E+0	25.8	340	315	8.25	3.64	3.17	36.81	1.97
h12	1.930	0.217	26.93	176	0.0996	0.00E+0	18.4	341	323	8.37	3.41	3.40	35.38	2.71
h14	1.275	0.492	21.44	100	0.0568	1.89E-04	10.7	341	330	7.77	2.46	3.50	22.61	3.35
h15	1.085	0.390	21.44	101	0.0572	1.06E-04	9.9	342	332	7.68	2.34	3.43	22.56	3.51
h16	0.878	0.284	21.54	102	0.0575	0.00E+0	9.3	337	328	6.55	1.70	2.94	22.85	3.15

Table 4-13 R134a condenser cycling data.

Test Point	Q_{cond} (kW)	T_{cai} (°C)	AFR_{Cond} (scfm)	m_{ca} (kg/s)	DP_{cr} (kPa)	P_{cro} kPa	T_{cao} (°C)	T_{cri} (°C)	T_{cro} (°C)	T_{cond} (°C)
i21	2.39	32.22	801	0.4534	41.34	1146	0.07	52.14	35.88	44.51
i22	2.201	31.91	800	0.4529	31.15	1094	0.07	49.19	36.10	42.74
i23	1.979	32.36	799	0.4525	37.35	1096	0.07	47.33	36.66	42.82
i24	1.579	32.59	799	0.4524	35.85	1049	36.29	44.53	35.67	41.17
i26	2.132	21.84	796	0.4508	34.12	882	26.43	41.57	23.57	34.78
i27	1.436	21.15	796	0.4506	42.03	787	24.02	38.54	22.62	30.72
i28	1.703	21.34	798	0.4516	36.74	789	25.22	36.50	23.30	30.83
i29	2.136	16.22	811	0.4593	38.65	746	20.75	35.62	17.32	28.85
i30	1.772	15.69	796	0.4509	37.32	683	19.74	32.82	17.13	25.86
i31	2.19	32.33	801	0.4537	33.07	1101	37.44	51.43	36.59	43.00
i32	1.959	26.78	798	0.4517	39.22	943	31.28	45.62	30.09	37.19
i33	1.344	26.88	799	0.4526	33.38	875	29.83	40.59	29.27	34.49
m9	3.707	43.93	952	0.5394	54.36	1617	51.08	76.35	50.93	58.35
m11	5.661	32.46	937	0.5306	65.94	1448	43.48	78.90	39.52	53.81
m12	4.179	32.45	948	0.5367	62.70	1284	40.64	68.90	38.22	48.97
m13	3.615	32.45	940	0.5321	62.49	1204	39.50	65.61	37.63	46.44
m14	3.194	32.30	948	0.5367	70.58	1158	38.71	62.29	36.92	44.91
m15	4.325	26.73	949	0.5372	62.66	1112	35.08	64.87	31.19	43.36
m16	2.939	26.83	952	0.5391	59.87	983	32.58	55.63	29.87	38.71
m18	5.537	21.09	940	0.5325	73.13	1105	31.71	70.72	25.87	43.14
m19	4.419	20.94	943	0.5339	66.45	985	29.45	62.36	23.98	38.79
m20	2.209	21.73	944	0.5344	60.26	844	25.76	49.73	22.26	33.20
m21	1.846	21.17	950	0.5378	56.40	809	24.66	48.53	21.13	31.69
m22	2.04	21.16	943	0.5339	56.64	799	24.71	46.15	22.03	31.26
m23	1.664	21.42	946	0.5355	46.97	778	24.63	41.83	22.40	30.33
m24	1.495	20.97	946	0.5360	56.81	765	23.65	40.12	21.81	29.74
m25	2.302	16.06	948	0.5366	56.25	721	20.29	44.86	16.33	27.71
m26	1.467	16.15	949	0.5371	43.04	670	18.89	37.80	16.26	25.21
h5	6.915	42.50	1252	0.7091	74.83	1873	52.38	103.50	49.67	64.64
h6	5.117	42.51	1254	0.7101	73.54	1655	49.79	91.50	47.98	59.34
h7	4.4	43.22	1255	0.7109	73.47	1600	49.46	88.63	48.26	57.92
h8	3.657	43.48	1223	0.6925	75.51	1542	48.85	84.57	48.39	56.37
h9	6.72	32.25	1227	0.6949	78.51	1466	42.02	90.95	38.04	54.31
h10	5.136	32.52	1228	0.6954	77.32	1317	40.09	83.28	36.46	49.97
h11	4.362	32.96	1214	0.6877	76.26	1259	39.37	80.12	36.18	48.19
h12	3.196	32.60	1235	0.6995	70.46	1134	37.28	72.36	34.93	44.11
h14	3.508	21.65	1226	0.6946	63.00	774	24.18	54.92	21.65	30.13
h15	3.252	21.68	1229	0.6959	58.02	758	23.64	51.03	21.47	29.43
h16	2.646	22.14	1229	0.6958	60.91	746	22.55	48.74	21.00	28.84

Table 4-14 Summary of all R744 data taken listed by test condition.

Point	Date	Comp	# runs	IHX	Flow	Pressure Range		COP Range		Rows	
						Low	High	Low	High	Start	Finish
i06	04/20/98	1	5	1.5	CC	13.1	13.6	1.52	1.56	5	9
i06	04/21/98	1	3	1.5	CC	13.2	13.3	1.53	1.57	13	15
i06	04/22/98	1	3	1.5	CC	13.2	13.4	1.53	1.56	16	18
i06	05/06/98	1	7	1.5	CC	12.9	13.8	1.42	1.58	92	98
i06	07/02/98	1	4	1.5	CC	11.2	13.8	1.13	1.28	121	124
i09	11/02/98	3	3	1.5	CC	9.5	11.6	1.71	1.89	277	279
i11	04/24/98	1	4	1.5	CC	10.1	10.8	1.93	1.99	48	51
i11	05/27/98	1	1	0.0	NA	10.6	10.6	1.49	1.49	102	102
i11	06/30/98	1	3	1.5	CC	9.7	11.3	1.63	1.76	114	116
i11	07/02/98	1	4	1.5	CC	9.8	11.2	1.61	1.68	117	120
i11	07/13/98	2	6	1.0	CF	9.5	11.5	1.67	1.81	125	130
i11	07/16/98	2	4	0.0	NA	10.8	12.0	1.40	1.51	131	134
i11	07/21/98	2	6	0.0	NA	12.0	14.6	1.41	1.54	142	147
i11	07/22/98	2	4	1.0	CF	11.5	13.5	1.60	1.78	157	160
i11	07/24/98	2	4	1.5	CF	11.0	12.6	1.72	1.85	172	175
i11	07/28/98	2	6	2.0	CF	9.6	12.0	1.77	1.90	186	191
i11	07/30/98	2	7	2.0	CC	9.6	13.2	1.68	1.83	206	212
i11	07/31/98	2	6	1.0	CC	10.2	13.0	1.66	1.80	221	226
i11	08/05/98	2	6	1.5	CC	9.8	12.7	1.61	1.73	243	248
i11	11/09/98	3	4	1.5	CC	10.0	12.0	1.63	1.70	308	311
i12	11/03/98	3	4	1.5	CC	10.0	11.5	1.63	1.68	286	289
i13	04/20/98	1	4	1.5	CC	10.4	10.8	1.86	1.90	1	4
i13	04/21/98	1	3	1.5	CC	10.5	10.8	1.84	1.86	10	12
i13	04/23/98	1	3	1.5	CC	10.3	10.9	1.78	1.83	29	31
i13	06/25/98	1	1	1.5	CC	10.7	10.7	1.62	1.62	111	111
i13	06/26/98	1	1	1.5	CC	10.8	10.8	1.65	1.65	112	112
i13	11/18/98	3	5	1.5	CC	9.6	12.0	1.46	1.59	340	344
i13R	04/23/98	1	3	1.5	CC	10.7	10.7	1.87	1.90	26	28
i16	04/27/98	1	3	1.5	CC	10.0	10.5	1.28	1.84	56	58
i17	04/27/98	1	4	1.5	CC	9.6	10.2	1.72	1.76	59	62
i17	11/18/98	3	5	1.5	CC	10.0	12.0	1.49	1.56	335	339
i19	04/24/98	1	4	1.5	CC	9.0	10.1	2.62	2.75	39	42
i19	05/27/98	1	3	0.0	NA	9.6	10.0	2.35	2.38	99	101
i19	07/21/98	2	7	0.0	NA	9.0	12.0	1.99	2.30	135	141
i19	07/22/98	2	9	1.0	CF	8.2	12.0	2.08	2.44	148	156
i19	07/23/98	2	7	1.5	CF	8.6	12.6	1.99	2.60	161	167
i19	07/28/98	2	6	2.0	CF	8.6	12.0	2.09	2.61	180	185
i19	07/29/98	2	5	2.0	CC	8.6	11.1	2.25	2.63	197	201
i19	07/31/98	2	8	1.0	CC	8.6	12.5	2.00	2.55	213	220
i19	08/05/98	2	6	1.5	CC	8.5	12.2	1.96	2.41	237	242
i19	09/09/98	2	4	1.5	CC	8.5	9.6	2.32	2.48	253	256
i19	09/11/98	2	6	1.5	CC	9.7	10.5	2.30	2.44	259	264
i19	10/16/98	3	1	1.5	CC	10.1	10.1	2.38	2.38	265	265
i19	10/21/98	3	4	1.5	CC	8.5	10.1	2.39	2.49	270	273
i19	10/29/98	3	3	1.5	CC	9.5	9.6	2.39	2.48	274	276
i19	11/16/98	3	6	1.5	CC	8.4	10.5	2.19	2.41	329	334

Table 4-14 Continuation of summary of all R744 data taken listed by test condition.

Point	Date	Comp	# runs	IHX	Flow	Pressure Range		COP Range		Rows	
						Low	High	Low	High	Start	Finish
i20	04/23/98	1	6	1.5	CC	8.5	10.3	2.34	2.57	20	25
i20R	04/23/98	1	1	1.5	CC	8.7	8.7	2.90	2.90	19	19
i34	11/03/98	3	7	1.5	CC	9.5	12.6	1.62	1.82	290	296
i35	11/05/98	3	5	1.5	CC	9.7	11.7	1.56	1.63	303	307
i36	11/04/98	3	6	1.5	CC	9.1	11.2	1.36	1.46	297	302
i36R	01/30/99	3	4	1.5	CC	8.1	8.7	1.22	1.81	357	360
i39	11/02/98	3	6	1.5	CC	10.8	13.0	2.19	2.31	280	285
i40	11/11/98	3	6	1.5	CC	9.5	11.7	1.63	1.79	318	323
i41	11/09/98	3	6	1.5	CC	9.5	12.0	1.58	1.73	312	317
i42	11/18/98	3	4	1.5	CC	10.0	11.6	1.26	1.36	345	348
i44	11/16/98	3	5	1.5	CC	8.0	9.3	2.76	2.90	324	328
i44sub	10/21/98	3	4	1.5	CC	7.1	8.3	2.10	2.91	266	269
i44sub	02/01/99	3	5	1.5	CC	7.3	9.0	1.81	3.04	361	365
m03	04/23/98	1	5	1.5	CC	11.1	11.6	1.54	1.58	32	36
m03	06/19/98	1	4	1.5	CC	11.2	11.3	1.45	1.48	103	106
m03	06/26/98	1	1	1.5	CC	11.5	11.5	1.46	1.46	113	113
m03R	04/29/98	1	5	1.5	CC	11.0	11.6	1.92	1.99	63	67
m05	04/24/98	1	5	1.5	CC	10.5	12.0	1.40	1.46	43	47
m05	07/23/98	2	4	1.0	CF	10.2	11.5	1.21	1.37	168	171
m05	07/24/98	2	4	1.5	CF	9.4	10.9	1.08	1.41	176	179
m05	07/28/98	2	5	2.0	CF	9.0	10.6	1.05	1.43	192	196
m05	07/29/98	2	4	2.0	CC	9.1	10.5	0.97	1.35	202	205
m05	08/03/98	2	4	1.0	CC	10.1	11.5	1.18	1.39	227	230
m05	08/04/98	2	6	0.0	NA	10.9	13.6	0.90	1.19	231	236
m05	08/06/98	2	4	1.5	CC	9.6	11.1	1.10	1.35	249	252
m05	09/09/98	2	2	1.5	CC	10.6	11.0	1.25	1.30	257	258
m05	11/19/98	3	3	1.5	CC	10.0	11.0	1.14	1.25	349	351
m08	04/27/98	1	4	1.5	CC	10.1	10.6	1.28	1.30	52	55
m10	04/24/98	1	2	1.5	CC	9.2	9.6	1.80	1.85	37	38
n01	11/19/98	3	5	1.5	CC	10.1	11.9	1.37	1.47	352	356
h03	05/05/98	1	5	1.5	CC	11.0	12.2	0.98	1.22	77	81
h03R	05/05/98	1	6	1.5	CC	11.5	12.6	1.26	1.48	82	87
h03R	05/06/98	1	4	1.5	CC	11.8	12.3	1.58	1.92	88	91

Table 4-15 Summary of all R744 data taken in chronological order.

Point	Date	Comp	# runs	SLHX	Flow	Pressure Range		COP Range		Rows	
						Low	High	Low	High	Start	Finish
First R744 System: Change accumulator location after evaporator (Reduced DPsuc)											
i06	04/20/98	1	5	1.5	CC	13.1	13.6	1.52	1.56	5	9
i13	04/20/98	1	4	1.5	CC	10.4	10.8	1.86	1.90	1	4
Second R744 System: Drain all oil from accumulator											
i06	04/21/98	1	3	1.5	CC	13.2	13.3	1.53	1.57	13	15
i13	04/21/98	1	3	1.5	CC	10.5	10.8	1.84	1.86	10	12
Third R744 System: Changed oil, this data published in OSLO											
i06	04/22/98	1	3	1.5	CC	13.2	13.4	1.53	1.56	16	18
i13	04/23/98	1	3	1.5	CC	10.3	10.9	1.78	1.83	29	31
Reduced Speed to same capacity of R134a											
i13R	04/23/98	1	3	1.5	CC	10.7	10.7	1.87	1.90	26	28
i20	04/23/98	1	6	1.5	CC	8.5	10.3	2.34	2.57	20	25
Reduced Speed to same capacity of R134a											
i20R	04/23/98	1	1	1.5	CC	8.7	8.7	2.90	2.90	19	19
Continue with test matrix											
m03	04/23/98	1	5	1.5	CC	11.1	11.6	1.54	1.58	32	36
i11	04/24/98	1	4	1.5	CC	10.1	10.8	1.93	1.99	48	51
i19	04/24/98	1	4	1.5	CC	9.0	10.1	2.62	2.75	39	42
m10	04/24/98	1	2	1.5	CC	9.2	9.6	1.80	1.85	37	38
m05	04/24/98	1	5	1.5	CC	10.5	12.0	1.40	1.46	43	47
i16	04/27/98	1	3	1.5	CC	10.0	10.5	1.28	1.84	56	58
i17	04/27/98	1	4	1.5	CC	9.6	10.2	1.72	1.76	59	62
m08	04/27/98	1	4	1.5	CC	10.1	10.6	1.28	1.30	52	55
Reduced Speed to same capacity of R134a											
m03R	04/29/98	1	5	1.5	CC	11.0	11.6	1.92	1.99	63	67
Increased RPM to 3000											
h03	05/05/98	1	5	1.5	CC	11.0	12.2	0.98	1.22	77	81
Reduced Speed to same capacity of R134a											
h03R	05/05/98	1	6	1.5	CC	11.5	12.6	1.26	1.48	82	87
h03R	05/06/98	1	4	1.5	CC	11.8	12.3	1.58	1.92	88	91
Continue with test matrix											
i06	05/06/98	1	7	1.5	CC	12.9	13.8	1.42	1.58	92	98
Removed suction line heat exchanger											
i11	05/27/98	1	1	0.0	NA	10.6	10.6	1.49	1.49	102	102
i19	05/27/98	1	3	0.0	NA	9.6	10.0	2.35	2.38	99	101
Replaced 1.5m suction line heat exchanger											
m03	06/19/98	1	4	1.5	CC	11.2	11.3	1.45	1.48	103	106
Continue with test matrix											
i13	06/25/98	1	1	1.5	CC	10.7	10.7	1.62	1.62	111	111
i13	06/26/98	1	1	1.5	CC	10.8	10.8	1.65	1.65	112	112
Compare repeatability using point m3 on 6/19 and 6/26											
m03	06/26/98	1	1	1.5	CC	11.5	11.5	1.46	1.46	113	113
Compare suction line pressure drop effects											
i11	06/30/98	1	3	1.5	CC	9.7	11.3	1.63	1.76	114	116
Continue with test matrix											
i11	07/02/98	1	4	1.5	CC	9.8	11.2	1.61	1.68	117	120
i06	07/02/98	1	4	1.5	CC	11.2	13.8	1.13	1.28	121	124
Change to second compressor											
Check suction line heat exchanger effects											
i11	07/13/98	2	6	1.0	CF	9.5	11.5	1.67	1.81	125	130
i11	07/16/98	2	4	0.0	NA	10.8	12.0	1.40	1.51	131	134
i11	07/21/98	2	6	0.0	NA	12.0	14.6	1.41	1.54	142	147
i19	07/21/98	2	7	0.0	NA	9.0	12.0	1.99	2.30	135	141

Table 4-15 Continuation of summary of all R744 data taken in chronological order.

Point	Date	Comp	# runs	SLHX	Flow	Pressure Range		COP Range		Rows	
						Low	High	Low	High	Start	Finish
i11	07/22/98	2	4	1.0	CF	11.5	13.5	1.60	1.78	157	160
i19	07/22/98	2	9	1.0	CF	8.2	12.0	2.08	2.44	148	156
i19	07/23/98	2	7	1.5	CF	8.6	12.6	1.99	2.60	161	167
m05	07/23/98	2	4	1.0	CF	10.2	11.5	1.21	1.37	168	171
i11	07/24/98	2	4	1.5	CF	11.0	12.6	1.72	1.85	172	175
m05	07/24/98	2	4	1.5	CF	9.4	10.9	1.08	1.41	176	179
i11	07/28/98	2	6	2.0	CF	9.6	12.0	1.77	1.90	186	191
i19	07/28/98	2	6	2.0	CF	8.6	12.0	2.09	2.61	180	185
m05	07/28/98	2	5	2.0	CF	9.0	10.6	1.05	1.43	192	196
i19	07/29/98	2	5	2.0	CC	8.6	11.1	2.25	2.63	197	201
m05	07/29/98	2	4	2.0	CC	9.1	10.5	0.97	1.35	202	205
i11	07/30/98	2	7	2.0	CC	9.6	13.2	1.68	1.83	206	212
i11	07/31/98	2	6	1.0	CC	10.2	13.0	1.66	1.80	221	226
i19	07/31/98	2	8	1.0	CC	8.6	12.5	2.00	2.55	213	220
m05	08/03/98	2	4	1.0	CC	10.1	11.5	1.18	1.39	227	230
m05	08/04/98	2	6	0.0	NA	10.9	13.6	0.90	1.19	231	236
i11	08/05/98	2	6	1.5	CC	9.8	12.7	1.61	1.73	243	248
i19	08/05/98	2	6	1.5	CC	8.5	12.2	1.96	2.41	237	242
m05	08/06/98	2	4	1.5	CC	9.6	11.1	1.10	1.35	249	252
Check effect of oil											
i19	09/09/98	2	4	1.5	CC	8.5	9.6	2.32	2.48	253	256
Continue with test matrix											
m05	09/09/98	2	2	1.5	CC	10.6	11.0	1.25	1.30	257	258
Check effect of accumulator charge and valve position											
i19	09/11/98	2	6	1.5	CC	9.7	10.5	2.30	2.44	259	264
Change to third compressor											
i19	10/16/98	3	1	1.5	CC	10.1	10.1	2.38	2.38	265	265
i19	10/21/98	3	4	1.5	CC	8.5	10.1	2.39	2.49	270	273
Ran subcritical point											
i44sub	10/21/98	3	4	1.5	CC	7.1	8.3	2.10	2.91	266	269
Check repeatability of i19											
i19	10/29/98	3	3	1.5	CC	9.5	9.6	2.39	2.48	274	276
Augmented test matrix											
i09	11/02/98	3	3	1.5	CC	9.5	11.6	1.71	1.89	277	279
i39	11/02/98	3	6	1.5	CC	10.8	13.0	2.19	2.31	280	285
i12	11/03/98	3	4	1.5	CC	10.0	11.5	1.63	1.68	286	289
i34	11/03/98	3	7	1.5	CC	9.5	12.6	1.62	1.82	290	296
i36	11/04/98	3	6	1.5	CC	9.1	11.2	1.36	1.46	297	302
i35	11/05/98	3	5	1.5	CC	9.7	11.7	1.56	1.63	303	307
i11	11/09/98	3	4	1.5	CC	10.0	12.0	1.63	1.70	308	311
i41	11/09/98	3	6	1.5	CC	9.5	12.0	1.58	1.73	312	317
i40	11/11/98	3	6	1.5	CC	9.5	11.7	1.63	1.79	318	323
i19	11/16/98	3	6	1.5	CC	8.4	10.5	2.19	2.41	329	334
i44	11/16/98	3	5	1.5	CC	8.0	9.3	2.76	2.90	324	328
i13	11/18/98	3	5	1.5	CC	9.6	12.0	1.46	1.59	340	344
i17	11/18/98	3	5	1.5	CC	10.0	12.0	1.49	1.56	335	339
i42	11/18/98	3	4	1.5	CC	10.0	11.6	1.26	1.36	345	348
m05	11/19/98	3	3	1.5	CC	10.0	11.0	1.14	1.25	349	351
n01	11/19/98	3	5	1.5	CC	10.1	11.9	1.37	1.47	352	356
Ran reduced speed											
i36R	01/30/99	3	4	1.5	CC	8.1	8.7	1.22	1.81	357	360
Ran subcritical points											
i44sub	02/01/99	3	5	1.5	CC	7.3	9.0	1.81	3.04	361	365
i25sub	02/04/99	3	7	1.5	CC	6.7	8.7	2.72	3.52	366	372

5 Internal Heat Exchanger

5.1 Introduction

This chapter explores the contribution of the internal heat exchanger (IHX) to the unexpectedly better performance of the R744 system. Both R744 and R134a are among a subset of refrigerants for which COP increases due to internal heat exchange for fundamental thermodynamic reasons explored in detail by Domanski et. al. (1994). However, conventional R134a systems have no internal heat exchanger because its cost and weight penalties have outweighed the marginal performance improvements. The potential benefits in the transcritical cycle are much greater because evaporator inlet qualities often exceed 50%, and the resulting thermodynamic irreversibility at the expansion valve is correspondingly large (Groll 1997). Moreover, the potential suction line pressure drop penalty is less severe for R744 due to the greater slope of its vapor pressure curve.

The purpose of this chapter is twofold. The first is to use component-level data from the aforementioned system tests to illustrate the effects of the internal heat exchanger on performance of the overall system. The second is to use the data set to develop and validate a component simulation model for parallel flow and counterflow concentric internal heat exchangers, such as those described in the next section. Using a subset of the experimental results, the effects of IHX are presented in Section 5.4, as a function of operating conditions. The simulation model is developed and validated in Section 5.5, and used to optimize the design in Section 5.6.

5.2 Apparatus and Test Conditions

Three internal heat exchangers, extruded aluminum of the concentric tube type, were used in these experiments. Figure 5-1 shows their identical cross sections. Lengths were 1.0, 1.5 and 2.0 m for both the parallel and counterflow configurations. The hot supercritical fluid flows in the inner tube while the cold low density fluid flows in the outer tube. The annulus is divided into six identical channels by radial webs connecting the two concentric tubes in a manner to

maximize the surface, thereby equalizing the circumferential wall temperature distribution for the cold stream.

Data were taken over a wide range of indoor and outdoor temperatures, humidity, compressor rpm and air flow rates over the evaporator and gas cooler. A thermodynamic analysis of the cycle indicated that the most significant contribution due to internal heat exchange could be expected at high ambient temperatures. Since capacity enhancement is needed most at low compressor (vehicle) speeds, most tests were performed at idle (950 rpm) and medium driving speed (1800 rpm) across the full range of non-cycling (pulldown) operating conditions. The three operating conditions used in this paper to illustrate key concepts are shown in Table 5-1; the complete test matrix is given by McEnaney et al. (1999).

A unique aspect of the transcritical cycle is the extra degree of freedom resulting from the ability to increase both COP and capacity by increasing high-side pressure. Therefore, several data points will be shown for each operating condition in the test matrix; they were taken to find the maximum capacity and maximum coefficient of performance of the system. Due to restrictions imposed by materials used, the compressor discharge temperature and pressure were not permitted to exceed 140°C and 15 MPa, respectively.

The internal heat exchangers were insulated from the ambient with 1" armoflex insulation, and positioned downstream of a suction accumulator and upstream of a filter as shown in Figure A-3. The position of the suction side inlet and exit of the internal heat exchanger were positioned downward to allow oil drainage. At most conditions, suction line inlet quality was between 0.95 and 1.00; superheat was far less common. Immersion thermocouples were installed in the elbows at each inlet and outlet. Pressure was measured at the evaporator outlet and compressor inlet, shown in Section 5.3, but the measurement uncertainty precluded accurate determination of the pressure drop in the heat exchanger. The result tended to confirm the near-negligible values of pressure drop on the suction line calculated by the model in Section 5.5. The quality at the low-pressure inlet was calculated from evaporator calorimetry as described by McEnaney et al. (1998).

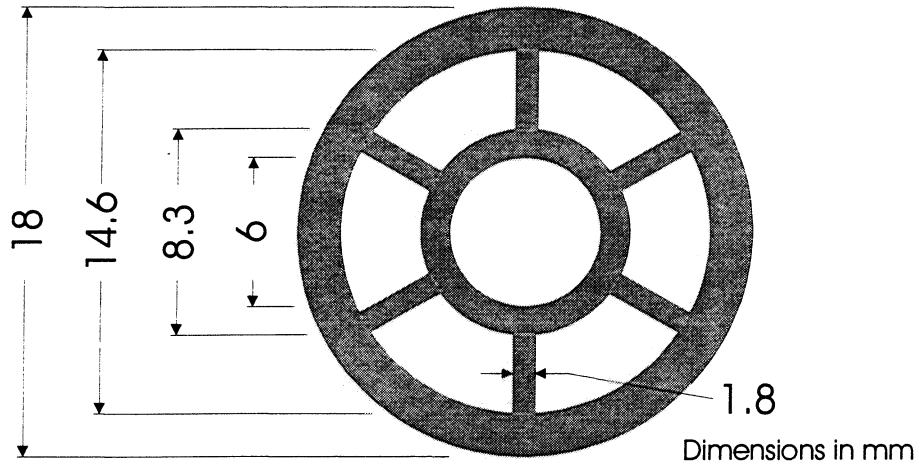

Figure 5-1 Cross section of the prototype internal heat exchanger I, II, and III.

Table 5-1 Test conditions for R744 system.

	Operating Condition		
	A	B	C
Compressor Speed (rpm)	950	950	1800
Gas Cooler Air Flow Rate (m^3/min)	22.7	22.7	27.0
Gas Cooler Air Inlet Temperature (°C)	32.2	43.3	43.3
Evaporator Air Flow Rate (m^3/min)	7.08	7.08	7.08
Evaporator Air Inlet Temperature (°C)	26.7	26.7	26.7
Evaporator Air Inlet Relative Humidity (%)	40	40	40

5.3 Pressure Drop in Suction Line

Only the pressure drop across the entire suction line (from evaporator exit to compressor inlet) was measured during the testing of the R744 system. Since the IHX pressure drop was not directly measured, a procedure is needed to determine the IHX contribution. Data was taken for suction line pressure drop using the three different IHXs and no IHX configurations. From this data, the suction line was broken into several parts with intention to determine pressure drop in the straight pipe section of the IHX suction side and entrance and exit losses. The breakdown of the various sections is shown in Figure 5-2.

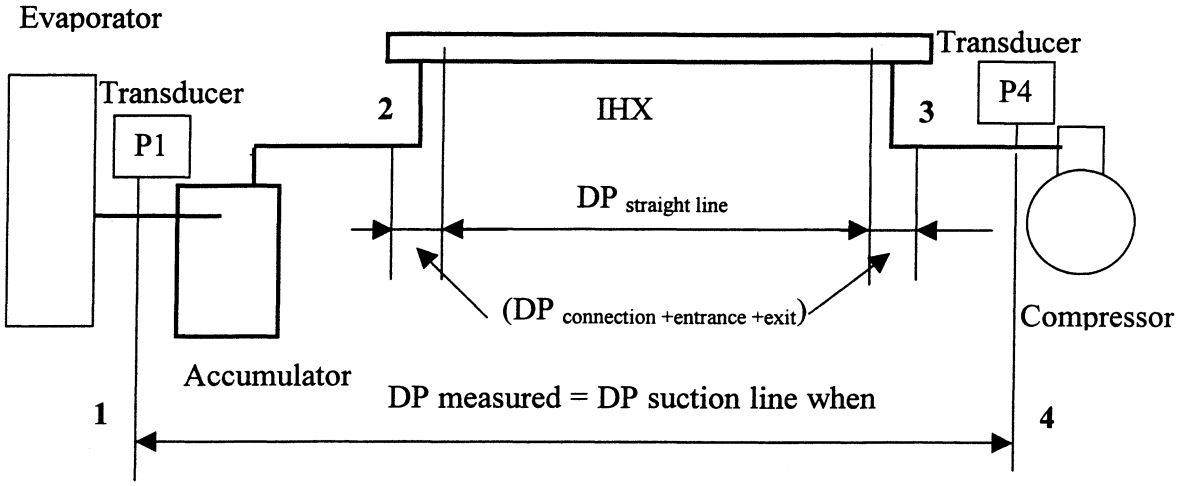

Figure 5-2 Schematic diagram of the R744 suction line.

The total pressure drop in the suction line ($DP_{measured}$) can be expressed as product of ρU^2 and a multiplier. The multiplier can then be further broken down into three parts, as shown in Figure 5-3:

a) straight pipe of the IHX suction side ($DP_{straight\ pipe}$),

b) suction line without internal heat exchanger ($DP_{suction\ line}$),

c) connections, entrance and exit of internal heat exchanger ($DP_{connection\ +entrance\ +exit}$).

The measured pressure drop data for the suction line with the three different internal heat exchangers yields the following three equations:

$$DP_{measured} = 0.0953\ \rho U^2 \quad \text{(for 2.0 m IHX)}$$

$$DP_{measured} = 0.0912\ \rho U^2 \quad \text{(for 1.5 m IHX)} \qquad (5.1)$$

$$DP_{measured} = 0.0871\ \rho U^2 \quad \text{(for 1.0 m IHX)}$$

The pressure drop of the suction pipe with the IHX is then determined from these equations. The differences between the three lines indicate the effect of the length of the IHX. This change in slope is a function of length and yields the following equation:

$$DP_{straight\ pipe} = 0.0082\ L\rho U^2 \quad (5.2)$$

Now subtracting equation 5.2 from equations 5.1, the pressure drop of the straight pipe ($DP_{straight\ pipe}$) and suction line ($DP_{suction\ line}$) remain.

The pressure drop in the suction line, which includes all elements between evaporator and compressor (suction accumulator, filter, fittings, pipes, valves etc.) but not the IHX or connections, is determined from data taken without an IHX in the system. These data without an IHX give the correlation:

$$DP_{suction\ line} = 0.0430\ \rho U^2 \quad (5.3)$$

Now, subtracting both equations 5.2 and 5.3 from equations 5.1, the pressure drop of the connections is found to be:

$$DP_{connections+entrance+exit} = 0.0359\ \rho U^2 \quad (5.4)$$

Putting all of the equations together, we come up with a relation for the suction line pressure drop with the IHX included.

$$DP_{measured} = (0.0789 + 0.0082\ L)\ \rho U^2 \quad (5.5)$$

The contributions of each part of the suction line pressure drop are shown in graphical form in Figure 5-3. Even though the graph differentiates pressure drops well, absolute values of pressure drop in the straight pipe are low. The pressure drop was determined using two 0 to 6.9 MPa pressure transducers ±0.25% FS, which makes pressure drop calculations for the straight pipe fairly uncertain.

5.4 System Performance Improvements

For each test condition, the system capacity and coefficient of performance were calculated as the expansion valve was controlled to achieve a wide range of compressor discharge pressures. The pressure range bracketed the maximum COP, but the maximum capacity point usually lay beyond the constraints on discharge pressure and temperature mentioned earlier.

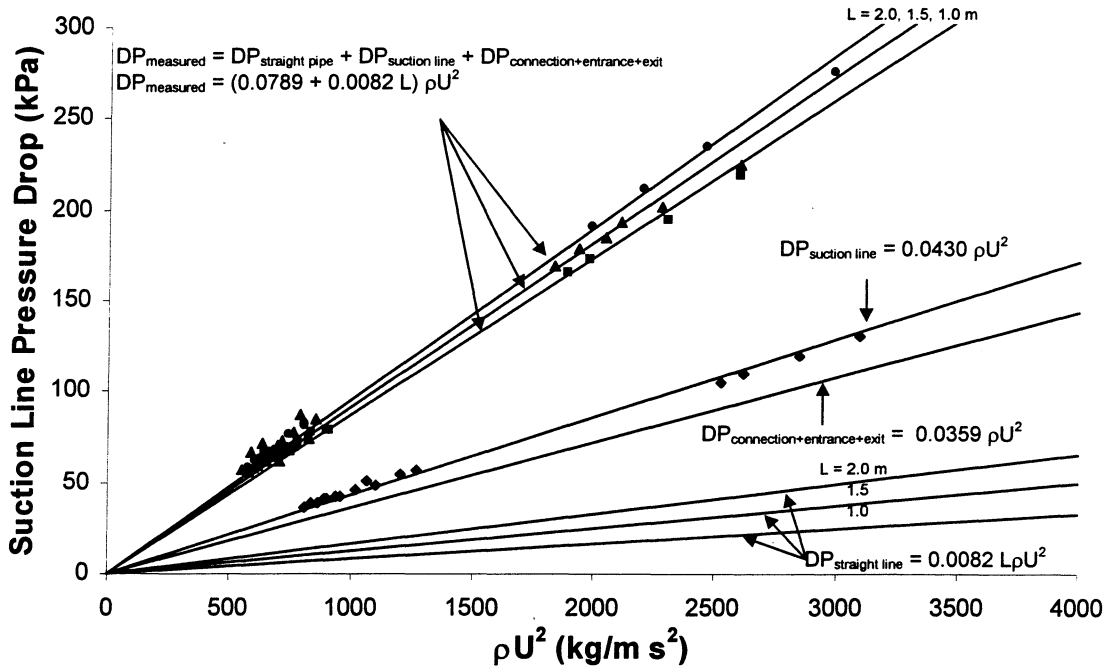

Figure 5-3 Graphical presentation of pressure drop elements in suction line.

Table 5-2 Idle and driving speed operating conditions at near-optimal COP.

Point	L_{ihx}	Counter or Parallel	$\dot{m}$ (g/s)	T_{hi} (°C)	T_{ho} (°C)	P_{hi} (kPa)	T_{ci} (°C)	T_{co} (°C)	x_{ci}	DP_{suc} (kPa)	Q_{ihx} (W)
A	None	-	27.2	37.2	37.5	9820	-	-	-	50	-
	1.0	PF	23.5	37.2	30.9	9370	5.9	22.1	1.00	70	690
		CF	26.0	37.7	35.6	8480	7.9	25.8	1.00	70	850
	1.5	CF	23.2	38.0	31.2	8940	6.4	29.1	0.98	80	970
	2.0	PF	22.4	36.8	28.3	9400	5.7	25.9	1.00	70	790
		CF	22.6	37.7	29.9	8980	6.2	30.8	0.99	70	990
B	None	-	28.0	47.0	47.2	11760	-	-	-	50	-
	1.0	PF	22.6	46.2	37.6	11460	7.5	26.2	0.99	60	790
		CF	22.7	46.6	38.5	10830	7.9	28.7	0.98	60	920
	1.5	CF	20.6	45.7	35.0	10450	7.7	34.6	0.96	40	1110
	2.0	PF	21.2	45.6	34.3	11900	7.3	29.6	1.00	60	840
		CF	21.5	46.2	34.9	10750	7.6	37.2	0.98	70	1120
C	None	-	39.3	48.3	48.4	13270	-	-	-	100	-
	1.0	PF	34.4	48.6	40.1	11140	2.6	25.8	0.98	160	1420
		CF	34.4	49.0	40.2	11100	2.2	28.4	0.98	160	1520
	1.5	CF	33.9	48.8	39.1	10530	2.5	34.5	0.96	160	1930
	2.0	PF	36.0	48.0	40.7	10040	3.6	34.1	0.97	190	1900
		CF	34.2	47.8	39.1	10150	3.0	38.4	0.97	180	1980

Table 5-2 shows results along with the inlet states and exit temperatures near the optimal COP for three operating conditions. The quality at the low-pressure inlet was calculated from the capacity determined on the high side. Shown for each test condition are only the values of the measured parameters near the optimal COP.

Table 5-2 also shows the impact of the presence of a one-meter IHX at idle speed (950 rpm) and low ambient temperature (condition A). Although capacity increased only 4-5%, COP increased approximately 13%. However, at idle speed and high ambient temperature, condition B, improvement due to IHX is much greater. Figure 5-4 shows that the optimal COP is increased by 23% for condition B. Moreover, at that COP-optimizing discharge pressure, the capacity is increased by 11%. The sharp maximum of the COP reflects the sensitivity of system performance to high-side pressure. Capacity is less sensitive to both high-side pressure and the presence of the internal heat exchanger. The positive effect of IHX is also evident at other operating conditions: COP is improved, Q is improved, and optimal pressures for both Q and COP are reduced. Most striking, however, is the fact that the distance between the two optimal pressures is also reduced by internal heat exchange. Therefore, it might be possible to use simple devices and algorithms for backpressure control.

Another interesting result illustrated in Figure 5-4 is the comparison of the system's performance while meeting a 2.8 kW load with and without IHX. In the conventional Evans-Perkins cycle, the high compressor suction temperatures caused by IHX translate directly into higher discharge temperatures, which can cause oil breakdown and impair reliability. In the transcritical cycle, however, the presence of the internal heat exchanger with its lower operating pressure offsets the tendency to increase the discharge temperature. Figure 5-4 shows that the system with no IHX achieves the 2.8 kW load at 14.0 MPa where COP is 1.47. The same system with the 2.0 m counterflow IHX could achieve the same 2.8 kW capacity at a 24% lower discharge pressure, resulting in a 10° increase (111°C to 121°C) in discharge pressure and a 30% increase in COP.

Figure 5-5 shows the effect of ambient temperature; other independent variables are held constant at idle conditions A and B. Clearly the presence of the IHX provides the greatest enhancement to both capacity and COP at precisely the condition where it is needed most.

As expected, the counterflow configuration outperformed the parallel flow. One reason for testing the latter was to evaluate its potential for avoiding excessively high compressor discharge

temperatures. For clarity and ease of comparison, the parallel flow configuration and the 1.5m internal heat exchanger have been omitted from Figure 5-4 and Figure 5-5. The 1.5m counterflow data fell between the 1.0m and 2.0m cases; they were shown in Boewe et al. (1999).

At driving speed condition C (1800 rpm), the compressor discharge temperature limited the high-side pressure range. The maximum COP point was reached only for the case without IHX, and capacity was constrained for all cases. Despite these limitations, the efficiency improvement due to internal heat exchange was 20%.

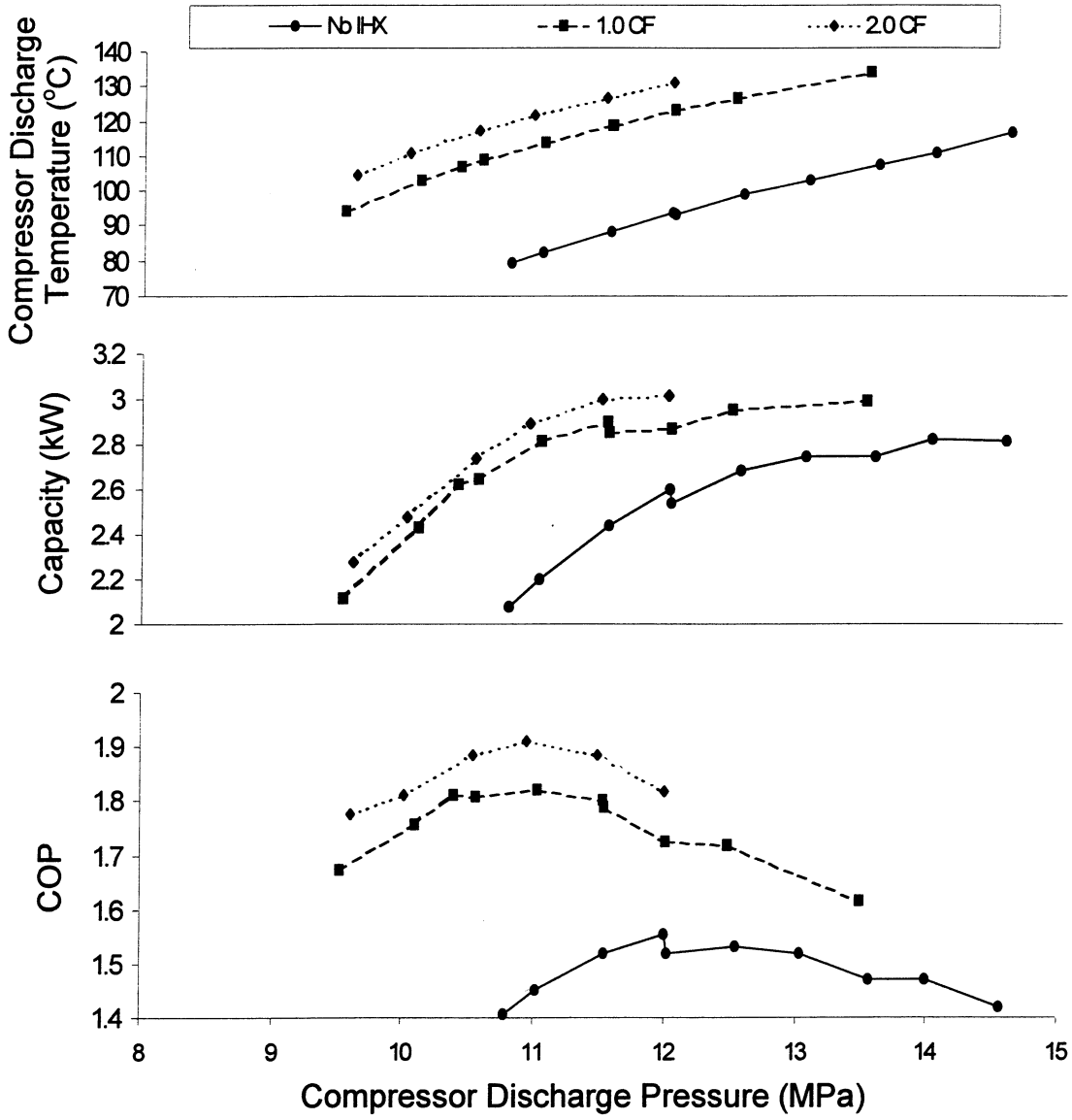

Figure 5-4 Influences of IHX length at hot idling condition B.

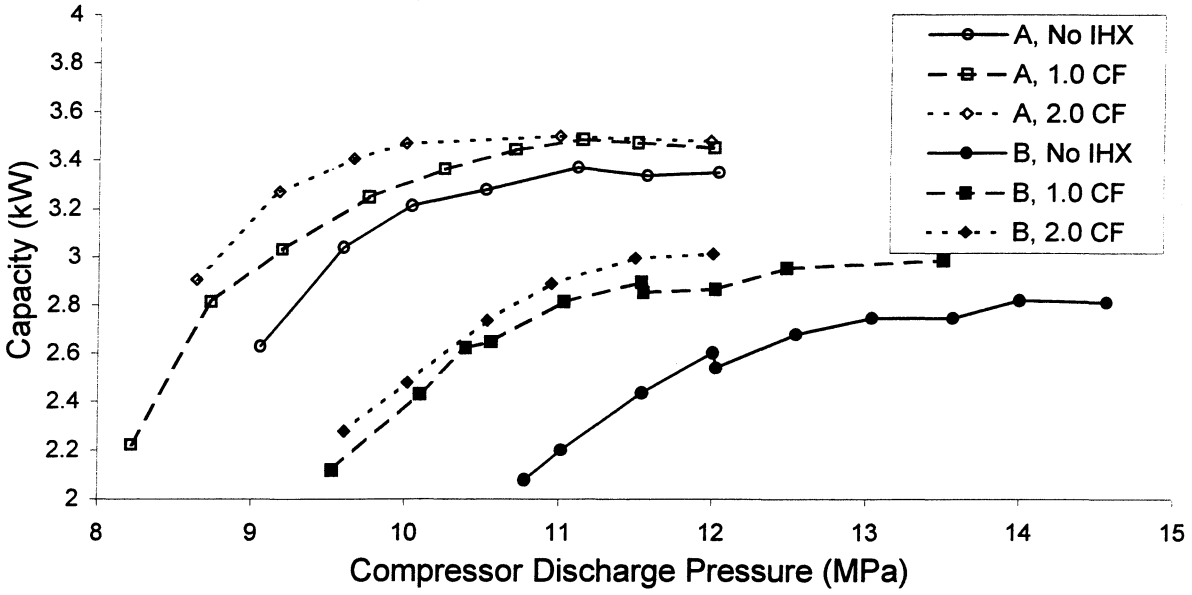

Figure 5-5 Effect of ambient temperature.

5.5 Simulation Model

The internal heat exchanger is simulated using a finite element approach; 10 segments were used for most of the simulations that follow. The model can handle any number and diameter of parallel ports for the hot and cold streams, arranged in a manner that ensures that each port is circumferentially isothermal. The equations neglect axial conduction, and approximate noncircular ports using their hydraulic diameter. The cold stream inlet may be two-phase fluid exiting the evaporator or suction accumulator, in which case the length of the first element is defined so its exit state is saturated vapor. For the supercritical hot stream and the single-phase region of the cold stream, the heat transfer coefficient is calculated using the Gnielinski (1976) correlation

$$Nu_D = \frac{(f/8)(\mathrm{Re}_D - 1000)\,\mathrm{Pr}}{1 + 12.7(f/8)^{1/2}(\mathrm{Pr}^{2/3} - 1)} \qquad 0.5 < \mathrm{Pr} < 2000;\ 2300 < \mathrm{Re_D} < 5 \times 10^6 \qquad (5.6)$$

which was found by Rieberer (1999) to be the best for R744 at transcritical and subcritical conditions. For the two-phase region, the heat transfer coefficient is calculated using the Chato-Wattelet (1994) correlation

$$\alpha = F\alpha_l \tag{5.7}$$

$$\alpha_l = 0.023\frac{k_l}{D}\mathrm{Re}_l^{0.8}\,\mathrm{Pr}_l^{0.4} \tag{5.8}$$

$$F = 1+1.925X_{tt}^{-0.83} \tag{5.9}$$

where X_{tt} is the Lockhart-Martinelli parameter

$$X_{tt} = \left(\frac{1-x}{x}\right)^{0.9}\left(\frac{\rho_v}{\rho_l}\right)^{0.5}\left(\frac{\mu_l}{\mu_v}\right)^{0.1} \tag{5.10}$$

The Chato-Wattelet correlation was originally developed for R12, R134a, and a mixture of R22/R124/R152a. It was later found by Rieberer (1999) to provide the best approximation for R744 evaporation.

The friction factors for all three regions of the heat exchanger are calculated using the smooth tube correlation developed by Petukhov

$$f = (0.790\ln \mathrm{Re}_D - 1.64)^{-2} \qquad 3000 < \mathrm{Re}_D < 5 \times 10^6 \tag{5.11}$$

in both the heat transfer and pressure drop calculations. The thermophysical properties of the R744 are obtained from the National Institute of Standards and Technology (REFPROP, 1998).

The internal heat exchanger pressure drop and heat exchange are calculated for each section and then summed to get the total pressure drop and heat exchange (Q_{ihx}). The effectiveness of the internal heat exchanger is defined as the total heat exchange divided by the maximum heat exchange possible (Q_{max}).

$$\varepsilon = \frac{Q_{ihx}}{Q_{max}} \tag{5.12}$$

For the counterflow configuration, the maximum heat exchange is the enthalpy found with the inlet temperature of the liquid line and the exiting suction pressure minus the enthalpy found with the inlet temperature and pressure (or quality) of the suction line.

$$Q_{max} = \dot{m}[h(T_{hi}, P_{co}) - h(T_{ci}, P_{ci} or X_{ci})] \tag{5.13}$$

For the parallel flow configuration, the maximum heat transfer is found by calculating the maximum enthalpy difference possible for the heat exchanger. This is done by simultaneously solving the following two equations (5.9 and 5.10) for Q_{max} and T_o.

$$Q_{\max} = \dot{m}[h(T_{hi}, P_{hi}) - h(T_o, P_{ho})] \tag{5.14}$$

$$Q_{\max} = \dot{m}[h(T_o, P_{co}) - h(T_{ci}, P_{ci} or X_{ci})] \tag{5.15}$$

Simulation results were compared to 178 sets of measured data taken over a two-year period with the prototype R744 mobile air conditioning system. The three internal heat exchangers (1.0, 1.5, and 2.0 m) were used in both parallel and counterflow configurations. Figure 5-6 shows the predictions of the IHX capacity. For these data, the IHX capacity ranges from 0.5 kW to 3.5 kW, enough to sometimes double the overall R744 system capacity. The model predicted IHX capacity with a standard deviation of 0.05 kW, which is 4.2% of the average IHX capacity.

Capacity is only one important indicator of the impact of IHX on the rest of the system; the other is density at the suction inlet, because of its relation to compressor work. Figure 5-7 therefore shows the predicted exit density for the suction side of the IHX; the standard deviation of this prediction is 1.2 kg/m^3, which is 1.2% of the average density. Compressor work will also be reduced due to the lower discharge pressure at which IHX-equipped systems will operate.

Optimal design of an internal heat exchanger will therefore involve a tradeoff between the effectiveness of the IHX and the suction-side pressure drop required to achieve it. High side pressure drop is not a problem, since it is immediately upstream of the throttling device. The pressure drop in the prototypes was too small to measure accurately, so the following analysis relies on model calculations.

The tradeoff between effectiveness and suction pressure drop is shown by the solid lines in Figure 5-9 and Figure 5-10 for idling and driving conditions A and C, respectively. For the cycle defined by the thermodynamic states measured at the idle condition, a 5% increase in effectiveness is worth a 10 kPa suction pressure drop without loss of COP. For the driving condition, a 5% increase in effectiveness is worth approximately 40 kPa. With this information, an improved internal heat exchanger can now be sought.

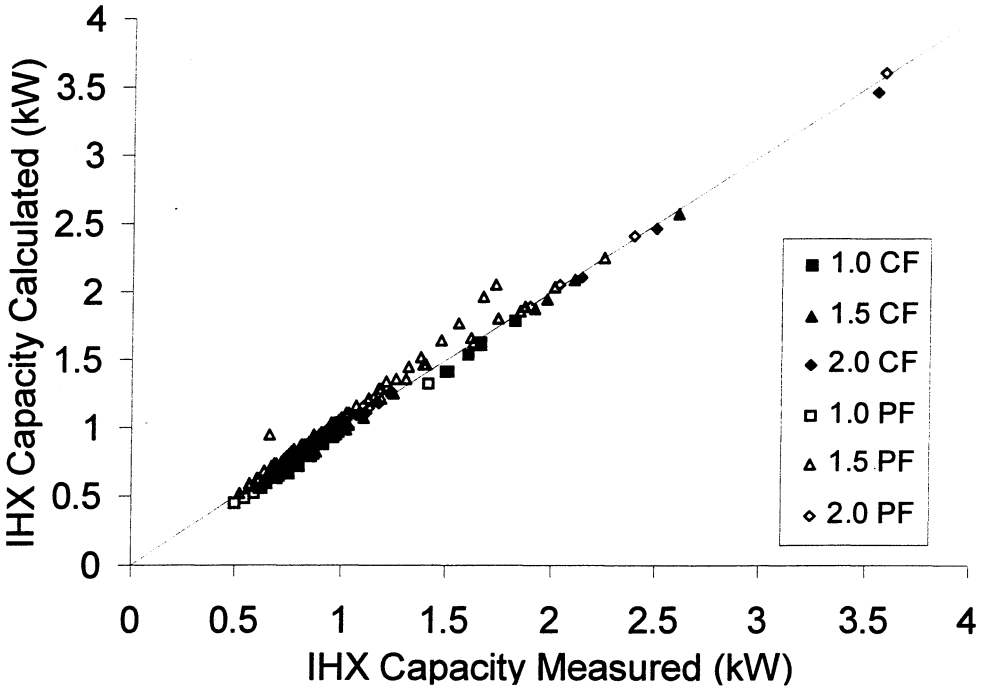

Figure 5-6 Predicted and measured capacity in parallel (PF) and counterflow (CF) configurations.

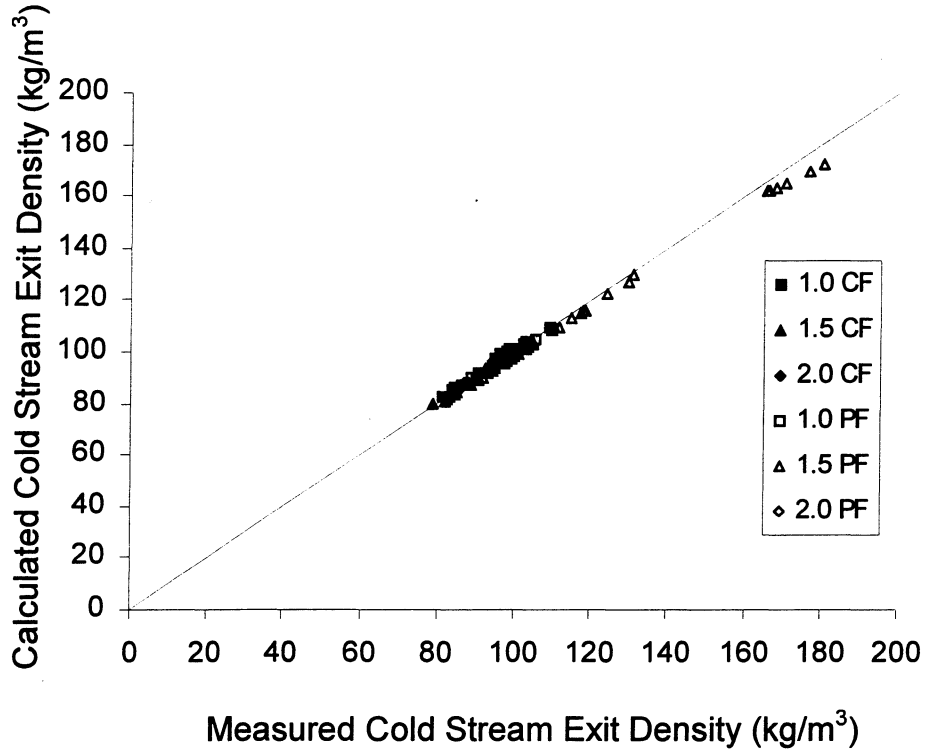

Figure 5-7 Predicted and measured compressor suction inlet density with IHX in parallel (PF) and counterflow (CF) configurations.

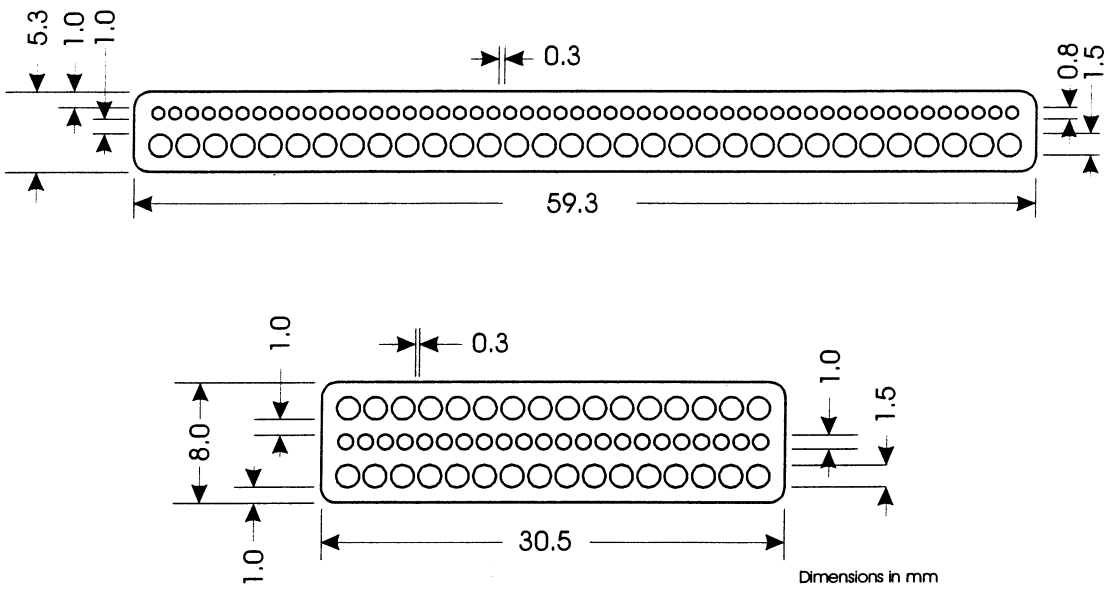

Figure 5-8 Proposed IHX designs IV (top) and V (bottom) with hot stream in smaller ports. Design V allows for limited bending about major axis.

5.6 Design Optimization

Figure 5-8 shows two candidate designs that appear to be easy to extrude, either as a single tube or as multiple tubes brazed or epoxied together. Flexible fittings could be attached to the ends. Both are only 1.0 m long, but that is sufficient to eliminate the separate suction and "liquid" lines that would otherwise be needed.

The performance of the three prototypes tested (internal heat exchangers I, II, and III) is shown on Figure 5-9 and Figure 5-10. Both suggested designs (IHXs IV and V) appear to offer substantial improvements in system COP, as a result of optimizing the tradeoff between pressure drop and IHX effectiveness. Table 5-3 shows that the proposed 1.0 m designs have half the aluminum mass of the original 2.0 m prototype, and significantly higher effectiveness. The predicted pressure drop penalty at driving speeds (high refrigerant mass flow rate) is not detrimental.

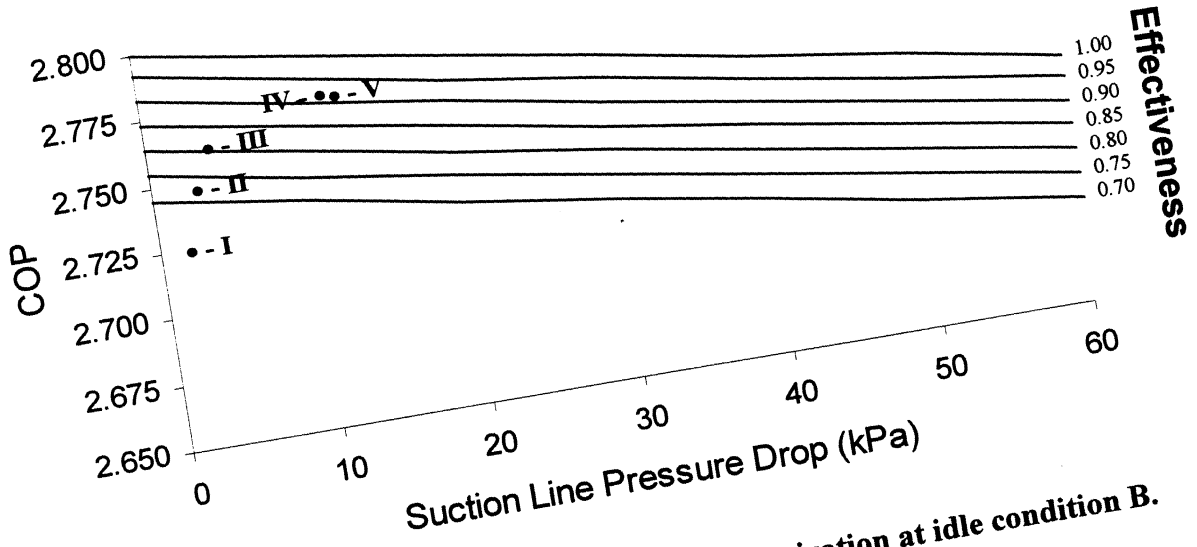

Figure 5-9 Efficiency improvement due to IHX optimization at idle condition B.

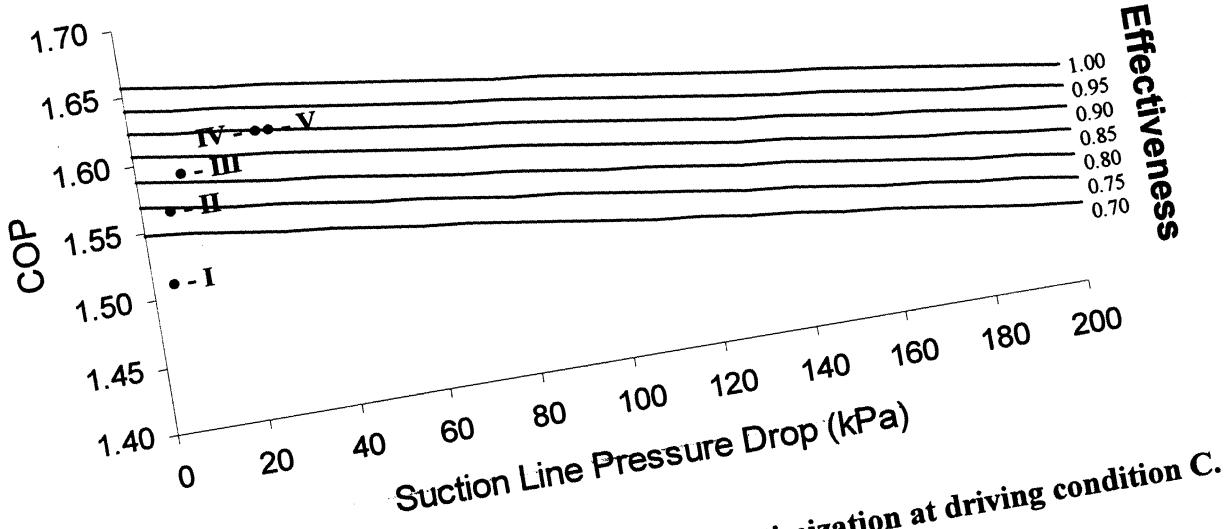

Figure 5-10 Efficiency improvement due to IHX optimization at driving condition C.

Table 5-3 Counterflow IHX performance at high ambient and driving conditions (B and C).

IHX	Liquid Ports # @ D_h (mm)	Suction Ports # @ D_h (mm)	Length (m)	Width (mm)	Height (mm)	Material Volume (cm^3)	Liquid DP (kPa)	Suction DP (kPa)	ε (%)
Idling									
I	1 @ 6.0	6 @ 3.6	1.0	18	18	254	2	2	60
II	1 @ 6.0	6 @ 3.6	1.5	18	18	382	2	3	73
III	1 @ 6.0	6 @ 3.6	2.0	18	18	509	3	4	80
IV	50 @ 0.8	32 @ 1.5	1.0	59.3	5.3	314	23	13	92
V	22 @ 1.0	32 @ 1.5	1.0	30.5	8.0	244	34	13	91
Driving									
I	1 @ 6.0	6 @ 3.6	1.0	18	18	254	3	5	59
II	1 @ 6.0	6 @ 3.6	1.5	18	18	382	5	8	74
III	1 @ 6.0	6 @ 3.6	2.0	18	18	509	8	11	81
IV	50 @ 0.8	32 @ 1.5	1.0	59.3	5.3	314	49	32	90
V	22 @ 1.0	32 @ 1.5	1.0	30.5	8.0	244	72	31	90

5.7 Conclusion

Results show the significant influence of the internal heat exchanger on system performance, increasing efficiency up to 25%. Internal heat exchange provides the greatest enhancement when it is needed most, while idling at high ambient temperatures. In systems without internal heat exchangers, the capacity- and efficiency-optimizing discharge pressures are far apart. Internal heat exchange brings them closer together, thus enabling simpler control systems and strategies.

Counterflow heat exchanger arrangement was shown to better than parallel, which was not unexpected. What was surprising was the fact that the IHXs lowering of discharge pressures offset its tendency to increase discharge temperature, eliminating the need to resort to parallel flow. In our experiments at idling speed, discharge temperatures at peak efficiency remained below the 140°C limit currently imposed on the prototype compressor. Once an upper limit is established as compressor designs mature, tradeoff analyses can determine whether to rely on an [active] compressor cutout switch or high-side pressure control, or a [passive] internal heat exchanger having lower effectiveness or parallel flow, as a means of limiting discharge temperatures at high-speed, high-ambient temperature conditions.

The simulation model proved effective in predicting performance of the prototype heat exchangers over a wide range of conditions, despite the relatively complex geometry and two-

phase inlet conditions. The model also proved to be a useful tool for optimizing the design, reducing material requirements by 50% while increasing effectiveness by 10%.

Acknowledgement

We acknowledge the contribution of Visiting Scholar Y. C. Park who has since returned to his position of Professor at Korea University, Seoul.

References

ANSI-ASHRAE Standard 40-1986, "Methods of Testing for Rating Heat Operated Unitary Air Conditioning Equipment for Cooling." 1986.

Boewe, D., Park, Y.C., Yin, J., Bullard, C.W., Hrnjak, P.S., "The Role of a Suction Line Heat Exchanger in Transcritical R744 Mobile A/C Systems." SAE International Congress and Exposition, Paper 1999-01-0583, 1999.

Domanski, P.A., Didion, D.A., Doyle, J.P., "Evaluation of Suction-Line/Liquid-Line Heat Exchange in the Refrigeration Cycle." Int. Journal of Refrigeration-Revue Internationale du Froid, Vol. 17, pp 487-493, 1994.

Gnielinski, V., "New Equations for Heat and Mass Transfer in Turbulent Pipe and Channel Flow." Int. Chem. Eng., Vol. 16, pp. 359-368, 1976.

Groll, E.A., Robinson, D.M., "Efficiencies of Transcritical CO2 Cycles with and wthout an Expansion Turbine." CO2 Technology in Refrigeration, Heat Pump and Air Conditioning Systems, Workshop Preceedings, Report No. HPC-WR-19, 1997.

Lorentzen, G., Pettersen, J., "A New, Efficient and Environmentally Benign System for Car Air-Conditioning." Int. Journal of Refrigeration, Vol. 16, No 1, pp 4-12, 1993.

McEnaney, R.P., Boewe, D.E., Yin, J.M., Park, Y.C., Bullard, C.W., Hrnjak, P.S., "Experimental Comparison of Mobile A/C Systems when Operated With Transcritical CO_2 Versus Conventional R134a." International Refrigeration Conference at Purdue, pp. 145-150, 1998.

McEnaney, R.P., Park, Y.C., Yin, J.M., Hrnjak, P.S., "Performance of the Prototype of Transcritical R744 Mobile A/C System." SAE International Congress and Exposition, Paper 1999-01-0872, 1999.

Park, Y.C., McEnaney, R., Boewe, D., Yin, J.M., Hrnjak, P.S., "Steady State And Cycling Performance Of A Typical R134a Mobile A/C System." SAE International Congress and Exposition, Paper 1999-01-1190, 1999.

REFPROP Version 6.0, "NIST Thermodynamic and Transport Properties of Refrigerants and Refrigerant Mixtures", U.S. Department of Commerce, Gaithersburg, Maryland, 1998.

Rieberer, R., "CO2 Properties." IIR Workshop on CO2 Technology in Refrigeration, Heat Pump and Air Conditioning Systems, 1999.

Thavenot, R., "A History of Refrigeration Throughout the World." Translated by J.C. Fidler. International Institute of Refrigeration, Paris, France.

Wattelet, J.P., Chato, J.C., Souza, A.L., Christoffersen, B.R., "Evaportive Characteristics of R-12, R-134a, and a Mixture at Low Mass Fluxes." ASHRAE Transactions, Vol. 100, Part I, pp 603-615, 1994.

Yin, J., Park, Y.C., Boewe, D., McEnaney, R., Beaver, A., Bullard, C.W., Hrnjak, P.S., "Experimental and model comparison of transcritical CO2 versus R134a and R410 system performance." Natural Working Fluids '98, IIR - Gustav Lorentzen conference, Oslo, pp. 331-340, 1998.

Yin, J.M., Pettersen, J., McEnaney, R., Beaver, A., "TEWI Comparison of R744 and R134a Systems for Mobile Air Condition." SAE International Congress and Exposition, Paper 1999-01-0582, 1999.

Appendix A - Mobile Air Conditioning System Components

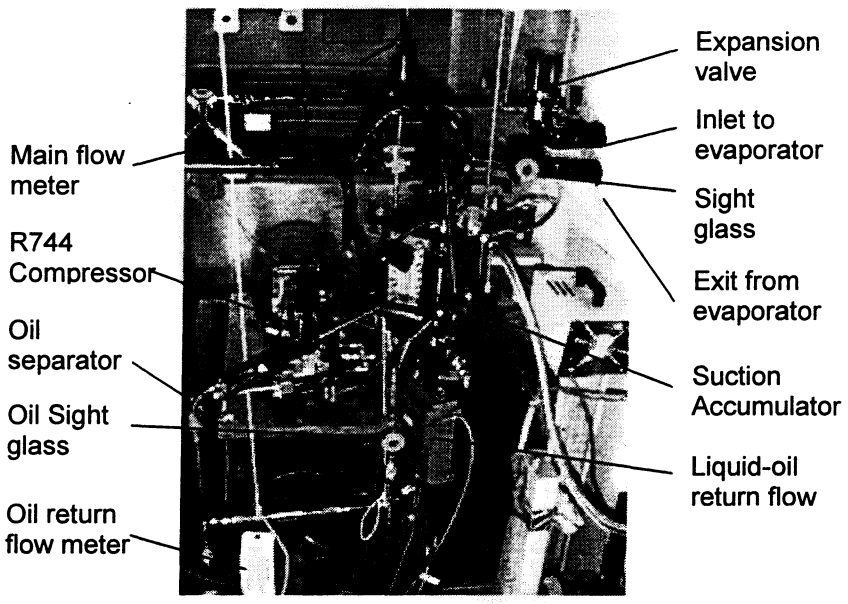

Figure A-1 Picture of some of the prototype R744 system components and instruments in the test facility.

Two mobile air conditioning systems were tested and compared over a two-year period at the Air Conditioning and Refrigeration Center (ACRC). The first system was a typical off the shelf R134a air conditioning system taken from a Ford Escort. The second system was a prototype R744 system. The R744 system was designed to have approximately the same size and weight components. Also, the face areas and package volumes of the heat exchangers were set to be approximately the same along with the same airside pressure drop. In this way, the comparison of the prototype R744 system and R134a system could be justified since they would both require the same amount of space, have the same overall weights, and take the same fan power in the automobile. It is also acknowledged that the Ford Escort system is an off the shelf, typical R134a system that was not necessarily optimized for energy efficiency. Nevertheless, the R744 prototype system, shown in Figure A-1, is in its infancy. Future research at the ACRC will be done to improve the R134a system performance.

Although the two systems mostly used the same components, the main difference was the inclusion of a suction line (internal) heat exchanger in the R744 system. The suction line heat exchanger helps the R744 system by increasing capacity and COP while also lowering the high side pressure for optimal performance. Also, the R744 system included an oil separator after the

compressor. This separator bypassed the oil exiting from the compressor back to the inlet of the compressor.

For measurement purposes, both systems were instrumented with pressure transducers, thermocouples, and mass flow meters. System schematics of both the R134a system and the R744 system are shown in Figure A-2 and Figure A-3. The placement of the instruments and sight glasses in the refrigerant lines are also shown. In the following sections, each system component is discussed in more detail.

A.1 Compressors

The Ford FS10 R134a compressor, shown in Figure A-4, is a typical open compressor for automotive applications. It is a relatively small reciprocating swash plate machine with 10 cylinders that draws refrigerant from the suction accumulator as low-pressure vapor. Once in the compressor, piston action compresses the refrigerant and sends it through the compressor outlet as a high-pressure vapor to the condenser. The compression ratio for the R134a compressor is on the order of 4 to 9.

The R744 compressor, shown in Figure A-4, is a prototype open compressor designed for automotive applications. Dimensions of the two compressors shown in Table A-1. The R744 compressor has nearly the same dimensions and weight as the R134a compressor. Once in the compressor, piston action compresses the refrigerant and sends it through the compressor outlet as a high-pressure vapor to the gas cooler. The compression ratio for the R744 compressor is on the order of 2 to 3.

Table A-1 Dimensions and characteristics of R134a compressor and R744 compressor.

	R134a Compressor	**R744 Compressor**
Type	Reciprocating	Reciprocating
Displacement (cm^3)	155	20.7
Mass (kg)	4.75	6.1
Length (cm)	19.0	21.0
Diameter (cm)	14.0	12.0

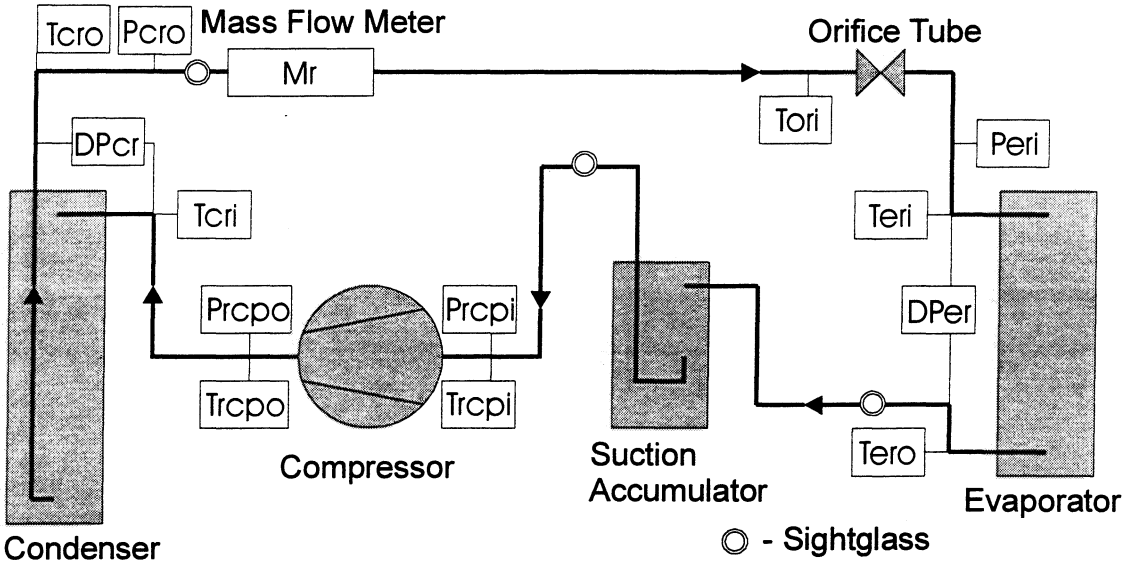

Figure A-2 Schematic of R134a air conditioning system components showing all refrigerant side measurements (excluding compressor torque meter and tachometer).

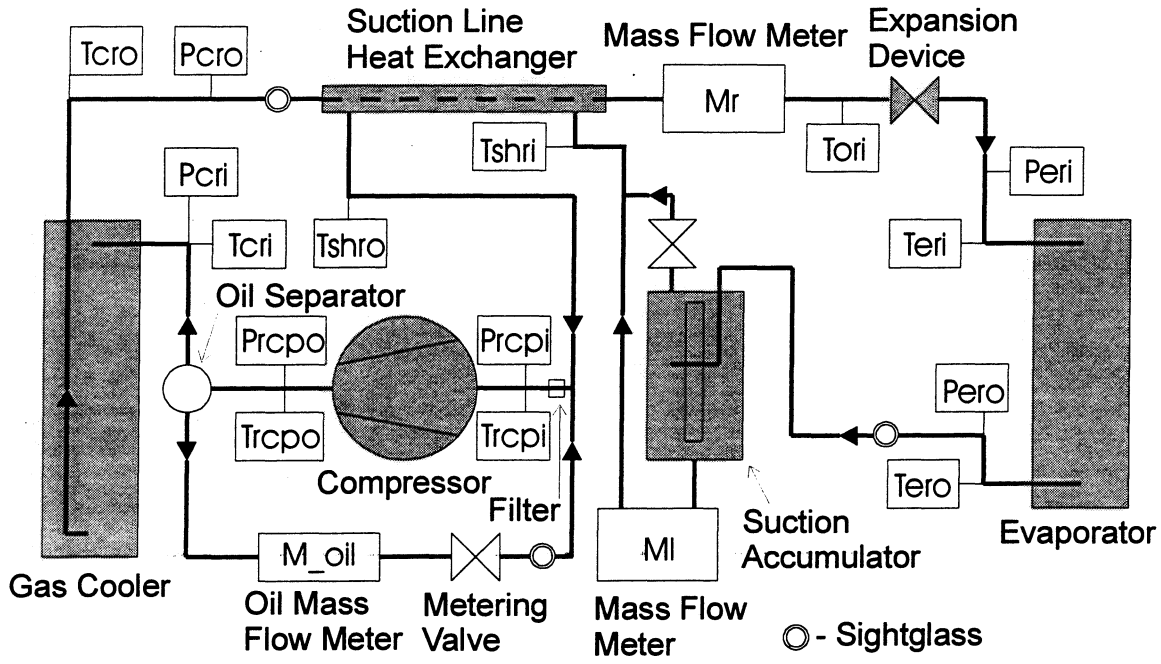

Figure A-3 Schematic of R744 prototype air conditioning system components showing all refrigerant side measurements (excluding compressor torque meter and tachometer).

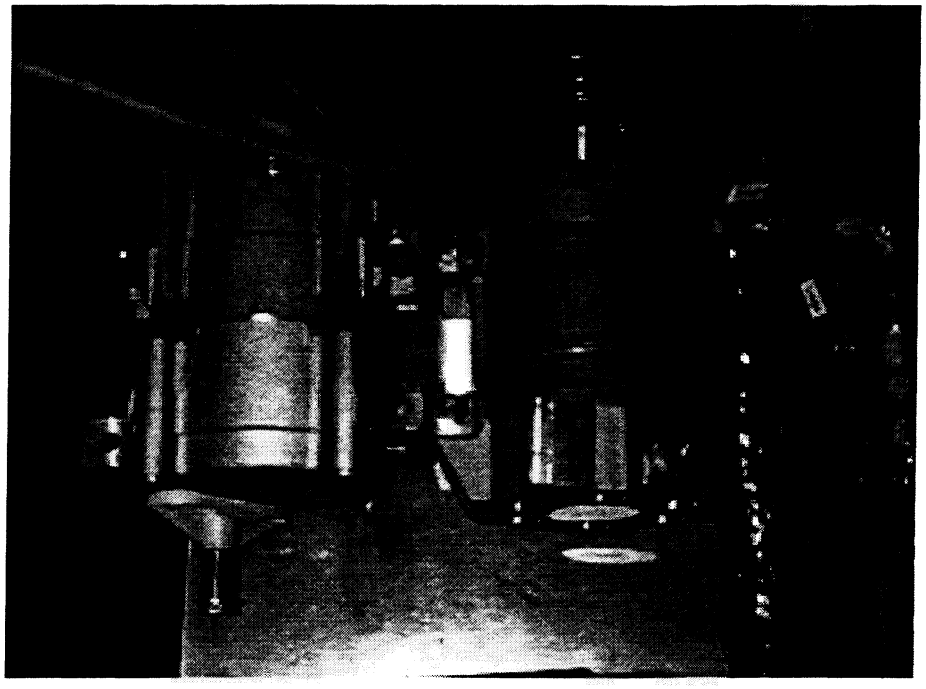

Figure A-4 Photo of R134a compressor (left) and R744 compressor (right) taken to show size comparison. At this time, R744 compressor is connected to refrigeration system being tested.

An oil separator at the compressor discharge returns most of the oil back to the suction line. To control the oil flow, a metering valve is placed in the bypass line. A mass flow meter measures the oil/refrigerant mixture flow rate and density. A sight glass was also used to visualize the flow through the bypass line.

Both compressors are run in steady and cycling conditions. For the cycling conditions, a magnetic clutch taken from the R134a system is used to control the compressor. The purpose of cycling is to prevent the evaporator from frosting. For the R134a system, a low-pressure switch is used to control the status of the compressor. The compressor is cycled off when the switch pressure lowers to around 155±5 kPa. Then, the compressor is cycled back on when the switch pressure comes back up to around 293±25 kPa. This is the actual switch used in the Ford Escort system and is located on the suction accumulator. It reads the actual suction accumulator pressure not the evaporating pressure. During testing, this switch was not changed in any way.

For the R744 system, the cycling was controlled a little differently. Instead of using a pressure switch, cycling was controlled using the exit air temperature of the evaporator. It was found that

the pressures in the system changed too rapidly to be used for good control of the system cycling. The switching temperatures were set based on the exit air evaporator temperatures in the R134a system. In this way, the cycling of the R744 could closely duplicate the R134a system cycle. Cycling is discussed in more detail in Ryan McEnaney's thesis.

A.2 Evaporator

The mobile air conditioning system evaporator is used to remove the heat from the indoor compartment. For the R134a system, the evaporator is a brazed aluminum plate (drawn cup, laminated) heat exchanger with 4 passes and 17 plates. The R134a evaporator is shown in Figure A-5 and described in Table A-2.

Our lab has three prototype R744 evaporators labeled: ZEV1, ZEV2, and ZEV3. All of the evaporators are made of aluminum and have the same dimensions and construction. The core is made of extruded microchannel tubes with louvered fins. The R744 evaporator is constructed with two slabs placed together and connected in series. A R744 evaporator is shown next to the R134a evaporator in Figure A-5. These R744 evaporators were designed to have the same face area, package volume, and airside pressure drop as the R134a evaporator. The only difference in the three evaporators is the number of passes and number of tubes in each pass. The dimensions and characteristics, which are common to all three evaporators, are listed in Table A-2. Profiles of the microchannel tubes and manifolds used in the R744 evaporator are shown in Figure A-6. The differences in passes and tubes per pass for the R744 evaporators are shown in Figure A-7. For all tests ran, the evaporator labeled ZEV2 was used.

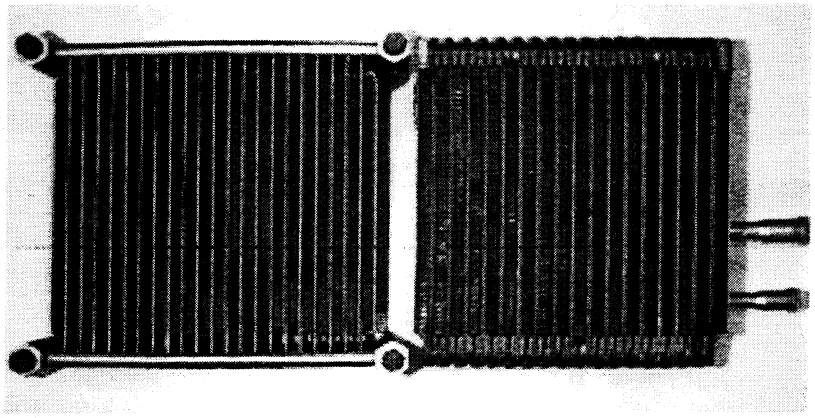

Figure A-5 Picture of R134a evaporator (right) and R744 evaporator (left).

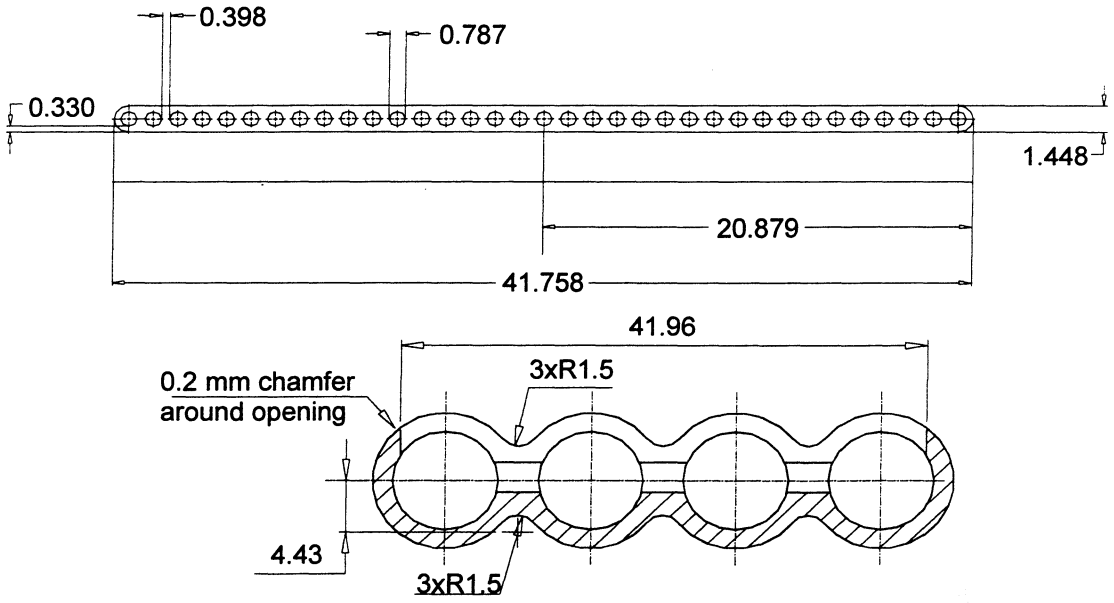

Figure A-6 Profile of evaporator microchannel tube (top) and manifold (bottom). All dimensions in mm.

Table A-2 Dimensions and characteristics of R134a evaporator and all three R744 evaporators.

	R134a Evaporator	**R744 Evaporator**
Description	Brazed Al Plate (drawn cup, laminated)	Microchannel, Brazed Al
Mass (kg)	1.8	2.2
Face Area (cm^2)	405	408
Core Depth (cm)	9.2	9.1
Core Volume (cm^3)	3720	3710
Airside Area (m^2)	3.5	4.2
Refrigerant Side Area (m^2)	0.55	0.67
Fin Density (fins/in)	-	17
Louver Angle (°)	-	30
Tube Length (mm)	-	187
Number of Ports	-	35
Port Diameter (mm)	-	0.787
Web Thickness (mm)	-	0.398
Wall Thickness (mm)	-	0.330
Fin Height (mm)	-	8.79
Fin Thickness (mm)	-	0.10
Louver Height (mm)	-	7.163
Louver Pitch (mm)	-	1.55
Number of Louvers	-	2 x 11
Louver redirection Length (mm)	-	2.6
Louver entry Length (mm)	-	2.6

ZEV1
(Two Slabs, Six Passes)
Second Slab
1st – 6 tubes
2nd – 7 tubes
3rd – 8 tubes
First Slab
4th – 6 tubes
5th – 7 tubes
6th – 8 tubes

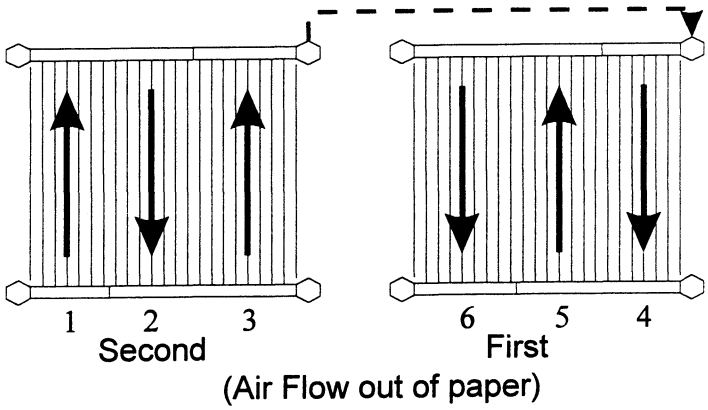

ZEV2
(Two Slabs, Seven Passes)
Second Slab
1st – 4 tubes
2nd – 5 tubes
3rd – 5 tubes
4th – 7 tubes
First Slab
5th – 6 tubes
6th – 7 tubes
7th – 8 tubes

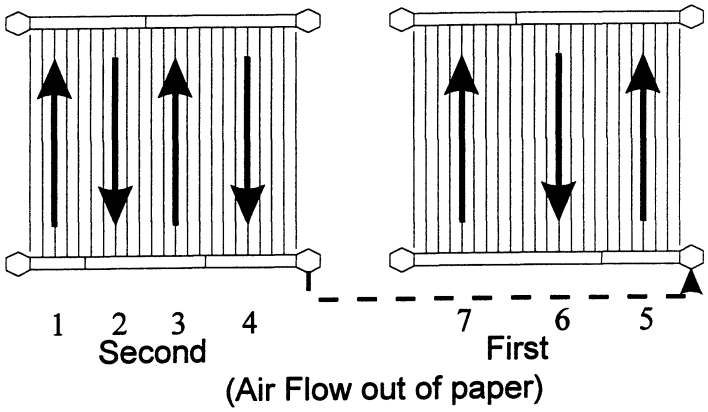

ZEV3
(Two Slabs, Five Passes)
Second Slab
1st – 6 tubes
2nd – 7 tubes
3rd – 8 tubes
First Slab
4th – 10 tubes
5th – 11 tubes

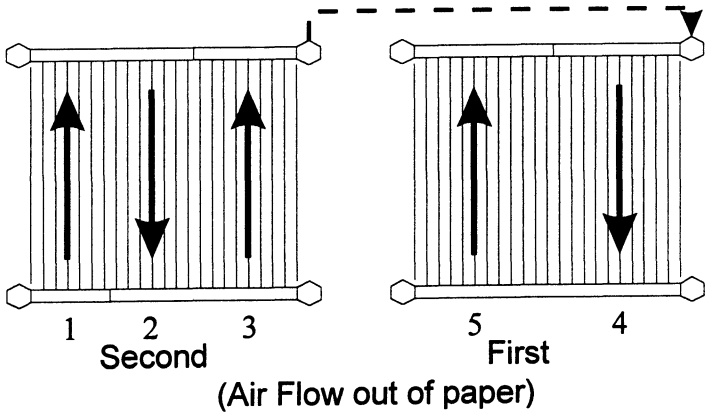

Figure A-7 Schematic showing the number of passes and number of tubes for each of the three evaporators available for use in the mobile air conditioning prototype system. The airflow is out of the paper through the first slab and then the second.

A.3 Condenser/Gas Cooler

The mobile air conditioning system condenser or gas cooler is used to remove heat from the refrigerant to the outside air. For the R134a system, the condenser is an aluminum wavy fin and round tube heat exchanger with 21 passes. The R134a condenser is shown in Figure A-8 and described in Table A-3. For the R744, a gas cooler takes the place of a condenser. The gas cooler operates in the supercritical region in the R744 cycle.

Our lab has three gas coolers labeled: ZGC1, ZGC2, and ZGC3. Each of these gas coolers are have the same dimensions and construction. Each gas cooler is made entirely of aluminum. The core is made up of extruded microchannel tubes with louvered fins. These heat exchangers were designed to have the similar face area, package volume, and air side pressure drop as the off the shelf R134a system. The package volume for the R744 is actually about 3/4 of R134a. The only difference in the three gas coolers is the numbers of passes and number of tubes in each pass. The dimensions and characteristics, which are common to all three gas coolers, are listed in Table A-3. A profile of the microchannel tube used in the gas cooler is shown in Figure A-9. The differences in passes and tubes per pass are shown in Figure A-10. For all tests ran, the gas cooler labeled ZGC2 was used.

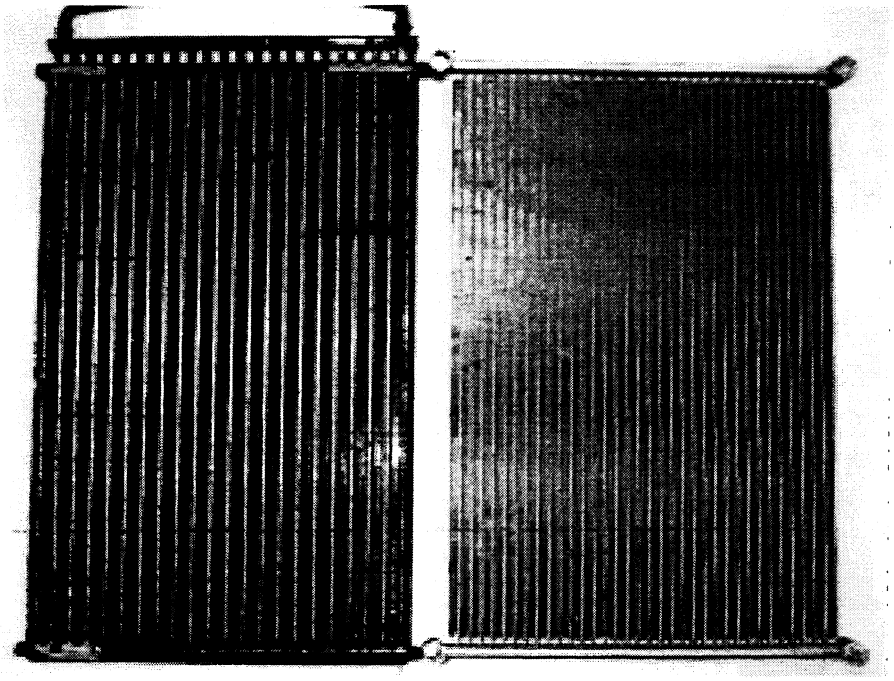

Figure A-8 Picture of R134a condenser (left) and R744 gas cooler (right).

Table A-3 Dimensions and characteristics of R134a condenser and all three R744 gas coolers.

	R134a Condenser	R744 Gas Cooler
Mass (kg)	2.0	2.3[A]
Face Area (cm^2)	1964	1950
Core Depth (cm)	2.2	1.65
Core Volume (cm^3)	4320	3320
Airside Area (m^2)	7.2	5.2
Refrigerant Side Area (m^2)	0.40	0.49
Fin Density (fins/in)	-	22
Louver Angle (°)	-	23
Tube Length (mm)	-	545
Number of Ports	-	11
Tube/Port Diameter (mm)	-	0.79
Web Thickness (mm)	-	0.70
Wall Thickness (mm)	-	0.43
Fin Height (mm)	-	8.89
Fin Thickness (mm)	-	0.10
Louver Height (mm)	-	7.16
Louver Pitch (mm)	-	0.99
Number of Louvers	-	2 x 6
Louver redirection Length (mm)	-	1.7
Louver entry Length (mm)	-	1.7

[A] Weight of gas cooler without aluminum blocks placed at corners for connections

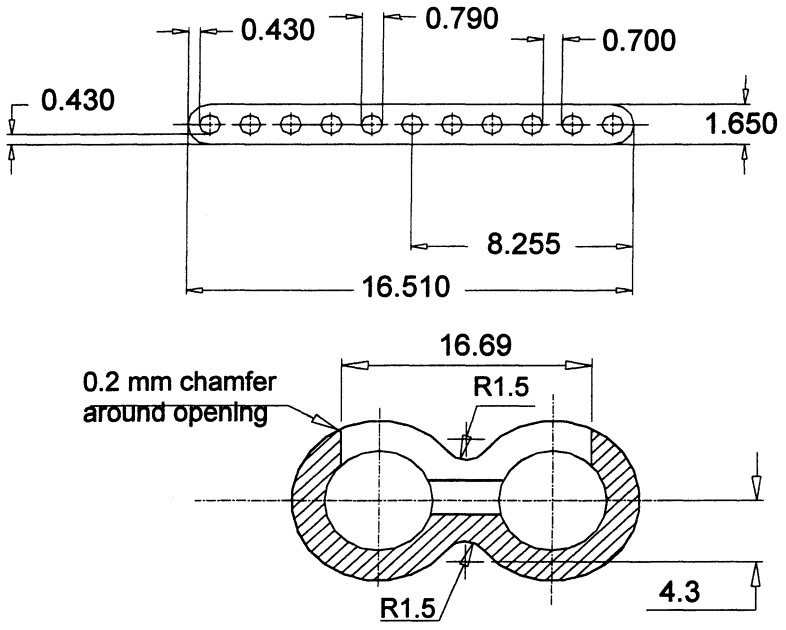

Figure A-9 Profile of gas cooler microchannel tube (top) and manifold (bottom). All dimensions in mm.

ZGC1
Four Passes
1st – 10 tubes
2nd – 9 tubes
3rd – 8 tubes
4th – 7 tubes

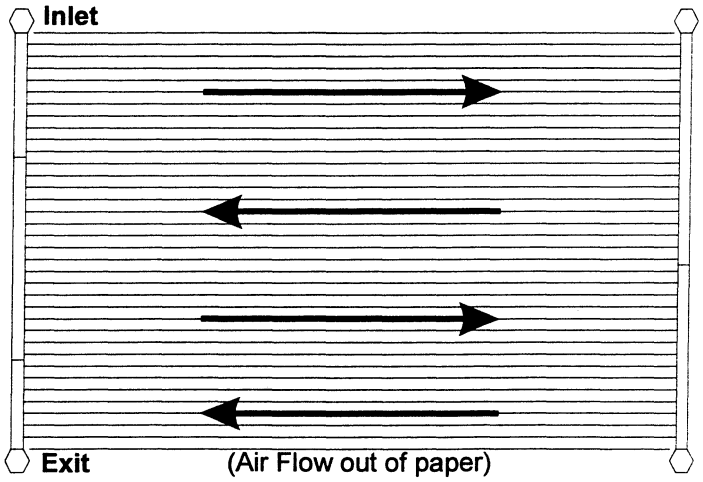

ZGC2
Three Passes
1st – 13 tubes
2nd – 11 tubes
3rd – 10 tubes

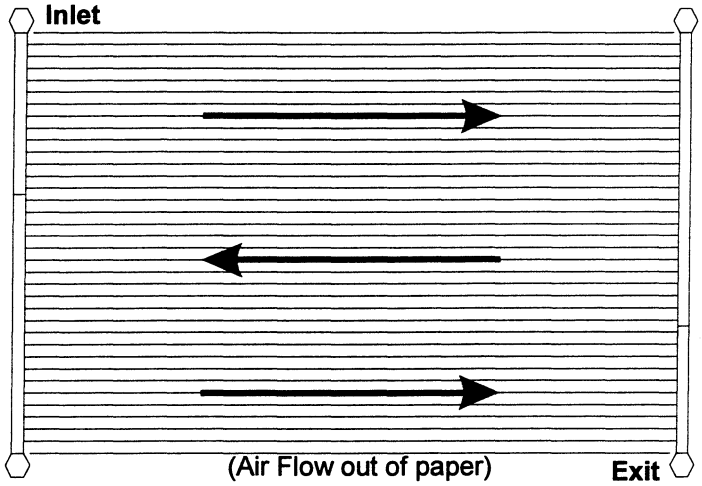

ZGC3
Five Passes
1st – 8 tubes
2nd – 7 tubes
3rd – 7 tubes
4th – 6 tubes
5th – 6 tubes

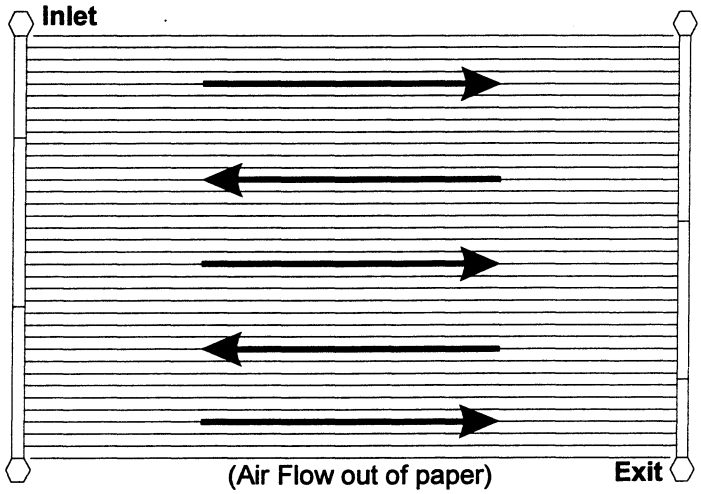

Figure A-10 Schematic showing the number of passes and number of tubes for each of the three gas coolers available for use in the mobile air conditioning prototype system.

A.4 Expansion Device

For the R134a system, a fixed orifice tube is used for the expansion device shown in Figure A-11. The orifice tube consists of a small brass tube molded into plastic with a screen mesh placed at the inlet and outlet of the tube. The screen acts as a filter for the orifice tube. The tube itself has an internal diameter calibrated for this specific R134a system with a fixed orifice diameter of 1.448 mm and length of 38.4 mm. The orifice tube was not changed during the testing of the R134a system.

For the R744 system, a manual valve was used as the expansion device. During the testing period, two different types of manual valves were used. In the beginning, a HOKE® 2300 Series Bar Stock Metering Valve was used. Later a second manual valve was added in parallel to the first valve. The second valve used was a TESCOM® 26-1700 Back Pressure Regulator. These valves are shown in Figure A-12.

Only one valve was used during testing at any given time. During steady state operation, the system performance behaves equally for both types of expansion valves. The pressure reducing valve is better suited during system cycling. This is due to the orifice size changing with the high to low side pressure ratio. This is explained in more detail in Ryan McEnaney's thesis.

A.5 Suction Accumulator

In both systems, a suction accumulator was used at the exit of the evaporator. The suction accumulator would hold the extra refrigerant charge of the system. A picture of the two suction accumulators is shown in Figure A-13. In the R134a system, the accumulator was the original accumulator taken from the Ford Escort system. It was a cylindrical vessel 21.6 cm long with a 9.0 cm radius. The accumulator receives the incoming vapor and oil mixture from the evaporator and the heavier oil separates to the bottom of the vessel. The exit tube of the accumulator draws in a small amount of oil from the bottom of the accumulator, which then goes with the exiting vapor to the compressor. Sight glasses are placed in the inlet and exiting streams to help visualize the R134a/oil mixture. A pressure switch is located at the top of the R134a accumulator which engages the compressor clutch during cycling operation.

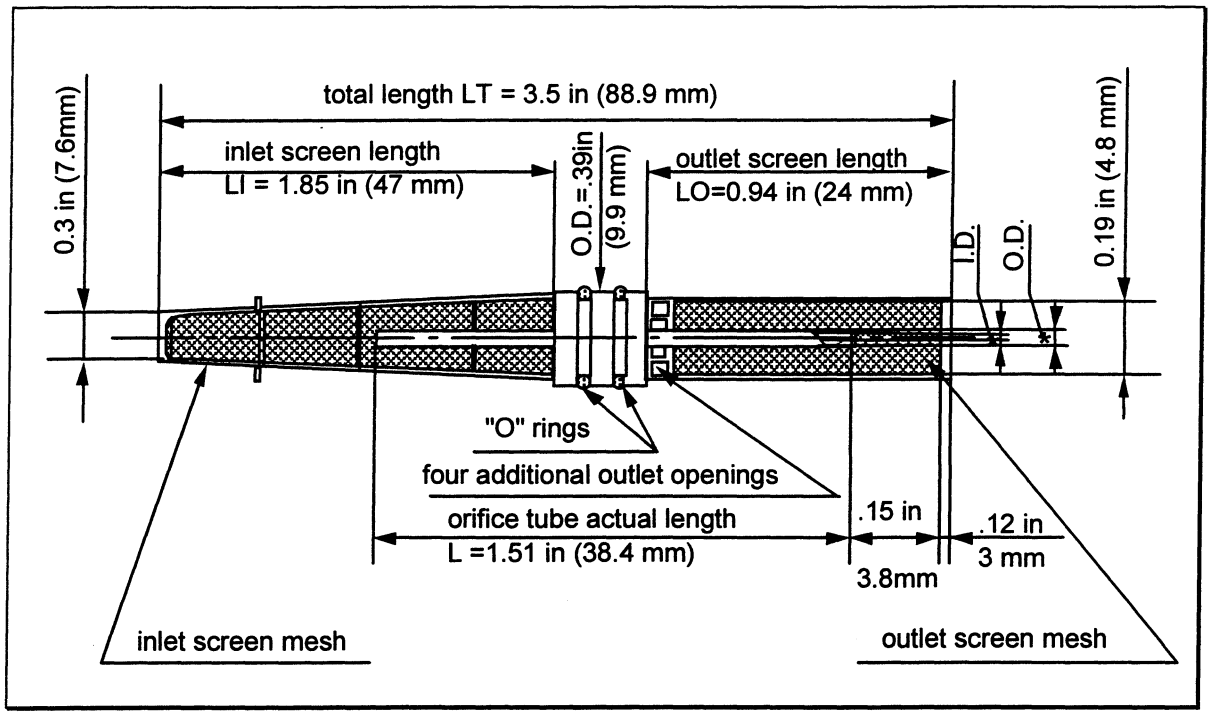

Figure A-11 Schematic of fixed orifice tube used in the R134a system.

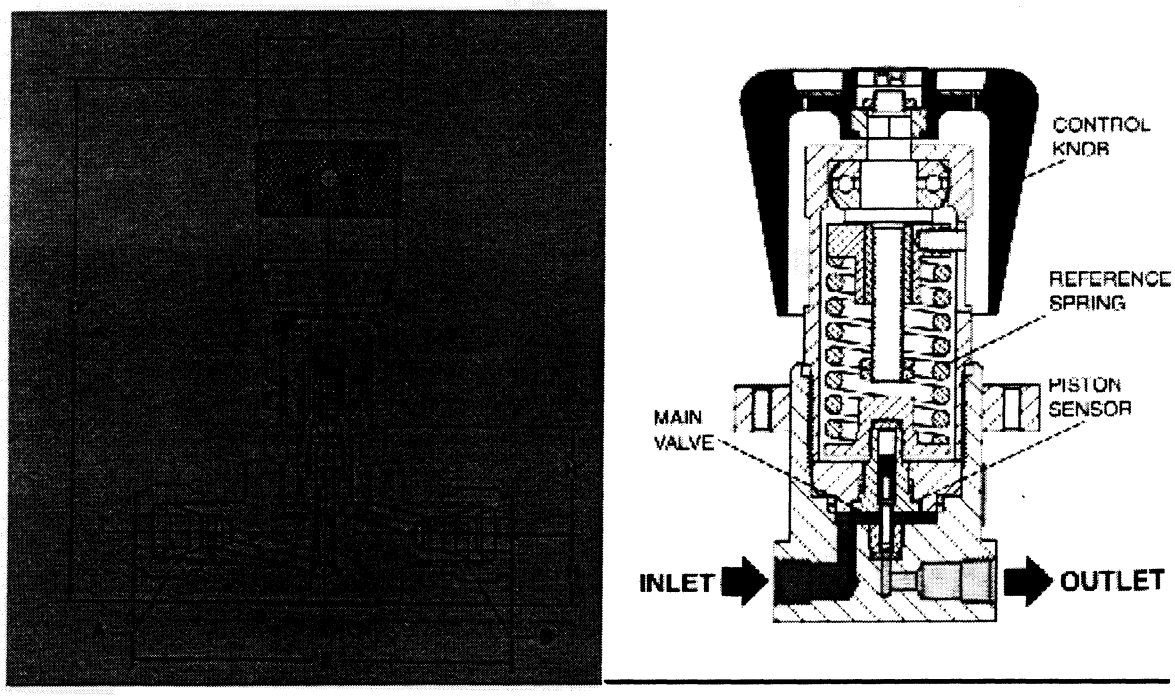

Figure A-12 Schematics of HOKE® 2300 Series Bar Stock Metering Valve (left) and TESCOM® 26-1700 Series Pressure Reducing Regulator (right) used for R744 expansion devices.

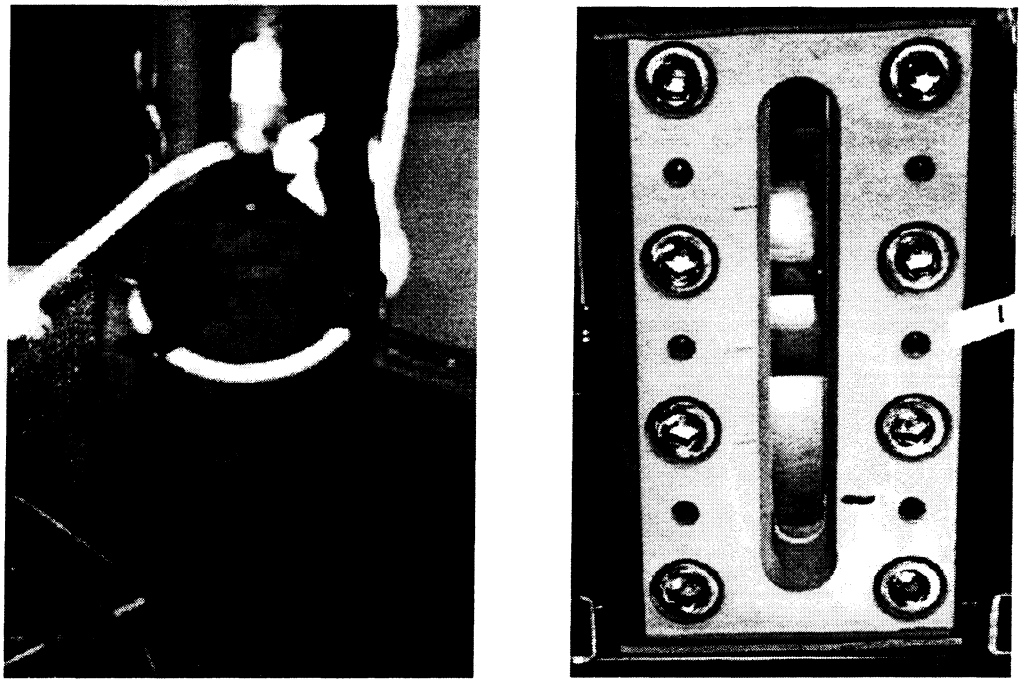

Figure A-13 Picture of R134a suction accumulator (left) and R744 suction accumulator (right).

For the R744 system, a suction accumulator was designed to include a large sight glass in the front and rear, and one more small sight glass in the bottom. The sight glasses are used to visualize the R744 in the accumulator. Inside the accumulator, the oil separates from the R744 to the bottom. The liquid and vapor R744 also separate, with only vapor R744 exiting from the top of the accumulator. A photograph of this separation can be seen in Figure A-14. This accumulator is large and bulky, over designed to suit our visualization purpose. An actual accumulator for the R744 would not to be of this size.

With such high operating pressures, extreme precaution was taken during the design of this vessel. PresSure® Products built and tested the suction accumulator with a rated pressure of 6.9 MPa. The accumulator has an internal volume of 1025 cm^2. The R744 exits the accumulator from the top and the oil exits from the bottom. The exiting oil goes through the mass flow meter located beneath the accumulator and then returns to the exiting R744 flow. The oil flow rate is regulated using a plug valve located in the R744 exit line. The plug valve creates a small pressure drop, which then allows the oil to be drawn from the bottom of the suction accumulator.

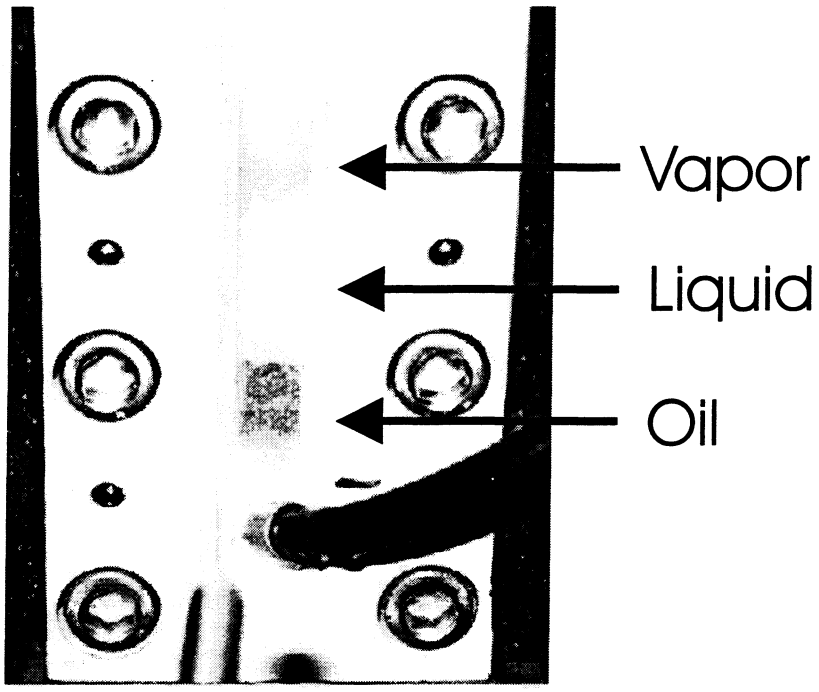

Figure A-14 Visualization of separation of vapor, liquid, and oil in R744 suction accumulator.

A.6 Internal Heat Exchanger

Although the two systems mostly used the similar components, the main difference was the inclusion of the internal heat exchanger in the R744 system. The internal heat exchanger helps the R744 system by increasing capacity and COP while also lowering the high side pressure for optimal performance. The R744 system schematic in Figure A-3 shows the placement of the internal heat exchanger. A photo of the position of the internal heat exchanger in the test system is shown in Figure A-15.

The internal heat exchanger is of the concentric tube type. The hot fluid flows in the inner tube and the cold fluid flows in the outer tube. The internal heat exchanger can be placed in either parallel or counter flow configurations. In the parallel flow arrangement, the hot and cold fluids flow in the same direction. In the counter flow arrangement, the hot and cold fluids flow in opposite directions. The outer tube is divided into six identical straight channels by webs. This

A.7 Valves

Several valves were used for system filling and discharging, component isolation, and flow regulation in the R744 system. The placement of these valves is shown in Figure A-3. The valve selection was based on valve use, operating pressure, material compatibility, and the valve flow coefficient (C_v). Valves placed in the high-pressure side were chosen to have at least a maximum operating pressure of 20 MPa. Valves placed in the low-pressure side were chosen to have at least a maximum operating pressure of 7 MPa. The valve materials were selected to be compatible and not interact with the R744. Buna N or Teflon was used for all sealing components.

For the high-pressure side and oil liquid flows, the valve flow coefficient is defined as the flow in U.S. gallons per minute of room temperature water that will flow through the valve with a pressure drop of 1 PSI across the valve. The valve flow coefficient is calculated using Equation (A.1).

$$C_v = Q\sqrt{\frac{SG}{DP}} \tag{A.1}$$

Where Q is mass flow rate (gal/min), SG is specific gravity of the fluid, and DP is the pressure drop (PSI) across the valve. Equation (A.1) is for liquid flows through valves, and the R744 is in the supercritical range at the expansion valve inlet. This difference could be reason for errors in predicting the pressure drops across the valves. But since we only needed to find the approximate range, this equation was used for the selection of valves on the high-pressure side and expansion valves. Figure A-18 uses this calculation to predict the pressure drop across the high-pressure valves for different R744 mass flow rates with the given valve flow coefficient.

For the low-pressure side, the flow calculations and charts differ due primarily to the compressibility. The valve flow coefficient is now calculated using Equation (A.2)

$$C_v = 16.05Q\sqrt{\frac{SG*T}{\left(P_1^2 - P_2^2\right)}} \tag{A.2}$$

increases the surface area and improves the heat transfer between the hot and cold fluids. A cross section of the internal heat exchanger used in all tests is shown with dimensions in Figure A-16.

Three separate internal heat exchangers were available for use while testing the R744 system. Each had the same cross section design with only a change in the heat exchanger length. The three lengths were 1.0 m, 1.5 m, and 2.0 m, with weights of 0.9 kg, 1.5 kg, and 1.8 kg respectively. They were all made from extruded aluminum.

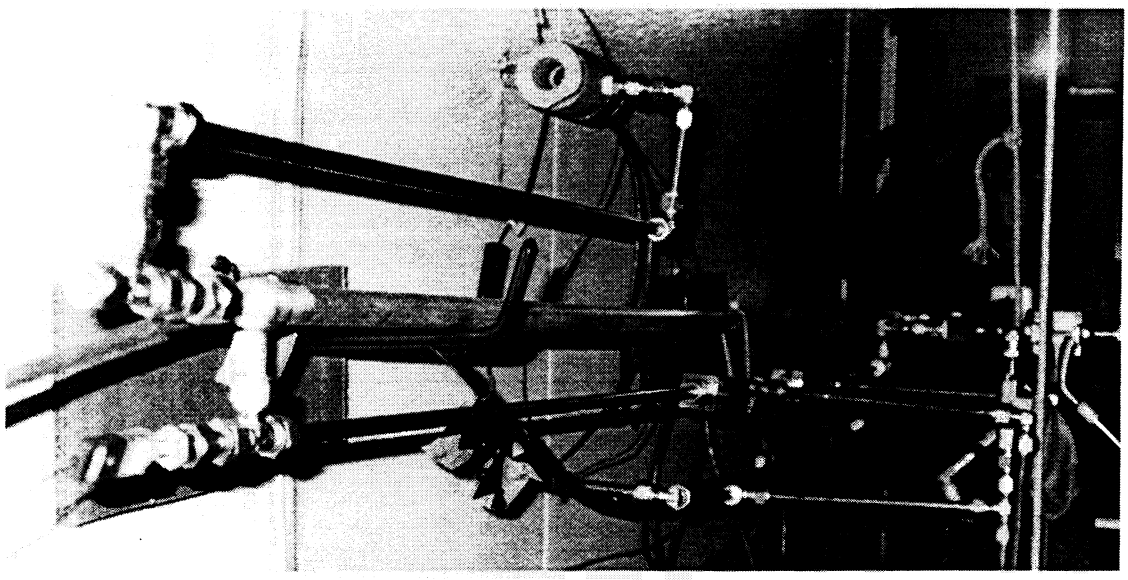

Figure A-15 A view of the suction line heat exchanger located on the wall of the environmental chamber.

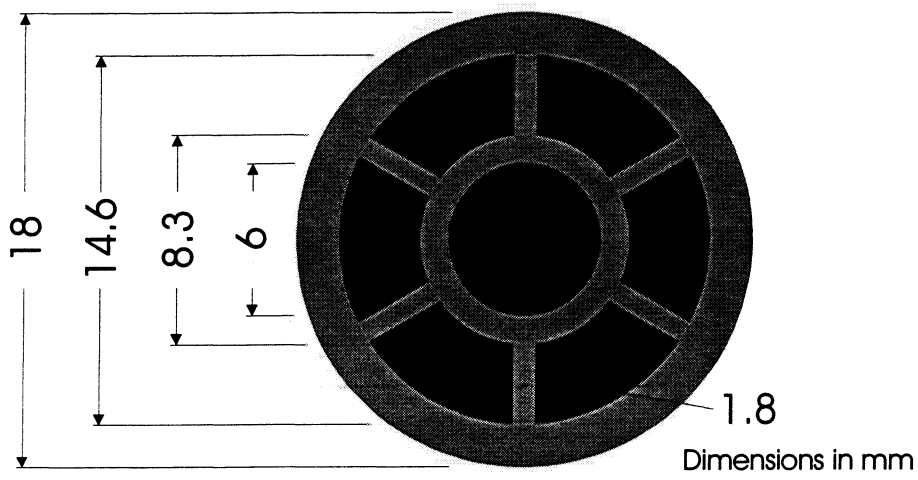

Figure A-16 A cross section of the internal heat exchanger used in all tests. The high pressure gas cooler exit flows through the inner tube and the low pressure accumulator exit flows through the outer channels.

where P_1 and P_2 are the inlet and outlet pressures (PSI) respectively, and T is the absolute temperature (°F+460) of the flowing gas. When the outlet pressure is approximately one half or less of the inlet pressure ($P_2 = 0.53P_1$), this condition becomes known as a critical pressure and then the valve flow coefficient formula becomes Equation (A.3) where P_1 is now $0.53P_1$.

$$C_v = 13.61Q\frac{\sqrt{SG*T}}{P_1} \qquad \textbf{(A.3)}$$

Figure A-19 uses Equation (A.2) to predict the pressure drop across low-pressure valves.

The type of valve used most in the R744 system is a Hoke® 7300 Series quarter-turn stainless steel plug valve. These plug valves are unidirectional valves with a maximum operating pressure of 20.7 MPa. They have a temperature range of –29°C to 205°C, which suits this application. The valve easily disassembles for quick replacement of all o-rings. One valve is used for filling and another one for discharging of the refrigerant in the system. This type of valve also has a low-pressure drop with a C_v of 0.74 when fully open and is used for compressor isolation with one at the inlet and one at the exit. The last use of this valve is to create the small increase in pressure drop at the R744 vapor exit of the suction accumulator in order to regulate the oil flow rate coming from the bottom of the suction accumulator.

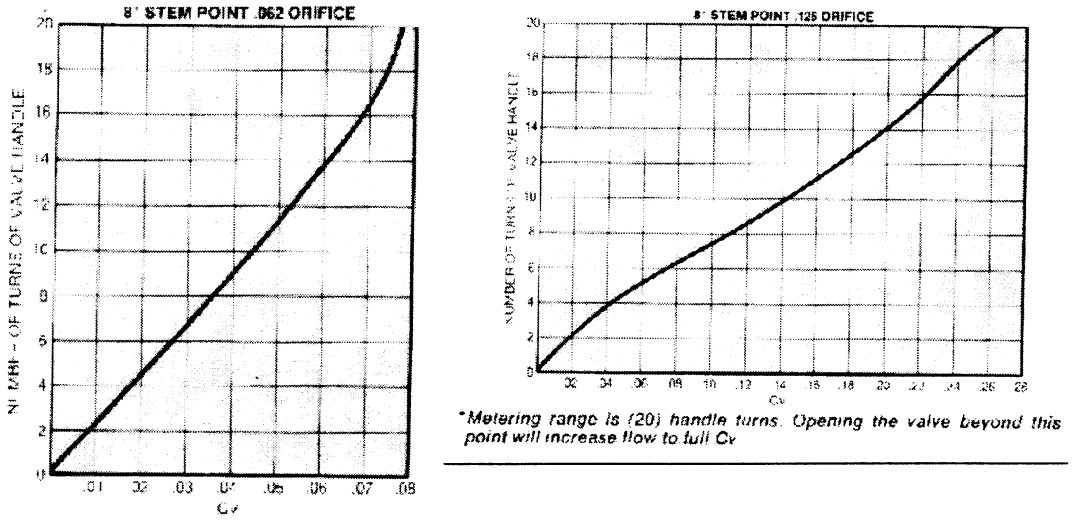

Figure A-17 Flow curves for the metering valve used as expansion device (left) and oil flow regulator (right). Graphs provided by HOKE®.

The other type of valve used in the system is a Hoke® 2300 Series bar stock metering valve. This type of valve is used for both the expansion device and regulation of the flow rate in the oil bypass to the compressor. The meter valve has a maximum operating pressure of 24.2 MPa at 93°C and a temperature range of –40°C to 93°C. The C_v curves for the two metering valves used are shown in Figure A-17.

A.8 Pipes

In order to get as close to the actual R134a system as possible, the components were not modified in any way. The only exception to this was the piping. The pipe dimensions for the R134a system are given in Table A-4 along with the original off the shelf system. The tube diameters were not changed, but the original pipe lengths were modified due to component placement in the test facilities.

Burst pressure and estimated pressure drop were used for pipe selection in the R744 system. On the high-pressure side, the selected pipes were 9.5 mm outside diameter with a wall thickness of about 1.6 mm. This pipe has a calculated burst pressure of 83.0 MPa. The pipe was connected using compression fittings. On the low-pressure side, the selected pipes were 9.5 mm outside diameter with a wall thickness of about 0.8 mm. This pipe has a calculated burst pressure of 37.9 MPa. The burst pressure data was taken from tubing data charts from HOKE®. The low-pressure pipes were also connected with compression fittings, but were bent at as many of the turns as possible. This was done to try to reduce pressure drop on the low side.

Table A-4 Connecting line dimensions for R134a and R744 systems.

Location	Original R134a Pipe Length (mm)	Modified R134a Pipe Length (mm)	R134a Inside Pipe Diameter (mm)	R744 Pipe Length (mm)	R744 Inside Pipe Diameter (mm)
Evaporator – Accumulator	1120	1440	12.7	1450	7.9
Accumulator – Compressor	610	1080	12.7	4500[A]	7.9
Compressor – Condenser	960	2210	9.5	2990	6.3
Condenser – Expn. Device	660	2740	9.5	5000	6.3
Expn. Device - Evaporator	1780	1510	9.5	990	6.3

[A] This includes 1.5 m suction line heat exchanger. Without suction line heat exchanger, length is 2260 mm.

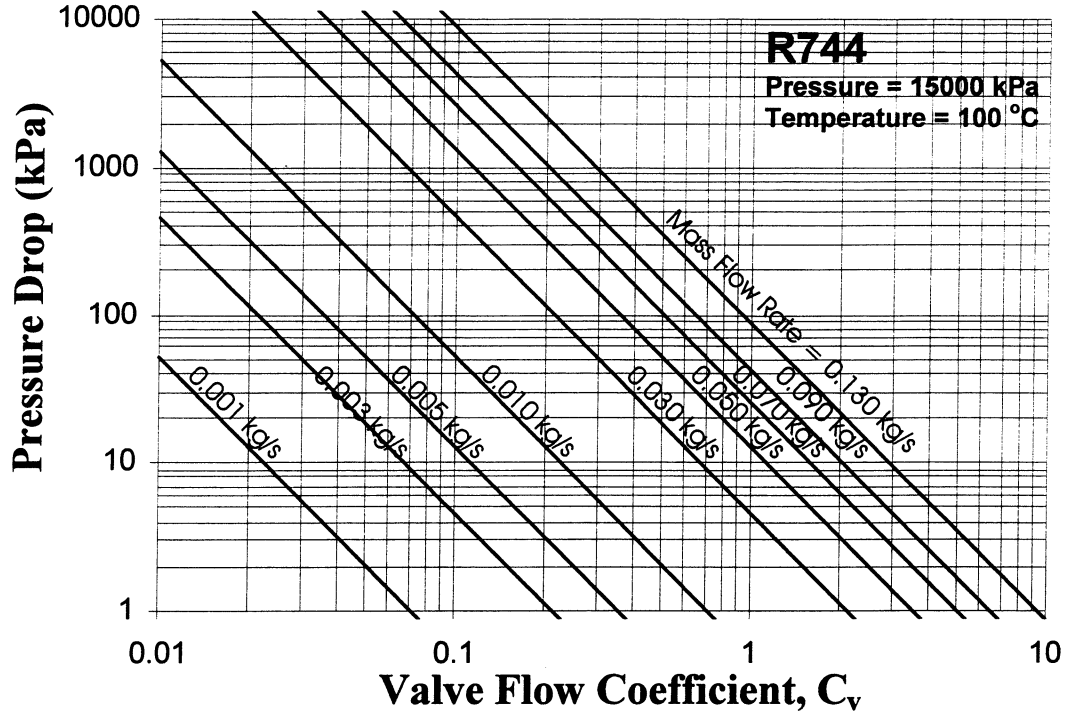

Figure A-18 Pressure drop predictions used in selection of valves placed on high-pressure side of R744 system.

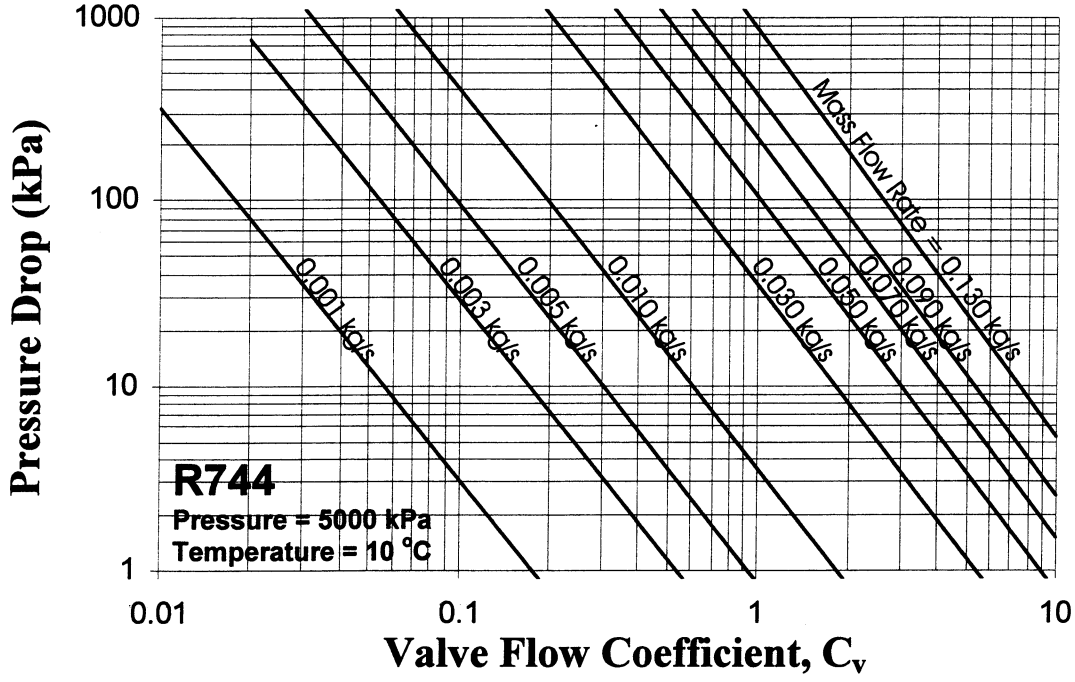

Figure A-19 Pressure drop predictions used in selection of valves placed on low-pressure side of R744 system.

A.9 Sight Glasses

In both the R134a system and the R744 system, sight glasses were used in various locations to visualize the refrigerant. In the R134a system, the sight glasses were See•All® Moisture and Liquid Indicators. They were placed directly into the flow of the refrigerant. One sight glass was placed at the exit of the condenser, inlet of the evaporator, exit of the evaporator, and exit of the accumulator.

In the R744 system, Bull's-Eye See-Thru sight glasses, shown in Figure A-20, made by PresSure® Products were used. On the high-pressure side, the sight glass had a maximum operating pressure of 20.7 MPa and was located at the gas cooler exit. On the low-pressure side, the sight glasses had a maximum operating pressure of 6.9 MPa and were located at the evaporator exit shown and compressor oil bypass line. Also, the R744 suction accumulator had a large sight glass in the front and rear.

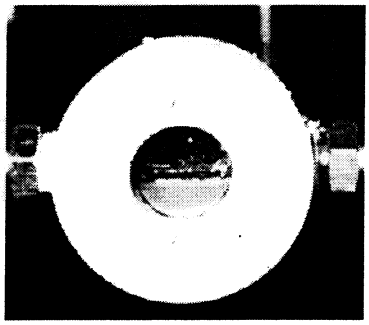

Figure A-20 Picture of sight glass located after evaporator in the R744 system. (System was not running at time of picture.)

Appendix B – Environmental Chambers

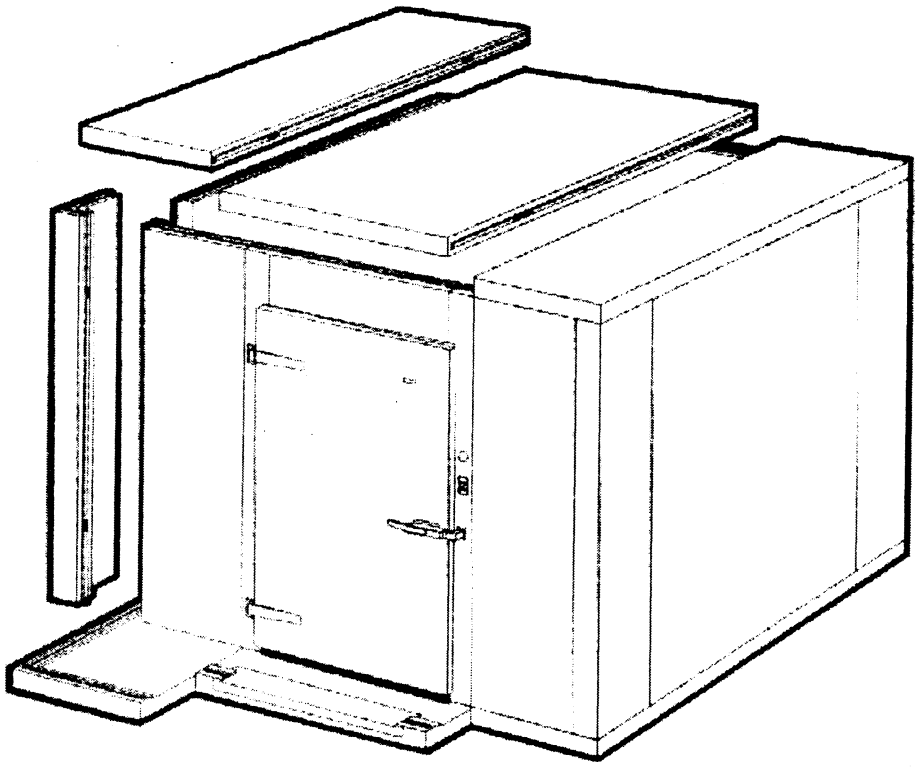

Figure B-1 Blow up of environmental chamber used in mobile air conditioning lab.

B.1 Evaporator and Condenser/Gas Cooler Chambers

The evaporator and condenser/gas cooler environmental chambers are Tyler walk-in coolers. Each chamber is constructed of 10.2 cm Class 1 Urethane panels with galvanized stucco embossed on interior and exterior of the panels. The prefabricated panel sections are assembled in the final location. Figure B-1 shows a blow up of a chamber. The panel sections are fastened together using lock and pin housings located inside the insulated panels as shown in Figure B-2. A hex cam wrench is used to turn the camlock in a clockwise direction to lock the two panels together.

The interior dimensions of the evaporator chamber is 3.55 m long x 1.83 m wide x 2.45 m high and the condenser/gas cooler chamber is 3.55 m long x 2.13 m wide x 2.45 m high. The door for each chamber measures 0.92 m x 2.13 m.

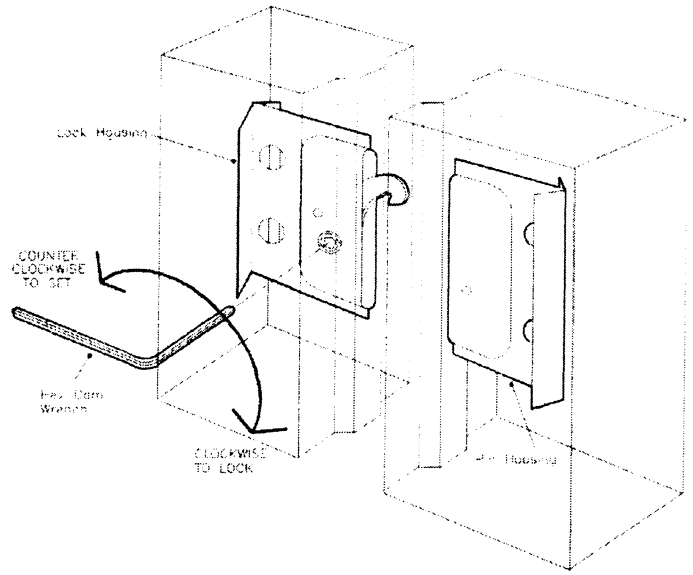

Figure B-2 Illustration of the panel locking system in the Tyler walk-in cooler.

Each chamber has added insulation to increase the overall R-value of the walls and ceiling. The insulation was added to the interior of the walls and to the exterior of the ceiling. Three layers of 5.1 cm polystyrene insulation and one layer of 5.1 cm Celotex insulation plus the 5.1 cm urethane make up the 30.5 cm thick walls of the chamber. The thermal conductivity of the urethane is 0.023 W/m K, polystyrene is 0.029 W/m K, and Celotex is 0.019 W/m K, which gives each chamber surface a total thermal conductivity of 0.025 W/m K.

The condenser/gas cooler chamber was calibrated to determine the heat loss through the walls. This calibration was used to determine the heat transfer coefficients of each surface. Each surface temperature was measured using welded type T thermocouples fixed to the interior and exterior surfaces of the chambers. To correlate the data, three temperature differences are used: wall, ceiling, and floor. On each wall surface, one thermocouple is installed at the center on the interior and exterior to yield the temperature difference. The four thermocouples inside and outside are averaged separately during the data taking process. Five thermocouples are used for each interior and exterior surfaces of the floor and ceiling. The average deviation of the calibration data is 0.8% with a maximum deviation of 1.7%. The calibration is shown in Figure B-3. The determined values of heat transfer coefficients were then carried over to the evaporator chamber calculations.

The overall heat loss due to transmission is the sum of the heat lost through each wall, ceiling, and floor. Equation (B.1) is the overall heat lost due to transmission.

$$Q_{tr} = U_f A_f \Delta T_f + U_w A_w \Delta T_w + U_c A_c \Delta T_c \quad \textbf{(B.1)}$$

where U is the heat transfer coefficient, A is the surface area (m^2), and ΔT is the temperature difference (°C) from inside to outside of surface for the floor, wall, and ceiling. Table B-1 gives the values of the heat transfer coefficients and surface areas for the evaporator and condenser/gas cooler chamber. For these chambers, overall heat losses are about 21.5 % through the walls, 28.5% through the ceiling, and 50% through the floor. The transmission losses are still only about 5% of the overall chamber energy balance.

Table B-1 Heat transfer coefficients and surface areas for transmission losses in environmental chambers.

	Heat transfer coefficient (W/m^2 °C)	Condenser/Gas Cooler Chamber Surface Area (m^2)	Evaporator Chamber Surface Area (m^2)
Floor	0.754	7.58	6.49
Ceiling	0.170	7.58	6.49
Walls	0.064	27.9	26.4

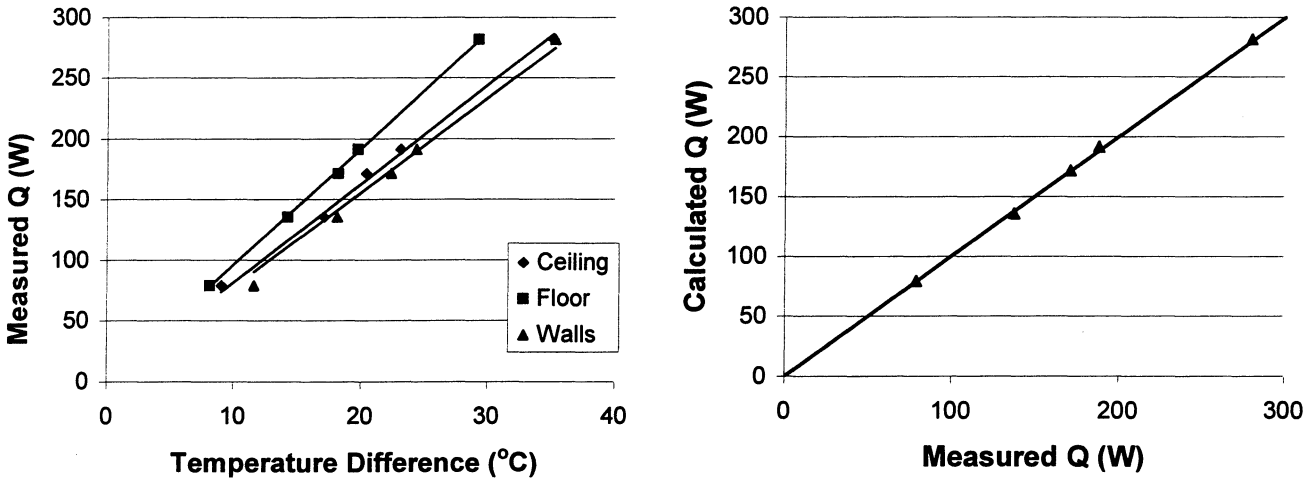

Figure B-3 Plot of data taken to calibrate the condenser chamber (left). Plot of measured heat transmission loss verses calculated loss using calibrated U values.

B.2 Compressor Chamber

The compressor stand is located inside a small chamber, which is constructed from 10.2 cm thick urethane panels. The compressor chamber is used to keep the surrounding air temperature of the compressor closer to actual under hood conditions. The panels are the same type used in the construction of the evaporator and condenser/gas cooler chambers. The internal dimensions of the chamber are approximately 1.2 m long x 0.7 m wide x 1.1 m high.

Appendix C - Evaporator and Condenser/Gas Cooler Wind Tunnels

The evaporator and condenser/gas cooler are each mounted in separate wind tunnels inside the environmental chambers. The same wind tunnels were used for both the R134a and R744 systems. A schematic of the test facility is shown in Chapter 2, Figure 2-1, and each component of the wind tunnels is discussed in more detail in the following section. The refrigerant heat exchangers are discussed in Appendix A.

C.1 Ducts

Both wind tunnels are constructed from sheet metal ducts. The duct sections for the evaporator wind tunnel are shown in Figure C-1 and listed in Table C-1. The evaporator ducts are insulated with 5 cm of Armoflex sheet insulation from the first thermocouple grid to just past the nozzle. The Armoflex insulation has a thermal conductivity of 0.039 W/m K. The duct sections for the condenser/gas cooler wind tunnel are shown in Figure C-2 and listed in Table C-2. The condenser/gas cooler ducts are insulated with 5 cm of Armoflex sheet insulation from the air inlet to just past the nozzle.

C.2 Air Straightener

Both the evaporator and condenser/gas cooler wind tunnels use air straightener to aid in getting a uniform airflow into the heat exchanger. The air straightener is 15 cm long and made of aluminum. The air straightener is located at the inlet of the wind tunnel before both the heat exchanger and thermocouple grid.

C.3 Thermocouple Grid

A thermocouple grid is located at the inlet and exit of the heat exchanger. The grid is made up of welded type T thermocouples averaged together to get a representative air temperature. The evaporator duct is divided into 9 equal sections with one welded thermocouple located at the center of each. The condenser/gas cooler duct is divided into 27 equal sections with one welded thermocouple located at the center of each.

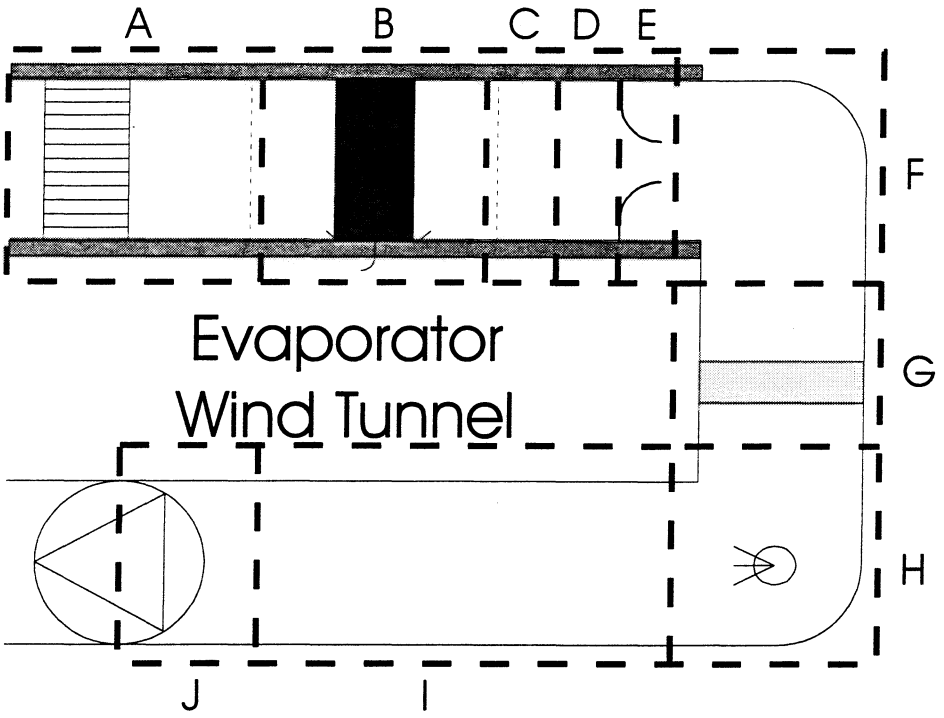

Figure C-1 Evaporator wind tunnel duct sections with wind tunnel components included.

Table C-1 Evaporator wind tunnel duct sections.

Test Section	Description	Length (cm)	Width (cm)	Height (cm)
A	Inlet duct w/flow straightener and inlet thermocouple grid	50	25	23
B	Evaporator test section	30	25	23
C	Expanding section w/exit thermocouple grid	30	-	-
D	Straight section inlet to nozzle	35	30	46
E	Straight section exit of nozzle	35	30	46
F	90° elbow section, 50 cm radius to outside edge	-	30	46
G	Straight section w/heaters	45	30	46
H	90° elbow section, 50 cm radius to outside edge, w/humidifier steam inlet	-	30	46
I	Straight section	90	30	46
J	Reducing section to 15 cm blower inlet diameter	30	-	-

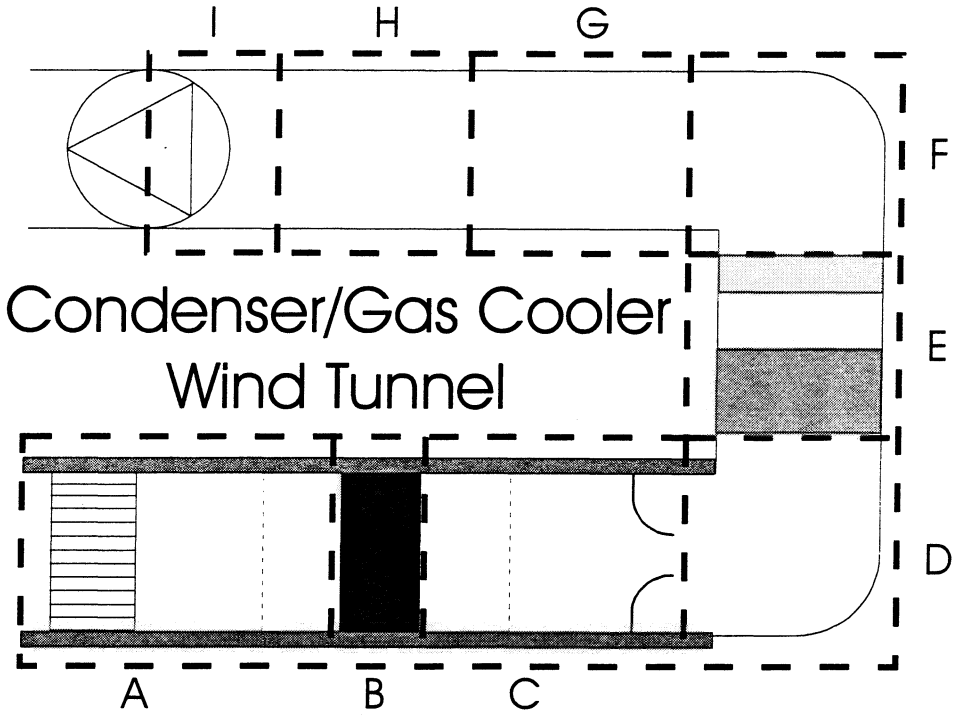

Figure C-2 Condenser/gas cooler wind tunnel duct sections with wind tunnel components included.

Table C-2 Condenser/gas cooler wind tunnel duct sections.

Test Section	Description	Length (cm)	Width (cm)	Height (cm)
A	Inlet duct w/flow straightener and inlet thermocouple grid	60	55	37
B	Condenser/Gas Cooler test section made of wood	5	55	37
C	Straight section w/exit thermocouple grid and nozzle	90	55	37
D	Reducing 90° elbow section, 50 cm radius to outside edge	-	-	-
E	Straight section w/cooling coil and heaters	34	61	31
F	Expanding 90° elbow section, about 50 cm radius to outside edge	-	-	-
G	Straight section	75	92	46
H	Straight section	55	92	46
I	Reducing section to 18 cm blower inlet diameter	40	-	-

C.4 Nozzles

The evaporator and condenser wind tunnels are both equipped with two identical nozzles. These nozzles are used to determine the air flow rate. Depending upon the desired flow rate, either both or only one nozzle is used. The nozzles for the evaporator wind tunnel have a 2.5" nominal diameter. The nozzles for the condenser wind tunnel have a 6.0" nominal diameter. The nozzles installed in wind tunnels comply with ANSI/ASHRAE Standard 40-1986. The following equations are used to determine the air flow rate.

$$v'_n = \frac{101.3 v_n}{(1+\omega_m)P_B} \tag{C.1}$$

$$Q_m = CA\sqrt{2P_v v'_n} \tag{C.2}$$

where,

Q_m	air flow rate (m^3/s)
C	nozzle discharge coefficient (0.98)
A	nozzle throat area (m^2)
P_v	pressure drop across the nozzle (Pa)
v'_n	specific volume of air at nozzle (m^3/kg)
v_n	specific volume of air at dry and wet bulb temperature conditions existing at nozzle but at standard barometric pressure (m^3/kg)
ω_m	humidity ratio of air at nozzle (kg water/kg dry air)
P_B	barometric pressure (kPa)

Each nozzle temperature is measured using a single welded type T thermocouple placed in the center of the exiting air stream. The pressure drop across the nozzle is measure using a Setra differential pressure transducer. The evaporator nozzle pressure transducer has a range of 0 to 250 Pa, and the condenser/gas cooler nozzle pressure transducer has a range of 0 to 625 Pa.

C.5 Heaters

The inlet air temperature is maintained constant using strip heaters placed directly into the airflow. A power controller and PID control the heaters to keep the air temperature at the test condition. In the evaporator wind tunnel, six 1.5 kW strip heaters are used to replace the heat taken by the evaporator.

In the condenser/gas cooler chamber, the heat added by the condenser/gas cooler is removed using a cooling coil. The only control on the cooling coil is the chilled liquid mass flow rate and is not easy to set to the exact required amount of cooling. Therefore, the cooling coil is actually set up to remove more heat than necessary and three additional 1.5 kW strip heaters are installed to bring the air temperature back up to the test condition. The heaters are controlled using a power controller and a PID.

C.6 Blowers

In both wind tunnels, the air flow is induced by connecting the duct to the inlet to a blower. The blower then sucks air through the duct (and all components). The blowers used are Dayton high-pressure, direct-drive blowers. For the evaporator wind tunnel, the blower has 15.2 cm circular inlet and 10.2 cm x 8.9 cm rectangular exit. The motor is a Dayton 3 phase, 1 HP motor with a maximum of 3450 rpm. For the condenser/gas cooler wind tunnel, the blower has a 17.8 cm circular inlet and a 12.7 cm x 10.2 cm rectangular exit. The motor is a Reliance Electric 3 phase, 5 HP motor with a maximum of 3500 rpm. For both wind tunnels, the blowers are controlled using a speed controller. The speed of the blower motor is set and the air flow rate is calculated from the nozzle measurement.

C.7 Humidifier

For the evaporator wind tunnel, the inlet humidity must be controlled and maintained. A humidifier is installed outside of the chamber and steam pipes go through the chamber wall into the duct before the blower. The steam pipes are insulated and configured to drain any condensed water outside of the chamber and only steam goes into the chamber.

The humidifier is a Standard Water "PS" Series Electric Humidifier made by Pure Humidifier Company. The humidifier consists of a tank with an immersion heater inside. The tank is filled with ordinary tap water. The "PS" Series utilizes a tri-probe conductive type water control system, which is designed for use with standard (hard or soft) tap water. The water level is controlled using the LC-942 water level controller. The LC-942 water level controller is a solid state logic controller, which controls the water level, fill, drain and safety circuit interlocks. The system also includes an automatic drain cycle that is not used.

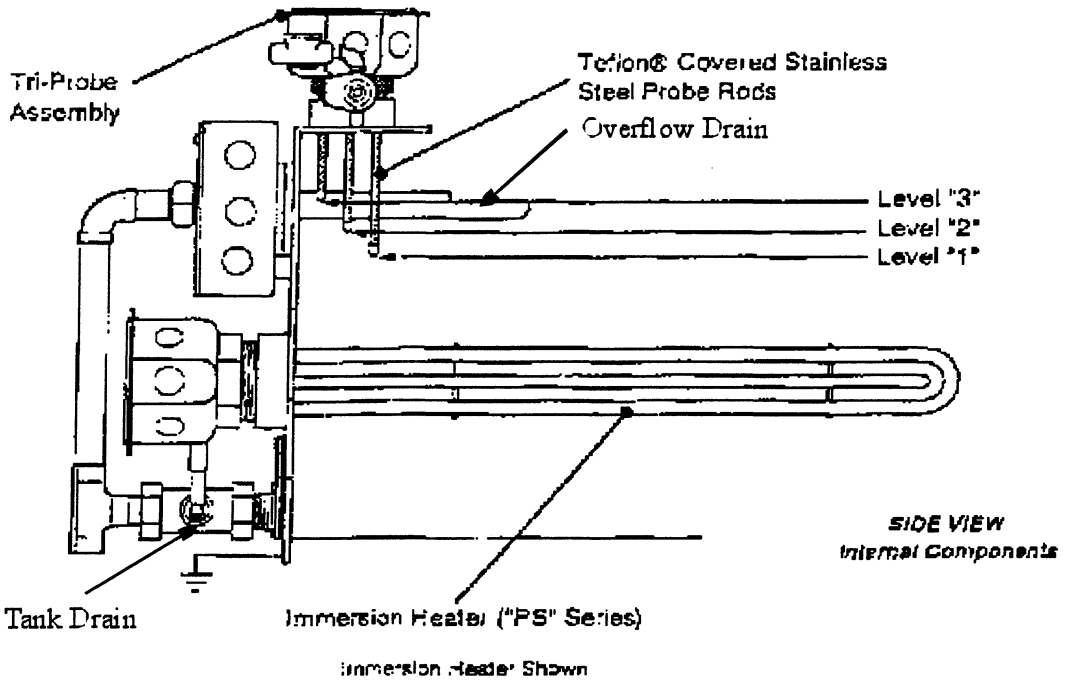

Figure C-3 Side view of internal components of humidifier.

The humidifier, shown in Figure C-3, has been modified to prevent the heater in the humidifier from cycling on and off. The tri-probe sensors inside the humidifier tank control the status of the humidifier. The water level of the tank triggers the sensors on and off. The top sensor (level "3") turns the heater on and the water fill off, the middle sensor (level "2") turns the water fill on, and the bottom sensor (level "1") turns the heater off. To prevent the sensor from cycling the water and heater on and off, the top sensor (level "3") can be disabled using a toggle switch located on the outside of the electrical control box. This allows the heater and water fill to remain on. The excess water flows out an overflow drain located at the top of the humidifier.

During normal operation, a switch located on the inside of the electrical box should be set to the 'normal operate' position. When the power to the humidifier is turned on, the humidifier automatically starts running. It is now necessary to make the humidifier run in a steady state mode (no cycling). The following steps are to start the humidifier and get to a steady state mode of operation.

1) Power up humidifier.
2) Put toggle switch in 'on' position.
3) 'Fill' light is on.
4) The humidifier fills until the 'heat ready' light comes on and the 'fill' light goes off.
5) Open the tank drain until the 'fill' light comes on.
6) Put toggle switch in 'off' position.
7) Let water fill to overflow drain.
8) Slow water flow rate to minimize overflow.

The humidifier may start in the middle of these steps due to the level of the tank. The humidifier will take some time to warm up before steam will go to the evaporator chamber. To aid this process, a water heater has been installed at the water inlet to the humidifier. The water heater is a 'point of use' water heater made by Ariston. The water heater has an adjustable thermostat from 18°C to 80°C.

C.8 Condensate Collection Stand

Condensate is collected from the exit of the evaporator. The condensate is then gravity fed from the bottom of the duct out of the chamber to the condensate collection stand shown in Figure C-4. The condensate is then collected in a bucket and weighed using an Omega strain gauge. The strain gauge has a maximum of 2.27 kg weighing capacity. The change in weight divided by time is used as the condensate flow rate. The strain gauge outputs a reading to both a Sensotec digital display and to the data acquisition system. In addition, the temperature of the exiting condensate is measured using a welded type T thermocouple. The temperature is measured in a water trap in the condensate line in order to get only the liquid temperature measurement. These numbers are used in the calculation of the evaporator chamber and in the air side energy balance.

C.9 Cooling Coil and Chiller System

A cooling coil is used to extract heat from the condenser/gas cooler chamber. The cooling coil is connected to a chiller system located on the roof outside the window. The chiller system consists of two chillers and two pumps. An aqueous ethylene glycol solution is pumped from the chillers to the chambers to achieve the desired level of cooling. The mobile and residential systems receive their cooling capacity from the chiller system. The chiller system can operate either independently for each lab (mobile and residential) or jointly for the both.

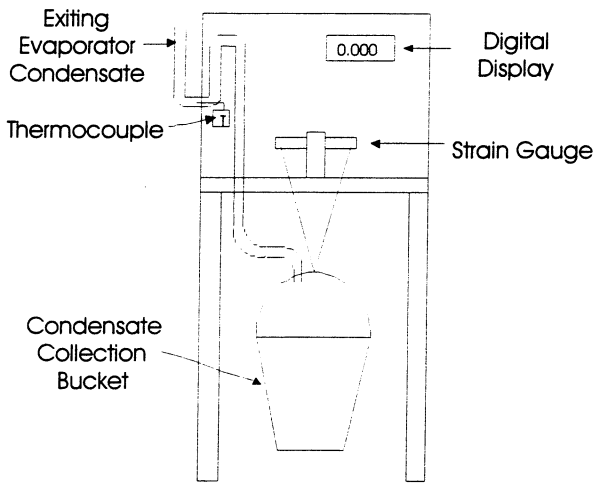

Figure C-4 Schematic of condensate collection stand.

Each chiller is a Continental Packaged Air Cooled Chiller Model CCA-5E. The chillers are charged with R-22 and cool an approximate 50% solution of aqueous ethylene glycol. Each chiller has an automatic low temperature shutoff that can be adjusted. This low temperature shutoff is located on the chiller unit on the roof. The aqueous ethylene glycol is pumped from the chiller to a heat exchanger in the chamber. Then the aqueous ethylene glycol is returned back to the chiller. The chiller system also has two expansion tanks located high enough to let all air in the system escape and allow expansion and contraction of the liquid during the cooling and heating process.

The power switch is located in the center of the east wall about a foot off the ground in room 361 MEL. The bottom switch is for the mobile system and the top switch is for the residential system. The switch has four positions. When the switch is turned all the way to the left, the first notch, the chiller and pump are off. Turn the switch right to the second notch for the pumps to turn on. Turn the switch right again to the third notch and the chiller system is in a preparatory mode. Turn the switch to the fourth and final notch and the chiller system turns on. Note the pumps are always on except when the switch is in the first notch, which is the off position. Sometimes it is necessary to run the chiller system with only the pumps (second notch). This allows the glycol and the condenser chamber to heat up to test conditions quicker. Then the chiller can be switched on (fourth notch).

During some testing, both chillers and/or pumps are necessary. The chiller systems are connected with piping to allow different modes of running to be achieved. Each configuration is outlined below. The valves are used for controlling the glycol flow rates and bypasses. All valves are standard gate valves used for water piping. Note these valves are very sensitive. The flow rate can jump a great deal with a very little amount of turn of the handle. In addition, the valves have dead zones. This mostly occurs when the turning direction of the handle is reversed. So, take it slow. A schematic of the chiller system is shown in Figure C-5

1) Standard Configuration – both systems separate
   - Valves 1, 2, 8, and 9 are closed
   - Valves 3, 5, 6, 7, 10, and 14 are open
   - 4 is the mobile bypass and 11 is the residential bypass
   - Valves 12 and 13 control flow between res. indoor and outdoor chambers

2) Parallel Flow Configuration – combined systems
   - Valves 8, and 9 are closed
   - Valves 1, 2, 5, 6, 7, 10, and 14 are open
   - Valve 4 is the mobile bypass and 11 is the residential bypass
   - Valves 12 and 13 control flow between res. indoor and outdoor chambers
   - Closing valve 3 changes the proportion sent to the mobile lab

3) Series Flow, Single Chiller, No 6 kW heater Configuration – high mass flow
   - Residential use only
   - Valves 1, 2, 3, 5, 7, and 10 are closed
   - Valves 6, 8, and 9 are open
   - Valve 11 is the residential bypass
   - Valves 12 and 13 control flow between res. indoor and outdoor chambers

4) Series Flow, Single Chiller, With 6 kW heater Configuration – high mass flow
   - Either residential, mobile or both
   - Valves 5, 7, 9 and 10 are closed
   - Valves 2, 6 and 8 are open
   - Valves 1 and 3 direct flow between mobile and residential
   - Valve 4 is the mobile bypass and 11 is the residential bypass
   - Valves 12 and 13 control flow between res. indoor and outdoor chambers

5) Series Flow, Double Chiller, Configuration – high mass flow
   - Either residential, mobile or both
   - Valves 5, 7 and 10 are closed
   - Valves 1, 2, 6 and 8 are open
   - Valve 9 controls the proportion of flow sent to each chiller unit
   - Valve 3 directs flow between mobile and residential
   - Valve 4 is the mobile bypass and 11 is the residential bypass

- Valves 12 and 13 control flow between res. indoor and outdoor chambers

The chiller systems were chosen to have a larger capacity than the mobile and residential systems. A 6 kW heater is used to take up some of this over capacity. The heater is controlled by a switch in the breaker box in the north east corner of room 361 MEL. When the glycol temperature is too low, the heater needs to be turned on. When the temperature is too high, the heater needs to be turned off.

As a built in safety, the chiller system has an automatic shut off when the system temperature is too low (approximately zero degrees Celsius). The system will remain pumping but stop cooling. The chillers will automatically come back on when the system temperature goes back up (approximately fifteen degrees Celsius). When the system goes into a cycling situation (chiller turns off and on constantly), the system temperature needs to be kept at a higher temperature. In general, this can be achieved using the 6 kW heater.

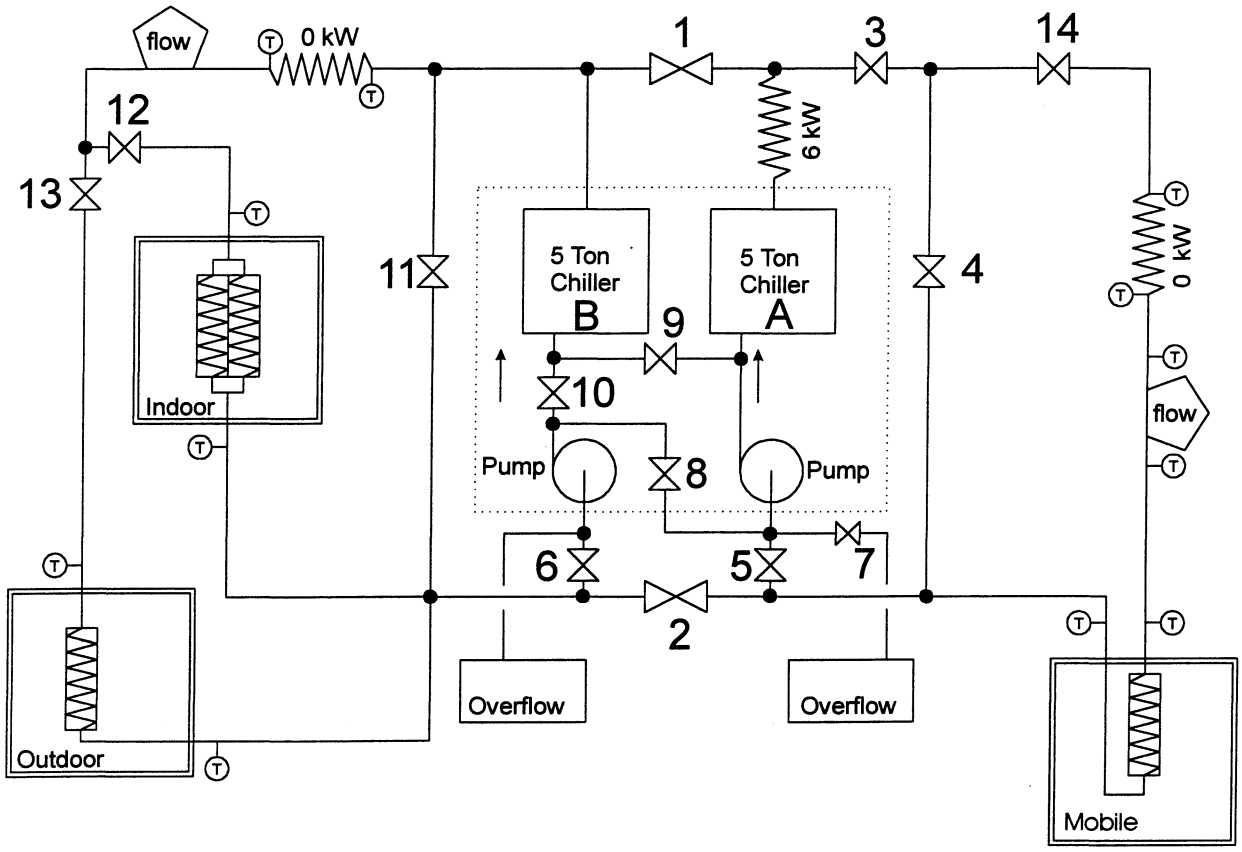

Figure C-5 A schematic of the mobile and residential chiller systems.

Appendix D – Compressor Stand

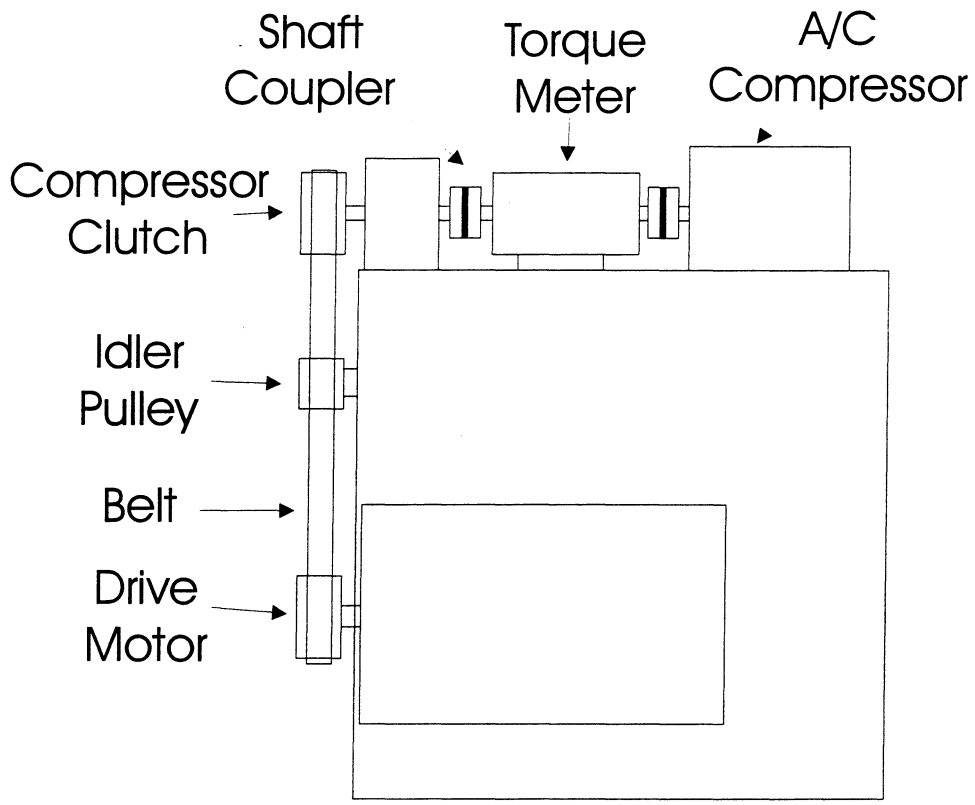

Figure D-1 Schematic of compressor stand.

The compressor test stand lies inside the compressor chamber between the two of the environmental chambers. The same compressor test stand was used for both the R134a and the R744 systems. The stand is a metal table that holds the air conditioning system compressor, torque meter, clutch assembly, and drive motor as shown in Figure D-1. The a/c compressor is belt driven with a 6-groove belt connected to a drive motor with a variable speed controller. The drive motor and compressor run at a 1 to 1 speed ratio. The drive motor is a 3 phase, 10 kW Baldor inverter drive motor with a maximum of 6000 rpm.

Directly coupled into the compressor shaft is torque meter located between the compressor and the clutch in order to measure compressor power at the shaft. This placement eliminates losses due to the drive belt and clutch. The torque meter is a MCRT non-contact torque meter made by S. Himmelstein & Co. with 0-56.5 Nm range and 8500 rpm.

A tachometer is used to find the speed of the compressor. The tachometer is a Panel Tachometer Model DT-5TG made by SHIMPO. This microprocessor-based tachometer can measure rotational, linear and flow rate speeds, and can function as an elapsed time counter and ratio meter. A SHIMPO DOP-FV analog output module is used with the tachometer. This module provides a voltage (0-10 VDC) or current (4-20 mA) proportional to the input frequency. This module allows full span analog output regardless of rpm range. The tachometer sensor is a Retro-Reflective Sensor Model RS220H by SHIMPO, which consists of an infrared source, sensing circuit, and amplifier, contained in a heavy-duty housing.

Appendix E - Instruments

This appendix lists all of the instruments used in taking the data. The list is broken into four tables. Table E-1 lists all instruments used in the chamber calculations. Table E-2 lists all instruments used in the air side calculations. Table E-3 lists all instruments used in the refrigerant side calculations. Table E-4 lists the accuracy of the data acquisition system.

Table E-1 List of all instruments used in calculating the chamber balance.

Environmental Chambers					
Measurement	**Instrument**	**Brand**	**Range**	**Accuracy**	**Description/Location**
Temperature	Type T Welded Thermocouple	Omega	-200 to 350°C	1°C or 0.75% above 0°C	Inside and outside surface temperatures
Temperature	Type T Thermocouple Probe	Omega	-200 to 350°C	1°C or 0.75% above 0°C	Glycol temperature into and out of chamber coil
Power	Model GW5 Watt Transducer	Ohio Semitronic	0 to 8 kW	0.2% of reading	Blower and heater power into evaporator chamber
Power	Model GW5 Watt Transducer	Ohio Semitronic	0 to 12 kW	0.2% of reading	Blower and heater power into cond./gas cooler chamber, lights and outlets in evaporator chamber
Glycol Flow Rate	Elite CMF050 Mass Flow Meter	Micro Motion	Nominal 0 to 0.94 kg/s Maximum 1.89 kg/s	±0.10% ±(0.00453/ Flow Rate (kg/s))%	Glycol mass flow into cooling coil
Condensate weight	Strain Gauge	Omega	0 to 2.5 kg	±0.10%FS	Weight of condensate exiting evaporator
Time	Computer	Gateway			Time used getting condensate flow rate

Table E-2 List of all instruments used in calculating the air side balance.

Air Side					
Measurement	**Instrument**	**Brand**	**Range**	**Accuracy**	**Description/Location**
Temperature	Type T Welded Thermocouple	Omega	-200 to 350°C	1°C or 0.75% above 0°C	Inlet and exit air temps for nozzle, evaporator, and condenser/gas cooler
Pressure Drop	Differential Pressure Transducer	Setra	0 to 1250 Pa	±0.17%FS	Pressure drop across condenser/ gas cooler
Pressure Drop	Differential Pressure Transducer	Setra	0 to 250 Pa	±0.17%FS	Pressure drop across evaporator
Pressure Drop	Differential Pressure Transducer	Setra	0 to 625 Pa	±0.17%FS	Pressure drop across condenser/gas wind tunnel cooler nozzle
Pressure Drop	Differential Pressure Transducer	Setra	0 to 250 Pa	±0.17%FS	Pressure drop across evaporator wind tunnel nozzle
Atmospheric Pressure	Pressure Transducer	Setra	80 to 110 kPA		Barometric pressure
Dew Point	Hygro M4 Dew Point Sensor	General Eastern	-40°C to 60°C	±0.1°C	Air inlet to evaporator
Condensate weight	Strain Gauge	Omega	0 to 2.5 kg	±0.10%FS	Weight of condensate exiting evaporator
Time	Computer	Gateway			Time used getting condensate flow rate

Table E-3 List of all instruments used in calculating the refrigerant side balance.

Refrigerant Side					
Measurement	**Instrument**	**Brand**	**Range**	**Accuracy**	**Description/Location**
Temperature	Type T Thermocouple Probe	Omega	-200 to 350°C	1°C or 0.75% above 0°C	All refrigerant temperatures
R744 High Pressure	Pressure Transducer	Sensotec	0 to 20.7 MPa	±0.25% FS	Compressor exit, gas cooler inlet and exit pressures
R744 Low Pressure	Pressure Transducer	Sensotec	0 to 6.9 MPa	±0.25% FS	Compressor inlet, evaporator inlet and exit pressures
R134a High Pressure	Pressure Transducer	Setra	0 to 3.5 MPa	±0.20%FS	Condenser inlet
R134a Low Pressure	Pressure Transducer	Setra	0 to 0.7 MPa	±0.20%FS	Evaporator inlet
R134a Differential Pressure	Differential Pressure Transducer	Setra	0 to 170 kPa	±0.17%FS	Condenser and evaporator pressure drop
Refrigerant Flow Rate	Elite CMF025 Mass Flow Meter	Micro Motion	Nominal 0 to 0.30 kg/s Maximum 0.61 kg/s	±0.10% ±(0.0015/ Flow Rate (kg/s))%	Refrigerant mass flow rate measured at gas cooler exit
Oil Bypass Flow Rate	Elite CMF010 Mass Flow Meter	Micro Motion	Nominal 0 to 0.023 kg/s Maximum 0.03 kg/s	±0.10% ±(0.00011/ Flow Rate (kg/s))%	Oil mass flow rate measured after the oil separator in R744 system
Accumulator exit Oil Flow Rate	Model D6 Mass Flow Meter	Micro Motion	Nominal 0 to 0.0075kg/s Maximum 0.015 kg/s	±0.10% ±(0.00017/ Flow Rate (kg/s))%	Oil mass flow rate measured after the accumulator in R744 system
Compressor Torque	MCRT non-contact torque meter	S. Himmelstein & Co.	0-56.5 Nm, 8500 max rpm	±0.1%FS	Torque measured at compressor shaft
Compressor Speed	Panel Tachometer Model DT-5TG	Shimpo	10-99999 rpm	±0.008% ±1 digit	Speed measured at compressor shaft

Table E-4 Data acquisition measurement accuracy.

Data Acquisition					
Measurement	**Instrument**	**Brand**	**Range**	**Accuracy**	**Description/Location**
Voltage measurements	Multimeter	Hewlett Packard	0 to 125 mV	0.033% + 5μV	Multimeter reading @ 16.7/20 ms
Voltage measurements	Multimeter	Hewlett Packard	0 to 1 V	0.023% + 15μV	Multimeter reading @ 16.7/20 ms
Voltage measurements	Multimeter	Hewlett Packard	0 to 8 V	0.020% + 50μV	Multimeter reading @ 16.7/20 ms

Appendix F - Data Reduction

All of the data reduction to get the system performance is done in an EES (Engineering Equation Solver) program. This EES data calculation model takes the raw data from HPVEE and calculates all system performance. A list of the more important variables are given in Section F.1 and F.2. Sections F.3 and F.4 give the EES code for the R134a and R744 models. The two models are almost identical for the two systems. Each code includes some comments and an explanation of the calculation being made.

F.1 Input to EES data calculation model

The More important variables used in the calculation models are given in the following tables.

Variable	Units	Description
A$	-	Filename or point
Clutch	-	Not used in calculations – used to signify when clutch is engaged
Count	-	Time
Deng	-	Glycol specific gravity
Denr	kg/m^3	Density of the refrigerant at mass flow meter
DenOIL	kg/m^3	Density of oil from separator
DPca	Pa	Condenser air side pressure drop
DPcn	Pa	Condenser nozzle pressure drop
DPcr	kPa	Condenser pressure drop
DPea	Pa	Evaporator air side pressure drop
DPen	Pa	Evaporator nozzle pressure drop
DPer	kPa	Evaporator refrigerant side pressure drop
Dslope	lb/s	Slope of G vs. time
ENN	-	Evaporator number of nozzles
Fc	in-lb	Compressor torque
G	lb	Mass of condensate
Mg	g/s	Glycol mass flow rate
Mr	g/s	Refrigerant mass flow rate
Patm	kPa	Atmospheric Pressure
Pcri	kPa	Condenser refrigerant inlet pressure (R744 only)
Pcro	kPa	Condenser refrigerant outlet pressure
Pero	kPa	Evaporator refrigerant exit pressure (R744 only)
Prcpi	kPa	Compressor refrigerant inlet pressure
RHe	%	Evaporator air inlet relative humidity
Rhen	°C	Evaporator nozzle dew point temperature
Tcai	°C	Condenser air inlet temperature
Tcc	°C	Compressor chamber air temperature
Tcic	°C	Condenser chamber inside ceiling temperature

Tcif	°C	Condenser chamber inside floor temperature
Tciw	°C	Condenser chamber inside wall temperature
Tcn2	°C	Condenser nozzle (2) air temperature
Tcoc	°C	Condenser chamber outside ceiling temperature
Tcof	°C	Condenser chamber outside floor temperature
Tcow	°C	Condenser chamber outside wall temperature
Tcri	°C	Condenser refrigerant inlet temperature
Tcro	°C	Condenser refrigerant outlet temperature
Tdpei	°C	Evaporator inlet dew point temperature
Teai	°C	Evaporator air inlet temperature
Teao	°C	Evaporator air exit temperature
Teic	°C	Evaporator chamber inside ceiling temperature
Teif	°C	Evaporator chamber inside floor temperature
Teiw	°C	Evaporator chamber inside wall temperature
Ten1	°C	Evaporator nozzle (1) air temperature
Ten2	°C	Evaporator nozzle (2) air temperature
Teoc	°C	Evaporator chamber outside ceiling temperature
Teof	°C	Evaporator chamber outside floor temperature
Teow	°C	Evaporator chamber outside wall temperature
Teri	°C	Evaporator refrigerant inlet temperature
Tero	°C	Evaporator refrigerant outlet temperature
Tgi	°C	Glycol inlet temperature
Tgo	°C	Glycol outlet temperature
Tori	°C	Expansion device refrigerant inlet temperature
Trcpi	°C	Compressor refrigerant inlet temperature
Trcpo	°C	Compressor refrigerant outlet temperature
Ts	°C	Steam temperature
Tw	°C	Condensate temperature
Vc	rpm	Compressor speed
Verdate	-	Version date
Wc	W	Condenser chamber energy (electricity) input – blowers, motors, etc.
We	W	Evaporator chamber energy (electricity) input = We1 + We2
We1	W	Evaporator chamber energy (electricity) input – blowers, motors, etc.
We2	W	Evaporator chamber energy (electricity) input – lights & outlets
Xoil	-	Oil concentration in refrigerant
Constants	**units**	**Description**
CDc	-	Condenser nozzle constant = 0.98
CDe	-	Evaporator nozzle constant = 0.975
Chmbrc	-	Condenser chamber number = 1
Chmbre	-	Evaporator chamber number = 2
Diac2	m	Condenser nozzle (2) diameter = 0.1525
Diae1	m	Evaporator nozzle (1) diameter = 0.06342
Diae2	m	Evaporator nozzle (2) diameter = 0.06348
Pstand	kPa	Standard Pressure = 101.3
RHc	-	Condenser relative humidity = 0.40
CPg	-	Constant for glycol equation = -1.842
Cpg1	-	Constant for glycol equation = 3.41
Cpg2	-	Constant for glycol equation = 0.003741

F.2 Output to EES data calculation model

Variable	Units	Description
η_{idia}	-	Compressor adiabatic efficiency
η_{Isen}	-	Compressor isentropic efficiency
η_m	-	Compressor mechanical efficiency
ηv	-	Compressor volumetric efficiency
$AFR_{m3,Cond}$	m^3/s	Condenser air flow rate
$AFR_{m3,Evap}$	m^3/s	Evaporator air flow rate
$AFR_{scfm,Cond}$	ft^3/min	Condenser air flow rate
$AFR_{scfm,Evap}$	ft^3/min	Evaporator air flow rate
COP	-	Coefficient of Performance
Cpcai	kg/m^3	Condenser air specific heat
DG_{gps}	g/s	Condensate removal rate
DG_{kgs}	kg/s	Condensate removal rate
DT_{sub}	°C	Condenser subcooling delta T
DT_{subF}	°F	Condenser subcooling delta T
DT_{sup}	°C	Evaporator superheat delta T
DT_{supF}	°F	Evaporator superheat delta T
Hci	kJ/kg	Condenser refrigerant inlet enthalpy based on T,P
Hco	kJ/kg	Condenser refrigerant outlet enthalpy based on T,P
h_{compin}	kJ/kg	Compressor refrigerant inlet enthalpy based on T,P
$h_{compout}$	kJ/kg	Compressor refrigerant outlet enthalpy based on T,P
Hei	kJ/kg	Evaporator refrigerant inlet enthalpy based on T,P
Heo	kJ/kg	Evaporator refrigerant outlet enthalpy based on T,P
h_{exit}	kJ/kg	Evaporator refrigerant outlet enthalpy based on chamber balance
Hs	kW	Steam energy input
Hw	kW	Water energy output
Mca2	g/s	Condenser air mass flow rate at nozzle (2)
Mdc2	g/s	Condenser dry air mass flow rate at nozzle (2)
Mde	g/s	Evaporator dry air mass flow rate
Mde1	g/s	Evaporator dry air mass flow rate at nozzle (1)
Mde2	g/s	Evaporator dry air mass flow rate at nozzle (2)
Mea	g/s	Evaporator air mass flow rate
Mea1	g/s	Evaporator air mass flow rate at nozzle (1)
Mea2	g/s	Evaporator air mass flow rate at nozzle (2)
Pcri	kPa	Condenser refrigerant inlet pressure (R134a only)
Pero	kPa	Evaporator refrigerant exit pressure (R134a only)
P_{ratio}	-	Compressor pressure ratio
Psei	kPa	Evaporator air inlet saturation pressure
PseN	kPa	Evaporator nozzle air saturation pressure
Pvei	kPa	Evaporator air inlet vapor pressure
PveN	kPa	Evaporator nozzle air vapor pressure
Qca	kW	Condenser air side capacity
Q_{cond}	kW	Condenser chamber side capacity
Qcr	kW	Condenser refrigerant side capacity
Qctr	kW	Condenser chamber transmission losses

Qea	kW	Evaporator air side capacity
Qer	kW	Evaporator refrigerant side capacity
Qetr	kW	Evaporator chamber transmission losses
Q_{evap}	kW	Evaporator chamber side capacity
Q_{glycol}	kW	Condenser chamber glycol capacity
Q_{latent}	kW	Evaporator latent capacity
Qcondan	kW	Air side gas cooler capacity based on nozzle temperature
Qcondag	kW	Air side gas cooler capacity based on grid temperature
Qcondr	kW	Gas cooler refrigerant side energy balance
Qcondcm	kW	Gas cooler chamber balance based on measure glycol Cp
Qcondcc	kW	Gas cooler chamber energy balance based on calculated glycol Cp
Qevapa	kW	Air side evaporator capacity
Qevapc	kW	Evaporator chamber energy balance
Qevapr	kW	Refrigerant side evaporator capacity
qm3sc1	m^3/s	Condenser air volumetric flow rate at nozzle (1)
qm3sc2	m^3/s	Condenser air volumetric flow rate at nozzle (2)
qm3se1	m^3/s	Evaporator air volumetric flow rate at nozzle (1)
qm3se2	m^3/s	Evaporator air volumetric flow rate at nozzle (2)
$Q_{sensible}$	kW	Evaporator sensible capacity
Rc	-	Condenser air Reynolds number at nozzle
Re	-	Evaporator air Reynolds number at nozzle
T_{cond}	°C	Condensing temperature
Tdpeo	°C	Evaporator outlet dew point temperature
T_{evap}	°C	Evaporating temperature
Velc2	m/s	Condenser nozzle (2) air velocity
Vele1	m/s	Evaporator nozzle (1) air velocity
Vele2	m/s	Evaporator nozzle (2) air velocity
Vndc2	m^3/kg	Condenser nozzle (2) air specific volume
Vnde1	m^3/kg	Evaporator nozzle (1) air specific volume
Vnde2	m^3/kg	Evaporator nozzle (2) air specific volume
WcN	-	Condenser nozzle humidity ratio
W_{comp}	kW	Compressor work
Wei	-	Evaporator air inlet humidity ratio
WeN	-	Evaporator nozzle humidity ratio
Xin	-	Evaporator refrigerant inlet quality
Xout	-	Evaporator refrigerant exit quality

F.3 R134a sample EES data calculation model

This is the most recent version of the R134a EES data calculation model used to calculate the system performance.

```
"----------Procedures----------"
"Gets R134a properties"
procedure TP(TC, P : Hkg)
      R134a=18;
        TK=TC+273.15
        CALL REFPROP(1, R134a ,1, TK, P : TK', P, V, H, S, Q)
        MW = 102.03; Hkg = H/MW
end

"Calculates air flow rate at each nozzle"
procedure AirFlowRate(CD,D,T,Pstand,Pn,Wn,DPn: Vel,ma,qm3s,Vn,Md)
An=3.1416*D**2/4
Vn=101.3*VOLUME(Air,T=T,P=Pstand)/Pn/(1+Wn)
qn=1414*CD*An*(DPn*Vn)**0.5
qm3s=qn/1000
Vel=qm3s/An
ma=qm3s/Vn
Md=ma/(1+Wn)
end

"Gets total air flow rate and air side balance two ways: (1.) using grid temp. (2.) using nozzle temp."
procedure NNum(ENN,qm1,qm2,Vn1,Vn2,
Tw,Patm,Mde1,Mde2,mea1,mea2,DGs,Tn1,Tn2,Teai, WN, Wi, Teao: Mde,mea,Qe,m3,scfm,Tn,
Qeg)
IF (ENN< 1.5) THEN
"For one nozzle"
m3=qm2
scfm=m3*2118.89/(Vn2)/1.2
Mde=Mde2
mea=mea2
Tn=Tn2
hvin=2501+1.805*Teai
hvout2=2501+1.805*Tn
heao2=Mde*SPECHEAT(Air,T=Tn)*Tn2+WN*Mde*hvout2
Heai=Mde*SPECHEAT(Air,T=Teai)*Teai+Wi*Mde*hvin
hea=heao2
Qe=Heai-hea-DGs*ENTHALPY(Water,T=Tw,P=Patm)
hvoutg=2501+1.805*Teao
Heaog=Mde*SPECHEAT(Air,T=Teao)*Teao+WN*Mde*hvoutg      {This value is still
dependent on nozzle temperature through air flow rate calculations}
```

```
Qeg=Heai-Heaog-DGs*ENTHALPY(Water,T=Tw,P=Patm)
ELSE
" Two nozzle "
m3=(qm1+qm2)
scfm=m3*2118.89/((Vn1+Vn2)/2)/1.2
Mde=Mde1+Mde2
mea=mea1+mea2
hvin=2501+1.805*Teai
hvout1=2501+1.805*Tn1
hvout2=2501+1.805*Tn2
heao1=Mde1*SPECHEAT(Air,T=Tn1)*Tn1+WN*Mde1*hvout1
heao2=Mde2*SPECHEAT(Air,T=Tn2)*Tn2+WN*Mde2*hvout2
hea=heao1+heao2
Tn=(Tn1+Tn2)/2
Heai=Mde*SPECHEAT(Air,T=Teai)*Teai+Wi*Mde*hvin
Qe=Heai-heao1-heao2-DGs*ENTHALPY(Water,T=Tw,P=Patm)
hvoutg=2501+1.805*Teao
Heaog=Mde*SPECHEAT(Air,T=Teao)*Teao+WN*Mde*hvoutg        {This value is still
dependent on nozzle temperature through air flow rate calculations}
Qeg=Heai-Heaog-DGs*ENTHALPY(Water,T=Tw,P=Patm)
ENDIF
END

"Calculates refrigerant side balance for both evap. (1) and cond. (2)."
procedure RefriBalance(Tri,Pri,Tro,Pro, Xoil, mr, chmbr:Qr,Qr_Refprop,T_2ph,DT_s, DT_sF,
h_in, h_out)
h_in=ENTHALPY(R134a,T=Tri,P=Pri)
h_out=ENTHALPY(R134a,T=Tro,P=Pro)
CALL TP(Tri,Pri: hcir)
CALL TP(Tro,Pro: hcor)
T_2ph=TEMPERATURE(R134a,x=0.02,P=Pro)

IF (chmbr< 1.5) THEN
DT_s=T_2ph-Tro
Qr_Refprop=(mr-mr*Xoil)*(hcir-hcor)/1000          +mr*Xoil/1000*(2.0499*(Tri-Tro)+2.261e-
3/2*(Tri^2-Tro^2))
Qr=(mr-mr*Xoil)*(h_in-h_out)/1000+mr*Xoil/1000*(2.0499*(Tri-Tro)+2.261e-3/2*(Tri^2-
Tro^2))
ELSE
DT_s=Tro-T_2ph
Qr_Refprop=(mr-mr*Xoil)*(hcor-hcir)/1000          +mr*Xoil/1000*(2.0499*(Tro-Tri)+2.261e-
3/2*(Tro^2-Tri^2))
Qr=(mr-mr*Xoil)*(h_out-h_in)/1000+mr*Xoil/1000*(2.0499*(Tro-Tri)+2.261e-3/2*(Tro^2-
Tri^2))
ENDIF
DT_sF=DT_s*9/5
END
```

```
"Evaporator chamber balance"
Procedure EvapChmbrBalan(Ts, Patm, Tw, Teif, Teof, Teic, Teoc, Teiw, Teow, DG_kgs,
We1,We2, QEvap_mean:Q_Evap, Qtr,Q_sensible,We, Q_Latent)
"Only add We2 to We if lights were on or outlets were being used in Evap. chamber"
We = We1"+We2"
Psteam=PRESSURE(Steam,T=Ts,x=0.5)
Hs=DG_kgs*ENTHALPY(Steam,T=Ts,P=Psteam-1)
Hw=DG_kgs*ENTHALPY(Water,T=Tw,P=Patm)
Qtr=(0.6571*6.493*(Teif-Teof)+0.2197*6.493*(Teic-Teoc)+0.073*(8.701+4.483)*(Teiw-
Teow))/1000
Q_Evap=We/1000+Hs-Hw-Qtr
Q_sensible=We/1000-Qtr
Q_Latent=QEvap_mean-Q_sensible
END

"Condenser chamber balance"
Procedure CondChmbrBalan(Tgi,Tgo,Tcif, Tcof, Tcic, Tcoc, Tciw, Tcow, Wc,mg:Q_Cond1,
Qctr, Q_glycol)
Cpg1=3.41          {constant 1 for glycol specific heat correlation}
Cpg2=0.003741      {constant 1 for glycol specific heat correlation}
Hgi1=mg*(Cpg1*Tgi+Cpg2*Tgi^2/2)/1000
Hgo1=mg*(Cpg1*Tgo+Cpg2*Tgo^2/2)/1000
Qctr=(0.6571*7.576*(Tcif-Tcof)+0.2197*7.576*(Tcic-Tcoc)+0.073*(8.701+5.230)*(Tciw-
Tcow))/1000
Q_Cond1=Wc/1000+Hgi1-Hgo1-Qctr
Q_glycol=Hgo1-Hgi1
END

"Calculates all compressor efficiencies"
procedure Efficiency(Tri,Pri,Tro,Pro,Q_cond1,W_comp, mrc,Trcpi,Prcpi,Vc:eta_isen, eta_idia,
eta_m, eta_v, h_compin, h_compout)
h_compin=ENTHALPY(R134a,T=Tri,P=Pri)
s_compin=ENTROPY(R134a,T=Tri,P=Pri)
h_compout_s=ENTHALPY(R134a,P=Pro,S=s_compin)
h_compout=ENTHALPY(R134a,T=Tro,P=Pro)

eta_isen=(h_compout_s-h_compin)/(h_compout-h_compin)
eta_idia=mrc*(h_compout-h_compin)/(W_comp*1000)
eta_m=eta_isen*eta_idia

V_suc=VOLUME(R134a,T=Trcpi,P=Prcpi)
Vdot_c=mrc*V_suc
{eta_v=Vdot_c/(85.9/1e6*Vc/60)/1000}  {suction volume of Sanden scroll compressor is 85.9
cc. Different expression for volumetric efficiency may be necessary}
eta_v=Vdot_c/(155/1e6*Vc/60)/1000      {volumetric efficiency for Ford Escort 10 piston
compressor P/N F7CH - 19D629 - AA}
END
```

```
"----------Model----------"
{Version 7 - improved R134a}
"inputs"
RHc=0.4              {Relative Humidity}
Xoil=0.01            { Oil Concentration }
ENN = 1              {for evaporator chamber, if use one Nozzle ENN=1, if two, then ENN=2 }
Pstand=101.325       {Standard Pressure, kPa}
Verdate=052299  {Date of Revision}

DG_kgs_o_m=0.45359*Dslope  { DG_kgs in Kilogram/sec }
DG_gps_o_m=DG_kgs_o_m*1000

DG_kgs=0.45359*Dslope_new_method
DG_gps=DG_kgs*1000

Pen=Patm-DPen/1000          {calculates air pressure at nozzle entrances}
Pcn=Patm-DPcn/1000

{ Calculate the Relative Humidity in the Evap. Chamber }

{Any of the following variables can be inputted as evaporator dew point:  Tdpe, RHe, or RHev}
{Tdpe = RHe
Tdpe = RHev}
Rhea_in=RELHUM(AirH2O,T=Teai,P=Patm,D=Tdpei)
Rhea_out=RELHUM(AirH2O,T=((ENN-1)*Ten1+Ten2)/(ENN),P=Pen,D=Tdpeo)

Rhea_in=RELHUM(AirH2O,T=Teai,P=Patm,W=Wei)
Rhea_out=RELHUM(AirH2O,T=((ENN-1)*Ten1+Ten2)/(ENN),P=Pen,W=WeN)

{---------- Air flow rate for Evaporator Side ---------- Uses new nethod for measuring condensate removal:  dew point sensors at inlet  of evaporator and exit of nozzle}
{Air flow rate for Evaporator Side  }
                    {Nozzle #1---->North  }
CDe=0.975;Diae1=0.06342
call    AirFlowRate(CDe,Diae1,  Ten1,Pstand,Pen,WeN,DPen:  Vele1,  mea1,qm3se1,Vnde1, Mde1)
Re=(9.6286-0.064834*Ten1+0.00025824*Ten1^2)*2.495*Vele1/0.3048*60

                    { Nozzle #2 --->South }
Diae2=0.06348  {2.5"}
call  AirFlowRate(CDe,Diae2, Ten2,Pstand,Pen,WeN,DPen: Vele2,mea2,qm3se2,Vnde2, Mde2)

{---------- Air flow rate for Evaporator Side ---------- Uses old condensate measuring method: weighs condensate removed}
{ Nozzle #1---->North  }
call                AirFlowRate(CDe,Diae1,          Ten1,Pstand,Pen,WeN_o_m,DPen:
Vele1_o_m,mea1_o_m,qm3se1_o_m,Vnde1_o_m, Mde1_o_m)
```

```
{ Nozzle #2 --->South }
call AirFlowRate(CDe,Diae2, Ten2,Pstand,Pen,WeN_o_m,DPen:
Vele2_o_m,mea2_o_m,qm3se2_o_m,Vnde2_o_m, Mde2_o_m)

{calculates Wei from Teai, Rhea_in, and Pvei instead of from EES built in function}
Wei_o_m=0.622*Pvei/(Patm-Pvei)
Pvei=Psei*Rhea_in
Psei=Pressure(Water,T=Teai,X=0.5)

{ Calculate the relative humidity at nozzle }
PveN=WeN_o_m*Patm/(0.622+WeN_o_m)
PseN=Pressure(Water,T=((ENN-1)*Ten1+Ten2)/(ENN),X=0.5)
Rhea_out_o_m=PveN/PseN

{calculates an exit dew point (Tdpeo) temperature for the old method}
Rhea_out_o_m=RELHUM(AirH2O,T=((ENN-1)*Ten1+Ten2)/(ENN),P=Pen,D=Tdpeo_old)


{----------Air Flow rate for Condenser Side----------}

{Air Flow rate for Condenser Side }
CDc=0.98;Diac2=0.15250 {6" }
call AirFlowRate(CDc,Diac2,Tcn2,Pstand,Pcn,WcN,DPcn: Velc2,mca2,AFR_m3_Cond,Vndc2,
Mdc2)
Rc=(9.6286-0.064834*Tcn2+0.00025824*Tcn2^2)*2.495*Velc2/0.3048*60

{Air Side Humidity Ratio }
WcN=0.622*RHc*pressure(Water,T=Tcai,x=0.5)/(Patm-RHc*pressure(Water,T=Tcai,x=0.5));
AFR_scfm_Cond=AFR_m3_Cond*2118.89/(Vndc2)/1.2

{---------- Energy Balance Calculations----------}

{ Condenser Air-Side }
Cpcai=(SPECHEAT(Air,T=Tcai) + SPECHEAT(air,T=Tcn2))/2
Qca=mca2*Cpcai*(Tcn2-Tcai)

{ Condenser Refrigerant Side }
chmbrc = 1
Call RefriBalance(Tcri,Pcri,Tcro,Pcro, Xoil, mr, chmbrc:Qcr,Qcr_Refprop,T_cond,DT_sub,
DT_subF, hci,hco)

{ Condenser Chamber }
Call CondChmbrBalan(Tgi,Tgo,Tcif, Tcof, Tcic, Tcoc, Tciw, Tcow, Wc,mg:Q_Cond1, Qctr,
Q_glycol)

{ Evaporator Air_Side }
```

```
call NNum(ENN,qm3se1,qm3se2,Vnde1,Vnde2,
Tw,Patm,Mde1,Mde2,mea1,mea2,DG_kgs,Ten1,Ten2,Teai, WeN,Wei,Teao:
Mde,mea,Qevap_air, AFR_m3_Evap, AFR_scfm_Evap,T_eao,Qeag)
WeN=Wei - DG_kgs/Mde   {calculates condensate removal rate in Kg/s}

{ Evaporator Refrigerant Side }
chmbre = 2
Call RefriBalance(Tori,Pcro,Tero,Pero, Xoil, mr, chmbre:Qer, Qer_Refprop,T_evap,DT_sup,
DT_supF, hei,heo)

{ Evaporator Chamber }
Call EvapChmbrBalan(Ts, Patm, Tw, Teif, Teof, Teic, Teoc, Teiw, Teow, DG_kgs, We1,We2,
QEvap_mean:Q_Evap, Qetr, Q_sensible,We, Q_latent)
{Q_latent=QEvap_mean-Q_sensible}

{ Compressor Energy Calculation }
W_comp=(Fc*.11298)*(Vc/9.5488)/1000   {KW, includes conversion factors}
COP=QEvap_mean/W_comp

{Error calculations}
QCond_mean=(Qca+ABS(Q_Cond1))/2      {Average of chamber and airside balance}
ErrCond_a=(QCond_mean-Qca)/QCond_mean*100
ErrCond_r=(QCond_mean-Qcr_Refprop)/QCond_mean*100
ErrCond_tot=(QCond_mean-ABS(Q_Cond1))/QCond_mean*100

QEvap_mean=(Qevap_air+Q_Evap)/2              {Average of chamber and airside balance}
ErrEvap_a=(QEvap_mean-Qevap_air)/QEvap_mean*100
ErrEvap_r=(QEvap_mean-Qer_Refprop)/QEvap_mean*100
ErrEvap_tot=(QEvap_mean-Q_Evap)/QEvap_mean*100

{Efficiency calculations}
mrc=ABS(Q_Cond1)*1000/(hci-hco)
Call Efficiency(Trcpi,Prcpi,Trcpo,Pcri, Q_Cond1,W_comp, mrc,Trcpi,Prcpi, Vc:eta_isen,
eta_idia, eta_m, eta_v, h_compin, h_compout)

{Pressure definitions }
Peri=Pero+DPer          {inlet pressure (absolute)}
Pcri = Pcro+DPcr        {inlet pressure (absolute)}
P_ratio=Pcri/Prcpi

{Evaporator quality}
h_exit = Q_Evap*1000/mrc + hei
x_out=(h_exit-ENTHALPY(R134a,P=Peri,x=0))/(ENTHALPY(R134a,P=Pero,x=1)-
ENTHALPY(R134a,P=Peri,x=0))
x_in=(hei-ENTHALPY(R134a,P=Peri,x=0))/(ENTHALPY(R134a,P=Pero,x=1)-
ENTHALPY(R134a,P=Peri,x=0))
```

{Other equations that invoke the humidity ratio at the evaporator exit - evaluates impact of new condensate measurement technique on data}
{Airside energy balance for old method}
call
NNum(ENN,qm3se1_o_m,qm3se2_o_m,Vnde1_o_m,Vnde2_o_m,Tw,Patm,Mde1_o_m,Mde2_o_m,mea1_o_m,mea2_o_m,
DG_kgs_o_m,Ten1,Ten2,Teai,WeN_o_m,Wei_o_m,Teao:Mde_o_m,mea_o_m,Qevap_air_o_m,
AFR_m3_Evap_o_m, AFR_scfm_Evap_o_m,T_eao_o_m,Qeag_o_m)

{ calculate the humidity ratio WeN after nozzle with old method }
WeN_o_m=Wei_o_m - DG_kgs_o_m/Mde_o_m

{Chamber energy balance for old method}
Pstm = PRESSURE(Steam,T=Ts,x=0.5)
Hs_o_m=DG_kgs_o_m*ENTHALPY(Steam,T=Ts,P=Pstm-1)
Hw_o_m=DG_kgs_o_m*ENTHALPY(Water,T=Tw,P=Patm)
Q_Evap_o_m=We/1000+Hs_o_m-Hw_o_m-Qetr
Q_latent_o_m=QEvap_mean_o_m-Q_sensible

COP_o_m=QEvap_mean_o_m/W_comp

QEvap_mean_o_m=(Qevap_air_o_m+Q_Evap_o_m)/2 {Average of chamber and airside balance}
ErrEvap_a_o_m=(QEvap_mean_o_m-Qevap_air_o_m)/QEvap_mean_o_m*100
ErrEvap_r_o_m=(QEvap_mean_o_m-Qer_Refprop)/QEvap_mean_o_m*100
ErrEvap_tot_o_m=(QEvap_mean_o_m-Q_Evap_o_m)/QEvap_mean_o_m*100

h_exit_o_m = Q_Evap_o_m*1000/mrc + hei

x_out_o_m=(h_exit_o_m-ENTHALPY(R134a,P=Peri,x=0))/(ENTHALPY(R134a,P=Pero,x=1)-ENTHALPY(R134a,P=Peri,x=0))

{Conversion of Data from Excel}
Tdpeo = Rhen
Tdpei = RHe

{Inputs from HPVEE, this is the measured system data}
DPen=229.982677
G=2.593412028
DPea=195.9398043
DPer=43.8037993
Pero=510.6440594
RHe=19.15897415
Patm=99.70469702
We1=3157.586068
Wg=-22.76129147
Clutch=6.89663366
Rhen=18.62523925

mr=37.20989244
Denr=0.999455044
We2=-17.61655449
Fc=172.1277179
Vc=949.5716981
Wc=3520.355706
DPcn=314.0468423
mg=57.32398895
Deng=1.079110567
DPcr=52.32744397
Pcro=2622.907152
DPca=77.86592863
Prcpi=504.7657323
count=0
Dslope=0.000191929
Teif=42.45099689
Teof=25.37772726
Teic=42.89433792
Teoc=31.11206566
Teiw=42.97355896
Teow=27.6588384
Teai=43.44884151
Teao=23.6545183
Ten1=23.5853567
Ten2=23.33209557
Tw=28.19392142
Ts=100.2170456
Teri=18.75580406
Tero=19.29728981
Tcc=33.31457264
Tcif=57.23772887
Tcof=25.50338151
Tcic=58.22334764
Tcoc=28.66860481
Tciw=58.67349632
Tcow=25.62780104
Tcai=59.63762236
Tcn2=70.34727774
Tgi=7.769835302
Tgo=48.57904585
Tcri=89.29635943
Tcro=71.07154698
Trcpi=18.24341302
Trcpo=89.93471736
Tori=70.90672925
A$='m990326I00_Baseline'

F.4 R744 sample EES data calculation model

```
"----------Procedures----------"
"Get R744 properties"
procedure TP(TC, P : Vkg,Hkg,Skg)
      R744=35;
        TK=TC+273.15
        CALL REFPROP(1, R744,1, TK, P : TK', P, V, H, S, Q)
      MW=44.01;   Vkg=V/MW;       Hkg=H/MW;       Skg=S/MW
end
procedure TQ(TC, Q : P, Vkg, Hkg, Skg)
      R744=35;
        TK=TC+273.15
        CALL REFPROP(1, R744 ,5, TK, Q : TK', P, V, H, S, Q)
      MW=44.01;  Vkg=V/MW;  Hkg=H/MW;   Skg=S/MW
end
procedure PQ(P, Q : TC, Vkg, Hkg, Skg)
      R744=35;
        CALL REFPROP(1, R744 ,6, P, Q : TK, P', V, H, S, Q)
      TC=TK-273.15
      MW=44.01;  Vkg=V/MW;  Hkg=H/MW;  Skg=S/MW
end
procedure PS(P, Skg : TC, Vkg, Hkg)
        R744=35;   MW=44.01
      S=Skg*MW
        CALL REFPROP(1 ,R744 ,4 , P, S : TK, P, V, H, S, Q)
        TC=TK-273.15
      Vkg=V/MW;  Hkg=H/MW
end
"Calculates air flow rate at each nozzle."
procedure AirFlowRate(CD,D, T,Pstand,Pn,Wn,DPn: Vel,ma,qm3s,Vn)
An=3.1416*D**2/4
Vn=101.3*VOLUME(Air,T=T,P=Pstand)/Pn/(1+Wn)
qn=1414*CD*An*(DPn*Vn)**0.5
qm3s=qn/1000
Vel=qm3s/An
ma=qm3s/Vn
end
"Gets total air flow rate and air side balance two ways: (1.) using grid temp. (2.) using nozzle
temp."
procedure                                                NozzleNum(ENN,qm1,qm2,Vn1,Vn2,
Tw,Pa,Heai,Mde1,Mde2,mea1,mea2,heao1,heao2,DGs,Tn1,Tn2: Mde,mea,Qe,m3,scfm,Tn)
IF (ENN< 1.5) THEN
{ One nozzle }
m3=qm2/(Vn2)/1.2
scfm=m3*2118.89
Mde=Mde2
```

```
mea=mea2
Heao=Heao2
Tn=Tn2
Qe=Heai-Heao2+DGs*ENTHALPY(Water,T=Tw,P=Pa)
ELSE
{Two nozzle}
m3=(qm1+qm2)/((Vn1+Vn2)/2)/1.2
scfm=m3*2118.89
Mde=Mde1+Mde2
mea=mea1+mea2
Heao=Heao1+Heao2
Tn=(Tn1+Tn2)/2
Qe=Heai-Heao1-Heao2+DGs*ENTHALPY(Water,T=Tw,P=Pa)
ENDIF
END
"----------Procedures----------"
"Input all measured system data... null are channels not used"
null100=99999
DPen=239.8002352
G=2.210314462
DPea=167.9967783
Peri=5240.58191
Pero=5150.286897
RHe=16.8007886
Patm=98.80940787
We1=2094.942572
Wg=-13.94401033
ML=0.729977031
DenOIL=0.942308662
Moil=3.202232028
Clutch=6.748770914
null114=99999
null115=99999
mr=32.62942107
Denr=0.496217291
We2=-16.87514095
Fc=113.743443
Vc=951.1900989
Wc=4068.718065
DPcn=294.5074066
mg=53.55670244
Deng=1.082063612
Pcri=9241.541396
Pcro=9093.292301
DPca=38.42491022
Prao=149.6055504
null213=99999
Prcpi=5054.361146
```

Prcpo=9456.975629
count=0
Dslope=0.000146466
Teif=31.60642409
Teof=22.70357656
Teic=31.72502871
Teoc=27.06885323
Teiw=31.75224742
Teow=25.26672774
Teai=32.13179398
Twbeai=31.99692312
Teao=18.47883097
Ten1=18.72899806
Ten2=18.86880452
Tw=24.11410043
Ts=99.07877634
Teri=17.75984978
Tero=17.15210247
Tcc=28.7127757
Tcif=42.34395989
Tcof=22.90368796
Tcic=42.28746634
Tcoc=23.92108785
Tciw=42.46586301
Tcow=22.4222214
Tcai=43.31171226
Tcao=48.24029774
Tcn1=46.1424
Tcn2=47.42364989
Tgi=-2.936239946
Tgo=35.47579591
Tcri=83.31620645
Tcro=45.48434301
Tcgi=-3.058478269
Tcgo=-2.91712871
Trcpi=37.45520419
Trcpo=85.94386301
Tshri=16.02586258
Tshro=31.62081
Tosri=79.3883571
Tosro=70.17909925
Trai=8.73785E+37
Tori=41.14797538
null508=9.80344E+37
null509=9.80344E+37
null510=9.91E+37
null511=9.91E+37
null512=9.91E+37

```
null513=9.91E+37
null514=9.91E+37
null515=9.91E+37
A$='C1102t4332i9hx15PF_A'

{Version 4 11/12/1998 by YCP}
ENN=2 { Evaporator duct nozzle number, 1 or 2 }
RHc=0.4; MW=44; Xoil=0.01  { Oil Concentration };NN=0 {for condenser chamber, if use one
Nozzle NN=0, if two, then NN=1 }
Pstand=101.325;{RHe=RHev*.01} {Convert Number to Decimal}
Cpg1=3.41;Cpg2=0.003741
We=We1;Pa=Patm {data loger variable change}

DG_kgs=0.45359*Dslope { DG_kgs in Kilogram/sec }
Pen=Pa-DPen/1000 { absolute pressures at nozzle throth }
Pcn=Pa-DPcn/1000

{ Calculate the RH value in Evap. Chamber }
T_dpe=RHe {data loger variable change}
Rhea=RELHUM(AirH2O,T=Teai,P=Pa,D=T_dpe)
Rhea=RELHUM(AirH2O,T=Teai,P=Pa,B=T_wbe) { calculate wet bubble temperature }

{Air flow rate for Evaporator Side }
                    {Nozzle #1---->North }
CDe=0.975 { if Re<=50,000 then CDe=0.97  if 50,000<=Re<=150,000 then CDe=0.98  if
Re>=200,000 then CDe=0.99}
Diae1=0.06342  { 2.497" }
call AirFlowRate(CDe,Diae1, Ten1,Pstand,Pen,WeN,DPen: Vele1,mea1,qm3se1,Vnde1)
                    { Nozzle #2 --->South }
Diae2=0.06348 {2.5"}
call AirFlowRate(CDe,Diae2, Ten2,Pstand,Pen,WeN,DPen: Vele2,mea2,qm3se2,Vnde2)
Re=(9.6286-0.064834*Ten1+0.00025824*Ten1^2)*2.495*Vele1/0.3048*60
                    { calculate the humidity ratio WeN after nozzle }
WeN=Wein-DG_kgs/mde

Mde1=mea1/(1+WeN)
Mde2=mea2/(1+WeN)
Wein=0.622*RHea*Pressure(Water,T=Teai,X=0.5)/(Pa-RHea*Pressure(Water,T=Teai,X=0.5))

                    { Calculate the relative humidity at nozzle }
RhN=WeN*Pa/(0.622+WeN)/Pressure(Water,T=T_eao,X=0.5)

{Air Flow rate for Condenser Side }
                    { Nozzle #1 ----> South }
CDc=0.98
Diac1=0.15238   {6.001"}
call AirFlowRate(CDc,Diac1, Tcn1,Pstand,Pcn,WcN,DPcn: Velc1,mca1,qm3sc1,Vndc1)
```

```
                    { Nozzle #2 --->North}
Diac2=0.15250      {6"      }
call  AirFlowRate(CDc,Diac2, Tcn2,Pstand,Pcn,WcN,DPcn: Velc2,mca2,qm3sc2,Vndc2)

Rc=(9.6286-0.064834*Tcn2+0.00025824*Tcn2^2)*2.495*Velc2/0.3048*60
AFR_m3_Cond=(qm3sc1*NN+qm3sc2)/(Vndc2)/1.2
AFR_scfm_Cond=AFR_m3_Cond*2118.89
                    {Air Side  Humidity  Ratio }
WcN=0.622*RHc*pressure(Water,T=Tcai,x=0.5)/(Pa-RHc*pressure(Water,T=Tcai,x=0.5));

{ Energy Balance Calculation   }
      {air temperature definition}
T_cao=Tcn2
mca=mca2

call                                        NozzleNum(ENN,qm3se1,qm3se2,Vnde1,Vnde2,
Tw,Pa,Heai,Mde1,Mde2,mea1,mea2,heao1,heao2,DG_kgs,Ten1,Ten2:
Mde,mea,Qevapa,AFR_m3_Evap,AFR_scfm_Evap,T_eao)

            { Condenser Air-Side  }
Cpcai=SPECHEAT(Air,T=Tcai)
Qcondan=(mca1*NN+mca2)*CPcai*(Tcn2-Tcai)  {nozzle temperature}
Qcondag=(mca1*NN+mca2)*CPcai*(Tcao-Tcai){grid temperature}
            { Condenser  Refrigerant Side  }
CALL TP(Tcri,Pcri: Vcri,Hcri,Scri)
CALL TP(Tcro,Pcro: Vcro,Hcro,Scro)
Qcondr=(Mr-Mr*Xoil)*(Hcri-Hcro)/1000+Mr*Xoil/1000*(2.0499*(Tcri-Tcro)+2.261e-
3/2*(Tcri^2-Tcro^2))
            { Condenser Chamber  }
CPg=Wg/(Tcgo-Tcgi)/Mg
;Hgi=Mg*(Cpg*Tgi+Cpg2*Tgi^2/2)/1000;Hgo=Mg*(Cpg*Tgo+Cpg2*Tgo^2/2)/1000
Qglycool=Hgo-Hgi
Qctr=(0.6571*7.576*(Teif-Teof)+0.2197*7.576*(Teic-Teoc)+0.073*(8.701+5.230)*(Teiw-
Teow))/1000
Qcondcm=Wc/1000+Hgi-Hgo-Qctr
Hgi1=Mg*(Cpg1*Tgi+Cpg2*Tgi^2/2)/1000;Hgo1=Mg*(Cpg1*Tgo+Cpg2*Tgo^2/2)/1000
Qcondcc=Wc/1000+Hgi1-Hgo1-Qctr
QCond=Qcondcc

            { Evaporator  Air_Side }
Heai=mde*SPECHEAT(Air,T=Teai)*Teai+Wein*Mde*Hvin
Heao1=Mde1*SPECHEAT(Air,T=Ten1)*Ten1+WeN*Mde1*Hvout1
Heao2=Mde2*SPECHEAT(Air,T=Ten2)*Ten2+WeN*Mde2*Hvout2
Hvin=2501+1.805*Teai;Hvout1=2501+1.805*Ten1;Hvout2=2501+1.805*Ten2

            { Evaporator Refrigerant Side }
call PQ(Pero,1:T_evap,Vv,Hv,Sv)
DT_sup=Tero-T_evap
```

```
CALL TP(Tero,Pero: Vero,Hero,Sero)
CALL TP(Tori,Pcro: Veri,Heri,Seri)
Qevapr=(Mr-Mr*Xoil)*(Hero-Heri)/1000-Mr*Xoil*(2.0499*(Tori-Tero)+2.261e-3/2*(Tori^2-
Tero^2))/1000
                { Evaporator Chamber }
psteam=PRESSURE(Steam,T=Ts,x=0.5)
Hs=DG_kgs*ENTHALPY(Steam,T=Ts,P=psteam-1)
Hw=DG_kgs*ENTHALPY(Water,T=Tw,P=Pa)
Qetr=(0.6571*6.493*(Teif-Teof)+0.2197*6.493*(Teic-Teoc)+0.073*(8.701+4.483)*(Teiw-
Teow))/1000
QEvap=We/1000+Hs-Hw-Qetr
Q_sensible=We/1000-Qetr
Q_latent=QEvap_mean-Q_sensible

{ Compressor and System Energy Calculation }
{W_comp=Fc*Vc/9.5488/1000  {KW}
H_compin=ENTHALPY(R134a,T=Trcpi,P=Prcpi+Pa)
H_compout=ENTHALPY(R134a,T=Trcpo,P=Pcro+DPcr)}
W_comp=(Fc*.11298)*(Vc/9.5488)/1000  {KW, includes conversion factors}
COP=(Qevapa+QEvap)/2/W_comp
QEvap_mean=(Qevapa+QEvap)/2


{ Efficiency Calculation }
CALL TP(Trcpi,Prcpi: Vrcpi,Hrcpi,Srcpi);call  PS(Pcri, Srcpi : Trcpos, Vrcpos, Hrcpos);call
TP(Trcpo,Pcri: Vrcpo,Hrcpo,Srcpo)
{Mrc=ABS(Q_Cond1)*1000/(Hcri-Hcro)}
QEvap=Mr*(H_exit-Heri)/1000
call PQ(Peri,0.0:T_evapi,Vl,Hl,Sl)
x_out=(H_exit-Hl)/(Hv-Hl)
x_in=(Heri-Hl)/(Hv-Hl)
Vdot=mr*Vrcpi
eta_isen=(Hrcpos-Hrcpi)/(Hrcpo-Hrcpi)
eta_idia=mr*(Hrcpo-Hrcpi)/(W_comp*1000)
eta_m=eta_isen*eta_idia
eta_v=Vdot/(20.7/1e6*Vc/60)/1000
P_ratio=Pcri/Prcpi

{ Suction line calculation }
DPsuc=Pero-Prcpi
CALL TP(Tori,Pcro: Vori,Hori,Sori)
CALL TP(Tshro,Pero: Vshro,Hshro,Sshro)
CALL TP(Tshri,Pero: Vshri,Hshri,Sshri)
Call  TQ(Tshri, X_shi : Pshi, Vshi, Hshi, Sshi)
CALL TP(Tcro,Pero: Vmax,Hmax,Smaxi)

call PQ(Pero,1.0:T_rcpi1,Vv_sh,Hv_sh,Sv_sh)
call PQ(Pero,0.0:T_rcpi2,Vl_sh,Hl_sh,Sl_sh)
```

```
QSH=mr*(hcro-hori)/1000
QSL=mr*(hshro-hshri)/1000
Q_max=mr*(hmax-hshi)/1000
eps_slhx=QSH/Q_max

QSH=mr*(Hshro-Hshri_cal)/1000
x_shi=(Hshri_cal-Hl_sh)/(Hv_sh-Hl_sh)
MOil_suc=mr-(x_shi*mr-ml)
MRatioRef=(Mr-MOil_suc)/mr*100
MRatioOil=MOil_suc/mr*100


{ mass flux in refrigerant}
Di_low=0.0146;Do_high=0.0083;t_w=0.0018
Area_low=Pi/4*(Di_low**2)-Pi/4*(Do_high**2)-t_w*(Di_low-Do_high)*6
Periameter_low=Pi*Di_low+Pi*Do_high+12*(Di_low-Do_high)-t_w*12

Rhoshri=1/Vshi
Dh=4*Area_low/Periameter_low
Areashri=Pi*Dh**2/4
{Mr/1000=Rhoshri*VELshri*Areashri}
Mr/1000=Rhoshri*VELshri*Area_low
Rhoyou2=Rhoshri*VELshri**2
```

Appendix G – Internal Heat Exchanger Model

The internal heat exchanger model was written in EES and is given below. This model is explained in more detail in Chapter 5.

```
"---------------------------------------------- Procedures ----------------------------------------------"
"The following four procedures call REFPROP to find properties of CO2. They
each require two given inputs."

procedure TP(TC, P :V,H,S)
        TK=TC+273.15
        CALL EESREFP6('Co2', 12, TK, P : TK2, P2, D2, V2, H2, S2, Q)
        V:=V2/44.01
        H:=H2/44.01
        S:=S2/44.01
end

procedure TQ(TC, x : V, H, S,P)
        TK=TC+273.15
        CALL EESREFP6('Co2', 17, TK, x : TK2, P, D2, V2, H2, S2, Q)
        V:=V2/44.01
        H:=H2/44.01
        S:=S2/44.01
end

procedure TRANSP( TC, RHO: MU, K)
     TK2:=TC + 273.15
        RHO2:=RHO/44.01
        CALL EESREFP6('CO2', 90, TK2, RHO2: MU2, K2)
        MU= MU2* 10^(-6)
        K= K2
end

procedure SPH(TC, P : CP)
        TK = TC+273.15
        CALL EESREFP6('Co2', 12, TK, P : TK2, P2, D2, V2, H_d1, S2, Q)
        CALL EESREFP6('Co2', 12, TK+0.1, P : TK2, P2, D2, V2, H_d2, S2, Q)
        CP = (H_d2-H_d1)/0.1 / 44.01
END

"---------------------------------------------- Main Program ----------------------------------------------"
"Units are:  m, kW, kPa and C unless otherwise stated."
"The length and number of ports are given. The value of Flow (+1 or -1) is used to
distinguish the direction of flow on the liquid side.  +1 is used for parallel flow and -1
```

```
is used for counter flow."
;Flow = -1
L_slhx = 1.0
N_port.liq = 1
N_port.suc = 6

"The perimeters and cross sectional areas of the liquid port and suction port are given.
It is assumed that all liquid ports and all suction ports are identical throughout the length
of the heat exchanger."
P_port.liq =  0.01885
A_port.liq =  0.00002827
P_port.suc =  0.01469
A_port.suc =  0.00001321

"The hydraulic diameter is calculated for both the liquid and suction ports."
D_h.liq = 4*A_port.liq/P_port.liq
D_h.suc = 4*A_port.suc/P_port.suc

"The internal heat exchanger is broken in NN sections after the two phase suction
side becomes vapor."
NN=10

"The inlet conditions for the liquid and suction sides are given from measured
data taken with the CO2 mobile air conditioning system."
Pllhxi[0] = 10827
Tllhxi[0] = 46.61
Tslhxi[0]= 7.905
xin = 0.9825
mdot = 0.02272

"Initial properties of the suction inlet are found using the procedures."
call TQ(Tslhxi[0], 1.0 : vv, hv, sv,Pv)
call TQ(Tslhxi[0], 0.0 : vl, hl, sl,Pl)
call TRANSP( Tslhxi[0], 1/Vv: mu_v, k_v)
call TRANSP( Tslhxi[0], 1/Vl: mu_l, k_l)
call SPH(Tslhxi[0],Pl+20:cp_l)

"The initial properties are transfered to the location 1, which is where the
two phase CO2 turns into single phase vapor CO2."
XLOC[0]=0.0
CP_suc[0]=CP_suc[1]
CP_liq[0]=CP_liq[1]
mu_suc[0]=mu_suc[1]
k_suc[0]= k_suc[1]

"The Lockhart-Martinelli number, G, and liquid Prandtl number are found."
Xtt=((1-Xin)/Xin)^0.9*(Vl/Vv)^0.5*(mu_l/mu_v)^0.1
G=mdot/(N_port.suc*A_port.suc)
```

```
hfg=hv-hl
Prl=mu_l*cp_l/(k_l/1000)

"Initial properties of the liquid inlet are found using the procedures."
call TP(Tllhxi[0], Pllhxi[0]:vllhxi[0], hllhxi[0], sllhxi[0])
call TQ(Tslhxi[0], Xin : Vslhxi[0], Hslhxi[0], Sslhxi[0],Pslhxi[0])

"The two phase suction part is between 0 and 1 in the internal heat exchanger."

duplicate i=1,1

    "Find all properties."
    call TP(Tllhxi[i], Pllhxi[i]: vllhxi[i], hllhxi[i], sllhxi[i])
    call TQ(Tslhxi[i], 1.0 : vslhxi[i], hslhxi[i], sslhxi[i],Pslhxi[i])
    call TRANSP( Tllhxi[i], 1/Vllhxi[i]: mu_liq[i], k_liq[i])
    call SPH(Tllhxi[i],Pllhxi[i]+5:cp_liq[i])
    call SPH(Tslhxi[i],Pslhxi[i]-5:cp_suc[i])
    call TRANSP( Tslhxi[i], 1/Vslhxi[i]: mu_suc[i], k_suc[i])
    rho_liq[i] = 1/vllhxi[i]
    rho_suc[i] = 1/vslhxi[i]

    "Find volumetric flow rate."
    Vdot_suc[i] = mdot* vslhxi[i]
    Vdot_liq[i] = mdot * vllhxi[i]

    "Find velocity."
    V_suc[i] = Vdot_suc[i]/(N_port.suc*A_port.suc)
    V_liq[i] = Vdot_liq[i]/(N_port.liq*A_port.liq)

    "Find friction factor  using Petukhov equation."
    f_suc[i] =(0.79*ln(Re_suc[i])-1.64)^(-2)    {Turbulent flow}
    f_liq[i] = (0.79*ln(Re_liq[i])-1.64)^(-2)

    "Find pressure drop."
    dP_suc[i]=f_suc[i]*(L2/D_h.suc)*V_suc[i]^2/2000/Vslhxi[i]+
                    (mdot/(A_port.suc*N_port.suc))^2*(Vslhxi[i]-Vslhxi[i-1])/1000
    dP_suc[i]=  Pslhxi[i-1] - Pslhxi[i]
    dP_liq[i] =  f_liq[i]*(L2/D_h.liq)*V_liq[i]^2/2000/Vllhxi[i]
    dP_liq[i]= (Pllhxi[i] - Pllhxi[i-1])*FLOW

    "Find Reynolds number."
    Re_suc[i]=rho_suc[i]*V_suc[i]*D_h.suc/mu_suc[i]
    Re_liq[i]=rho_liq[i]*V_liq[i]*D_h.liq/mu_liq[i]

    "Find Prandtl number."
    Pr_liq[i] = mu_liq[i]*cp_liq[i]/(k_liq[i]/1000)
    Pr_suc[i] = mu_suc[i]*cp_suc[i]/(k_suc[i]/1000)
```

```
        "The liquid side heat transfer coefficient is found using the Gnielinski correlation."
        Nusselt_liq[i]=
        (f_liq[i]/8)*(Re_liq[i]-1000)*Pr_liq[i]/(1+12.7*(f_liq[i]/8)^0.5*(Pr_liq[i]^(2/3)-1))
        h_liq[i]=Nusselt_liq[i]*k_liq[i]/D_h.liq

        "The two phase heat thansfer coefficient is found using the Chato-Wattelet correlation."
        Rel=1/vl*V_suc[i]*D_h.suc/mu_l *(1-Xin)
        h_l=0.023*k_l/D_h.suc*(Rel)^0.8*Prl^0.4
        Frl=G^2/(1/vl)^2/9.314/D_h.suc
        F=1+1.925*Xtt^(-0.83)
        h_suc[i]=F*h_l
        Nusselt_suc[i]=h_suc[i]*D_h.suc/k_suc[i]

        "The resistance and UA values are found. The UA value is calculated by UP*L_hx
        for ease of convergence. (k in EES is in W/m-K so the values are divided by 1000 to
        get kW/m-K.)"
        R_suc[i] = 1000/(Nusselt_suc[i]*k_suc[i]*N_port.suc*P_port.suc/D_h.suc)
        R_liq[i] = 1000/(P_port.liq*N_port.liq*Nusselt_liq[i]*k_liq[i]/D_h.liq)
        UP[i] = (R_suc[i] + R_liq[i])^(-1)
        UA[i] = UP[i]*L2

        "The heat transfer is calculated for the two phase region of the suction line. Also, the
        wall temperature is found."
        Q[i]=mdot*(hslhxi[i] - hslhxi[i-1])
        Q[i]=mdot*(hllhxi[i] - hllhxi[i-1])*FLOW
        Q[i]=UA[i]*(Tllhxi[i]-Tslhxi[i])
        Q[i]=(Tllhxi[i]-Twall[i])/R_liq[i]*L2

end

"The vapor phase  region of the suction side is broken NN sections."
XLOC[1]=L2
duplicate i=2,NN+1
        L_suc[i] =( L_slhx-L2)/(NN)
        L_liq[i] = (L_slhx-L2)/(NN)
        L_hx[i] = (L_slhx-L2)/(NN)
        XLOC[i]=L2+L_hx[i]*(i-1)
END
"The vapor phase suction part is between 1 and NN in the internal heat exchanger."
duplicate i=2,NN+1
        "Find all properties."
        call TP(Tllhxi[i], Pllhxi[i]: vllhxi[i], hllhxi[i], sllhxi[i])
        call TP(Tslhxi[i], Pslhxi[i]: vslhxi[i], hslhxi[i], sslhxi[i])
        call TRANSP( Tllhxi[i], 1/Vllhxi[i]: mu_liq[i], k_liq[i])
        call SPH(Tllhxi[i],Pllhxi[i]+10:cp_liq[i])
        call SPH(Tslhxi[i]+0.2,Pslhxi[i]:cp_suc[i])
        call TRANSP( Tslhxi[i]+0.2, 1/Vslhxi[i]: mu_suc[i], k_suc[i])
        rho_liq[i] = 1/vllhxi[i]
```

```
rho_suc[i] = 1/vslhxi[i]

"Find volumetric flow rate."
Vdot_suc[i] = mdot* vslhxi[i]
Vdot_liq[i] = mdot * vllhxi[i]

"Find velocity."
V_suc[i] = Vdot_suc[i]/(N_port.suc*A_port.suc)
V_liq[i] = Vdot_liq[i]/(N_port.liq*A_port.liq)

"Find friction factor using Perukhov equation."
f_suc[i] =(0.79*ln(Re_suc[i])-1.64)^(-2)    {Turbulent flow}
f_liq[i] = (0.79*ln(Re_liq[i])-1.64)^(-2)

"Find pressure drop."
dP_suc[i] = f_suc[i]*(L_suc[i]/D_h.suc)*V_suc[i]^2/2000/Vslhxi[i]
dP_suc[i]=  Pslhxi[i-1] - Pslhxi[i]
dP_liq[i] =  f_liq[i]*(L_liq[i]/D_h.liq)*V_liq[i]^2/2000/Vllhxi[i]
dP_liq[i]= (Pllhxi[i] - Pllhxi[i-1])*FLOW

"Find Reynolds number."
Re_suc[i]=rho_suc[i]*V_suc[i]*D_h.suc/mu_suc[i]
Re_liq[i]=rho_liq[i]*V_liq[i]*D_h.liq/mu_liq[i]

"Find Prandtl number."
Pr_liq[i] = mu_liq[i]*cp_liq[i]/(k_liq[i]/1000)
Pr_suc[i] =mu_suc[i]*cp_suc[i]/(k_suc[i]/1000)

"Find the heat transfer coefficient using the Gnielinski correlation."
Nusselt_liq[i]=
(f_liq[i]/8)*(Re_liq[i]-1000)*Pr_liq[i]/(1+12.7*(f_liq[i]/8)^0.5*(Pr_liq[i]^(2/3)-1))
h_liq[i]=Nusselt_liq[i]*k_liq[i]/D_h.liq

Nusselt_suc[i]=
(f_suc[i]/8)*(Re_suc[i]-1000)*Pr_suc[i]/(1+12.7*(f_suc[i]/8)^0.5*(Pr_suc[i]^(2/3)-1))
h_suc[i]=Nusselt_suc[i]*k_suc[i]/D_h.suc

"The resistance and UA values are found.  The UA value is calculated by UP*L_hx
for ease of convergence.  (k in EES is in W/m-K so the values are divided by 1000 to
get kW/m-K.)"
R_suc[i] = 1000/(Nusselt_suc[i]*k_suc[i]*N_port.suc*P_port.suc/D_h.suc)
R_liq[i] = 1000/(P_port.liq*N_port.liq*Nusselt_liq[i]*k_liq[i]/D_h.liq)

UP[i] = (R_suc[i] + R_liq[i])^(-1)
UA[i] = UP[i]*L_hx[i]

"The heat transfer is calculated for the two phase region of the suction line.  Also, the
wall temperature is found."
```

```
        Q[i]=mdot*(hslhxi[i] - hslhxi[i-1])
        Q[i]=mdot*(hllhxi[i] - hllhxi[i-1])*FLOW
        Q[i]=UA[i]*(Tllhxi[i]-Tslhxi[i])
        Q[i]=(Tllhxi[i]-Twall[i])/R_liq[i]*L_hx[i]

end

"The suction pressure drop, liquid pressure drop,  and Q_slhx for each section are summed
to get the total. "
DP_Low=sum(DP_suc[I],I=1,NN+1)
DP_High=sum(DP_liq[I],I=1,NN+1)
Qslhx =sum(Q[i],i=1,NN+1)

"The effectiveness for the internal heat exchanger is found.  If the flow is counter Qmax_counter
is used, and if the flow is parallel, Qmax_parallel is used."

Qmax_parallel = mdot*(hlmax - hllhxi[0])
Qmax_parallel = mdot*(hsmax - hslhxi[0])
call TP(Tmax, Pslhxi[NN+1]: vsmax, hsmax, ssmax)
call TP(Tmax, Pllhxi[NN+1]: vlmax, hlmax, slmax)

Qmax_counter = mdot*(htmax - hslhxi[0])
call TP(Tllhxi[0], Pslhxi[NN+1]: vtmax, htmax, stmax)

eps_calc=(1-Flow)/2*Qslhx/Qmax_counter + (1+Flow)/2*Qslhx/Qmax_parallel
```